University of Durham

Surfactant-Induced Crystallisation of Dl-Aspartic acid

Seema Al-Mannai

A dissertation submitted in partial fulfilment of the requirements for the degree of Master in Chemistry at the University of Durham

January 2001

Declaration

The work reported in this thesis was carried out in the Department of Chemistry at the University of Durham between October 1999 and September 2000 under the supervision of Dr. s. Cooper. The work is original, unless otherwise stated in the text. No part of this work has been submitted for a degree at this or any other university.

ABSTSTRACT

Crystallisation of dl-aspartic acid beneath monolayers at the air-water interface was studied using seven different monolayer films namely stearic acid, methyl stearate, o-octadceyl carbonyl-l-tyrosine methyl ester hydrochloride, polycaprolactone, poly-l-isoleucine, poly-γ-benzyl-l-glutamate, and nylon 6 6. These films were chosen to study the effect of small molecule and polymeric surfactants on the nucleation of dl-aspartic acid. The crystallisation was studied using optical microscopy and external reflection FTIR. The dl-aspartic acid crystal morphology was analysed using molecular modelling. It was found that the polymeric monolayers were more likely to nucleate dl-aspartic acid than the small molecule ones. In particular, nylon 6 6 and polycaprolactone were the best monolayer films at nucleating dl-aspartic acid. The crystals grown beneath these two films were typically grown in groups or lines, the nucleation density was larger and the crystals were also larger than for the other films. The {1 1 0} and { $\bar{1}$ 1 1} crystal faces were the main crystal faces that grew beneath all the films. External reflection FTIR was shown to be a good method of studying crystallisation beneath films, because peaks due to the film and dl-aspartic acid crystals can be seen. FTIR evidence of film reorganisation during dl-aspartic acid crystallisation was found for the stearic acid, methyl stearate and nylon 6 6 films (spread from phenol-toluene). The FTIR data suggested that the nylon 6 6 and l-tyrosine monolayer films nucleated dl-aspartic acid crystals at earlier times compared with the other films.

Acknowledgement

I would like to thank my supervisor, Dr. S. J. Cooper, for all her kind help during my studies and in her help in improving this thesis. In addition, I would like to thank my husband Fawaz and my family for their love and support.

Contents

Chapter 1: Introduction

1.1. Crystallisation Beneath Monolayer 1
1.2. Project Objective 1
1.3. Crystallisation Theory 2
1.3.1. Equilibrium Shape of a Crystal 4
1.3.2. Equilibrium of infinitely large phase 4
1.3.3. Supersaturation 5
1.3.4. Equilibrium of Finit Phases 6
1.3.4.1.Laplace Equation 6
1.3.4.2. Equation of Cibbs-Thomson 6
1.3.5.1. Nucleation 8
1.3.5.1.1. Classical Homogeneous Nucleation Theory 9
1.3.5.1.2. Classical Heterogeneous Nucleation Theory 12
1.3.5.1.2.a Cap- shaped nuclei 13
1.3.5.1.2.b Disc-shaped nuclei 15
1.3.5.1.2.c Monolayer disc 16
1.3.5.1.2.d Anisotropic 3-dimensional nuclei 16
1.3.5.2. Crystal Growth 18
1.3.5.2.1 Crystal Growth Mechanism 19
1.3.5.2.1a Continual Growth Mechanism for atomically rough faces 19
1.3.5.2.1b Layer growth of Flat Faces 20
1.3.5.2.2. Crystal Morphology 21
1.3.5.2.2a Equilibrium Crystals and Macroscopic Crystals 21
1.3.5.2.2b Predicting Crystal Morphologies 22
1.4. Monolayer Films 22
1.4.1. Description 22
1.4.2. Monolayer States 24
1.4.2.1 Gaseous Monolayer 25
1.4.2.2 Expanded Monolayer 25
1.4.2.3 Condensed Monolayers 26
26

1.4.3 Monolayer Stability
1.4.3.2 Solution 27
1.4.3.3 Collapse and Fracture 27
1.4.4 Factors Determining Film Behaviour 29
1.4.4.1 Solute 29
1.4.4.2 Impurities 29
1.4.4.3 Vibration 29
1.5 External Reflection FTIR Spectroscopy 19

Chapter 2. ExperimentalMethods and π-A Isotherms 30
2.1 Introduction 30
2.2 Equipment 30
2.2.1. PFTE Langmuir Trough and Barriers 30
2.2.2. Wilhelmy Plate Balance 31
2.2.3. Evaporation from the troughs 32
2.3. Ensuring a Contamination Free Environment 32
2.3.1. Trough Cleaning Procedure 32
2.3.2. Wilhelmy Plate Cleaning 32
2.3.3. Purity of Chemicals Used 33
2.3.4. Criteria for a Clean Subphase Surface 33
2.4. Film Spreading 33
2.5. Experimental Details 34
2.5.1. Preparation of Supersaturated Solutions 34
2.5.2. Nucleation Experiments 35
2.5.3. Removal of Surface Crystals 35
2.5.4. Analytical Techniques 35
2.5.4.1. Optical Microscopy 35
2.5.4.2. FTIR Spectroscopy 36
2.6. π-*A* Curve Results 36
2.6.1. π-*A* Curves of Stearic Acid over Pure Water and dl-Aspartic Acid Subphases 37
2.6.2. π-*A* Curves of Methyl Stearate over Pure Water and dl-Aspartic Acid Subphases 38

2.6.3. π-A Curves of L-Tyrosine-O-Octadecylcarbonyl Hydrochloride MethylEster over Pure Water and dl-Aspartic Acid Subphases 39

2.6.4. π-A Curves of Polycaprolactone over Pure Water and dl-Aspartic Acid Subphases 40

2.6.5. π-A Curves of Poly-l-Isoleucine over Pure Water and dl-Aspartic Acid Subphases 41

2.6.6. π-A Curves of Poly-γ-Benzyl-Glutamate over Pure Water and dl-Aspartic Acid Subphases 42

2.6.7. π-A Curves of Nylon 6 6 over Pure Water and dl-Aspartic Acid Subphases 43

Chapter 3. Results and Discussion of the Nucleation Experiments 44

3.1 Introduction 44

3.2 The Monolayer Films Used 46

3.3 Nucleation Experiments 47

3.4 The Effects of Film Surface Pressure upon Crystallisation 47

3.4.1. Stearic acid 48

3.4.2. Methyl stearate 49

3.4.3. l-tyrosine 54

3.4.4. Polycaprolactone 56

3.4.5. Poly-l-isoleucine 59

3.4.6. Poly-γ-benzyl-glutamate 59

3.4.7. Nylon 6 6 62

3.5. Comparison of the Films' Ability to Crystallise dl-Aspartic Acid 67

3.5.1. Stearic acid 67

3.5.2. Methyl stearate 67

3.5.3. l-tyrosine 69

3.5.4. Polycaprolactone 70

3.5.5. Poly-l-isoleucine 72

3.5.6. Poly-γ-benzyl-glutamate 72

3.5.7. Nylon 6 6 73

3.6 Conclusion 75

Chapter 4. Morphology Studies and FTIR Results 76
4.1. Introduction 76
4.2. The Morphology 76
4.2.1. Computational modelling 76
4.2.2. Crystal habit of dl-aspartic acid in aqueous solution 78
4.2.3. Investigation of crystal habit beneath each monolayer film 79
4.2.3.1.Crystal habits of dl-aspartic acid grown beneath stearic acid monolayer film 81
4.2.3.2.Crystal habits of dl-aspartic acid grown beneath methyl stearate monolayer film 82
4.2.3.3. Crystal habits of dl-aspartic acid grown beneath l-tyrosine monolayer film 83
4.2.3.4.Crystal habits of dl-aspartic acid grown beneath polycaprolactone monolayer film 84
4.2.3.5. Crystal habits of dl-aspartic acid grown beneath poly-l-isoleucine monolayer film 85
4.2.3.6. Crystal habits of dl-aspartic acid grown beneath poly-γ-benzyl-glutamate monolayer film 86
4.2.3.7. Crystal habits of dl-aspartic acid grown beneath nylon 6 6 monolayer film 87
4.3 The Results of External Reflection FTIR Spectroscopy 88
4.3.1. Stearic acid 88
4.3.2. Methyl stearate 89
4.3.3. l-tyrosine 94
4.3.4. Polycaprolactone 97
4.3.5. Poly-l-isoleucine 100
4.3.6. Poly-γ-benzyl-glutamate 104
4.3.7. Nylon 6 6 110
4.3.8 Nylon 6 6 (spread from phenol-toluene solvent) 113
4.4. The Conclusion 118

Chapter 5. Conclusion 119
References 122

CHAPTER 1

INTRODUCTION

1- Background:

1.1. Crystallisation Beneath Monolayers:

At an air-water interface a surfactant monolayer will spontaneously organise, and may form a condensed, close-packed film if sufficiently compressed. Such a film will be an ordered layer upon which heterogeneous and indeed epitaxial (ie. oriented), nucleation and growth may preferentially occur. Lahav *et al*[1-4] were the first to explain such epitaxial growth beneath monolayers, for the case of glycine crystals growing with their {0 1 0} faces attached to resolved α-amino acid surfactants. The film was acting as a 2-D template for the required nucleating face of the overgrowth, and in common with the analogous 3-D systems, an exact or close correspondence between the lattice structures of film and overgrowth produced the desired epitaxial growth.

The current application of new techniques[5,6] for determining the structure and packing of monolayers, however, shows that coherent films can possess some degree of order at lower surface pressures. Hence this suggested that heterogeneous and epitaxial nucleation may also occur upon such partially compressed or uncompressed films, even in the absence of film island formation, as has been shown recently [7-9]. For such films, any decrease in order, as compared with their fully compressed counterparts, may be compensated by the greater dynamical freedom and compressibility of these more expanded films. Thus, a larger degree of lattice mismatch between the film and nucleating species may be tolerated.

1.2. Project Objective:

The objective of this thesis is to study the crystallisation of dl-aspartic acid beneath seven different monolayer films under different surface pressure and supersaturation conditions. We are particularly interested in comparing small molecular and polymeric surfactant behaviour, to see if polymers offer any advantage over their small molecule analogues. Consequently the following readily available surfactant films were chosen:

1. Stearic acid.
2. Methyl stearate.
3. o-octadecyl carbonyl-l-tyrosine methyl ester hydrochloride.
4. Polycaprolactone.
5. Poly-l-isoleucine.
6. Poly -γ-benzyl-l- glutamate.
7. Nylon 6 6

This research involves:

1. Characterisation of monolayer films at the air-water interface.
2. Study of the crystallisation rate as a function of film material, surface pressure and supersaturation.
3. Comparison between small molecule and polymeric surfactant behaviour.
4. Investigation of the nucleation of dl-aspartic acid by external reflection FT-IR spectroscopy at the air-water interface.

1.3. Crystallisation Theory:

Crystallisation involves the production of crystalline daughter phase from a parent phase.

1.3.1- Equilibrium Shape of a Crystal

The formation of any new phase from a bulk parent phase needs the creation of an interface between the two phases. This interface needs an amount of work, dependant upon the surface tension, γ, of the interface. The surface tension is defined as the work required to create unit area of interface; and is given by:

$$\gamma = \left(\frac{\partial G}{\partial A}\right)_{pT} \qquad (1)$$

where: ∂G is the Gibbs free energy change, ∂A is the area change, p is the pressure, and T is the temperature.

The equilibrium crystal shape can be determined by the Gibbs-Wulff theorem. Gibbs (1878) recommended that for the equilibrium shape of a crystal, the total Gibbs surface function of formation should be a minimum for constant volume of crystal:

$$d\sum_n A_n\gamma_n = \sum_n \gamma_n dA_n = 0 \qquad (2)$$

where: A_n is the area of the n^{th} crystal face, and γ_n is the surface tension of the n^{th} face, which is assumed constant over the whole face and independent of the crystal shape. Wulff (1901) stated that equation 2 would lead to a constant value for $\frac{\gamma_n}{h_n}$, where h_n is the distance to the n^{th} face from a point in the crystal known as the Wulff point. This enables the equilibrium shape of the crystal to be drawn by means of a Wulff plot.

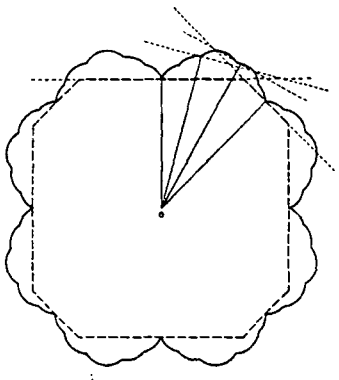

Fig. 1.1. Wulff plot in two dimensions[10].

Wulff plot :

1- Draw vectors normal to all possible crystallographic faces from an arbitrary point.

2- The distances proportional to γ_n are marked on the vectors.

3- Planes normal to the vectors are constructed through the marks.

4- The resulting closed polyhedron is the equilibrium form.

1.3.2- Equilibrium of Infinitely Large Phases:

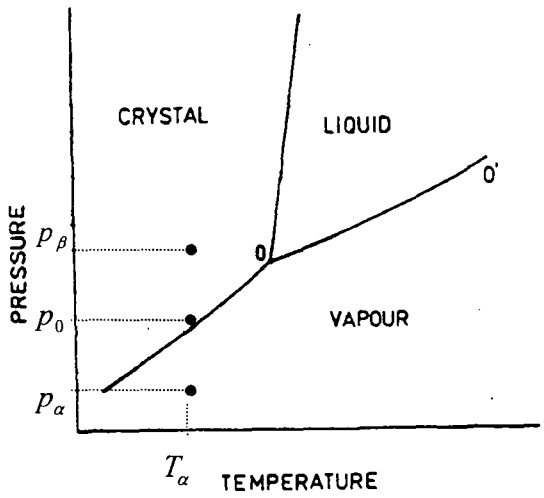

Fig. 1.2. Phase diagram of a single component system in P-T coordinates[11].

The pressure-temperature diagram of a typical material is divided into three parts (phases):

1- The crystal phase is thermodynamically favoured at high pressure and low temperatures.

2- The liquid phase is stable at high temperatures and high pressures.

3- The gas (vapour) phase is stable at high temperature and low pressure.

The three phases are simultaneously in equilibrium at the triple point (0) (see fig 1.2), and any two phases are in equilibrium along the lines of the curves. At point (0`) the critical point, the liquid and gas are indistinguishable.

1.3.3- Supersaturation:

The supersaturation, $\Delta\mu$, is the difference between the chemical potential of the vapour and crystalline phase, so $\Delta\mu = \mu_v - \mu_c$; it represents the thermodynamic driving force for the phase transition. As shown in fig. 1.2. of the phase diagram of a single component system in p-T coordinates, the chemical potentials of the phases are equal only at equilibrium. If we increase the pressure on a gas initially at pressure p_α and temperature T_α, then at pressure p_0, the gas will be in equilibrium with its crystal. Any further increase in the pressure, say to pressure p_β, will make the gas unstable with respect to the bulk, infinitely large crystal, and the chemical potential of the gas will be higher than that of the infinite crystal ($\mu_v \rangle \mu_c$).

Table 1.1. Lists the different expressions for the supersaturation with regard to processes of condensation, crystallisation, bubble formation and electrodeposition of metals.

Different expressions for the supersaturation:

Process	**Expressions† for the supersauration, $\Delta\mu$**	
Condensation of vapour to liquid or crystal	$\Delta\mu = kT \ln \frac{p}{p_0}$	$\Delta\mu = \frac{\Delta_{trans} H \Delta T}{T_{trans}}$
Crystallisation from solution	$\Delta\mu = kT \ln \frac{C}{C_0}$	$\Delta\mu = \frac{\Delta_{sol} H \Delta T}{T_{sat}}$
Crystallisation from the melt	$\Delta\mu = \frac{\Delta_{melt} H \Delta T}{T_m}$	
Formation of gas bubbles in liquid	$\Delta\mu = -kT \ln \frac{p}{p_0}$	$\Delta\mu = \frac{\Delta_{evap} H \Delta T}{T_b}$
Electrocrystallisation of metals	$\Delta\mu = ze\eta$	

Table 1.1

† Assuming ideal systems and entropy/enthalpy of the transitions are independent of T.

In table 1.1: p_0 is the equilibrium pressure of the infinitely large condensed phase, C and C_0 are the actual and equilibrium concentrations of the solute, the $\Delta H's$ represent the enthalpy of the transition, the T_{trans} are the equilibrium temperatures for the

transition with the subscripts *sat*, *b* and *m* referring to saturation, boiling and melting, respectively. *z* is the valence of the neutralising ions, *e* is the elementary electric charge and η is the over potential.

1.3.4- Equilibrium of Finite Phases:

The process of formation of a new phase always goes through the formation of small crystallites, droplets or bubbles. By studying the equations of Laplace and Thomson-Gibbs, we can consider:

1- the mechanical equilibrium of small particles with their ambient phase, and

2- the thermodynamic equilibrium of small particles or their equilibrium vapour pressure as a function of their size.

1.3.4.1- Laplace Equation:

$$p_l - p_v = \frac{2\gamma}{r} \qquad (3)$$

The pressure in a small droplet (p_l) is always higher than the surrounding vapour pressure (p_v) by an amount $2\gamma/r$, known as the Laplace or capillary pressure. When the phase boundary is flat (r→∞), the capillary pressure is zero and $p_l = p_v$.

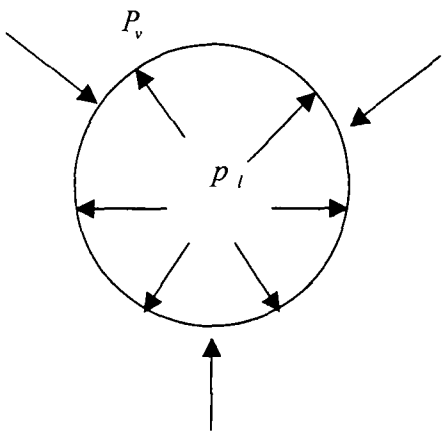

Fig. 1.3. Liquid droplet showing that $p_l \rangle p_v$.

1.3.4.2- Equation of Gibbs-Thomson:

The thermodynamic equilibrium of small particles is considered by the expression for the Gibbs free energy for the chemical potential of the molecules in a small droplet,

$$\Delta\mu = \frac{2\gamma v_l}{r} \qquad (4)$$

where: v_l is the volume occupied by one molecule in the liquid droplet, and r is the radius for the droplet.

By using the equation of condensation of vapour to liquid (see table 1.1):

$$\Delta\mu = kT \ln \frac{p}{p_0}$$

we will have:

$$kT \ln \frac{p}{p_0} = \frac{2\gamma v_l}{r} \qquad (5)$$

where: k is the Boltzmann constant, and T is the temperature.

This equation demonstrates that the vapour pressure of the liquid droplet increases with decreasing droplet radius. The physical reason for this is simple to understand when one considers that an atom on a curved convex surface will be more weakly bound than in the case of an atom on a flat surface.

For the formation of an equilibrium crystal, application of the Gibbs-Wulff theorem shows that:

$$\Delta\mu = \frac{2\gamma_n v_c}{h_n} \qquad (6)$$

where: v_c is the volume occupied by one molecule in the crystal, and h_n is the length of the crystal face from the Wulff point.

1.3.5- How Does The New Phase Form?

This question can be solved, by studying two processes, nucleation and crystal growth.

1.3.5.1 Nucleation:

Nucleation is the process describing the initial formation of small clusters of the crystallising material from individual atoms or molecules, where there is a free energy barrier to the formation of the new phase. The free energy barrier arises because, the formation of any new phase from a bulk parent phase needs the creation of an interface between the two phases; this interface needs an amount of work. Hence initially there is an increase in the Gibbs free energy of the system, when the new phase starts to form, as shown in fig 1.4

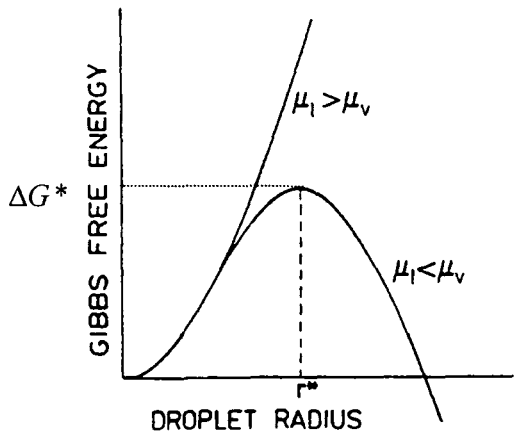

Fig. 1.4.Gibbs free energy as a function of droplet radius[12] .

At all conditions above or below the saturation temperature, fluctuations in density, heat content, etc. occur in the solution phase. These fluctuations always increase the free energy of the local environment when the solution is above its equilibrium temperature. Moreover, below the saturation temperature, these same fluctuations can lead to the formation of stable nuclei of the solid phase, by providing the energy, ΔG^*, required to form the new phase.

We can distinguish two different types of nucleation: *homogeneous nucleation* is the spontaneous formation of nuclei in the bulk of the supersaturated system, and *heterogeneous nucleation*, which occurs upon a foreign substrate.

1.3.5.1.1. Classical Homogeneous Nucleation Theory:

In classical homogeneous nucleation theory, to consider the rate of nucleation, *J*, it is important to go through two processes.

1- The formation of a near equilibrium concentration, *n (i*)*, of critical nuclei.

2- Impingement at a rate, *W**, of the condensable species upon these nuclei, which causes them to become essentially free growing and thus eventually bulk, condensed phase.

Thus:

$$J = W^* n(i^*) \tag{7}$$

The equilibrium concentration of critical nuclei is given by a Boltzmann distribution:

$$n(i^*) = n\exp\left[\frac{-\Delta G^*}{kT}\right] \tag{8}$$

where: n is the concentration of the condensable phase, and ΔG^* is Gibbs free energy of formation of critical nuclei.

To determine ΔG^*, we need to consider the change in the Gibbs free energy on formation of a cluster containing i monomers:

$$\Delta G_i = -i(\Delta\mu) + \sum_n \gamma_n A_n \tag{9}$$

For a spherical cluster, Eq. (9) becomes:

$$\Delta G_i = -\frac{4\pi r^3}{3v_c}(\Delta\mu) + 4\pi r^2\gamma \tag{10}$$

Where: $4\pi r^2$ is the surface area of a spherical cluster, $(4/3)\pi r^3$ is the volume of a spherical cluster, and v_c is the volume occupied by one molecule in the cluster.

Maximising ΔG_i with respect to r gives the radius of the critical nucleus:

$$\frac{d\Delta G_i}{dr} = -\frac{4\pi r^2}{v_c}\Delta\mu + 8\pi r\gamma = 0$$

This gives:

$$r^* = \frac{2\gamma v_c}{\Delta\mu}$$ i.e. the Gibbs-Thomson equation.

Substituting the Gibbs Thomson equation into (10) gives the Gibbs free energy of formation of the critical nucleus in terms of the supersaturation as:

$$\Delta G^* = \frac{16\pi\gamma^3 v_c^2}{3\Delta\mu^2} \qquad (11)$$

Or in surface free energy terms as:

$$\Delta G^* = \frac{1}{3}A\gamma \qquad (12)$$

The Gibbs free energy of formation of the critical nucleus for a crystal is given by:

$$\Delta G^* = -\frac{V_c^*}{v_c}\Delta\mu + \sum_n A_n\gamma_n$$

where: V_c^* is the volume of the crystalline critical nucleus.

The volume of any crystal = the sum of pyramid volumes, where each pyramid has a crystal face as its base, and the Wulff point as its apex. Hence:

$$V_c^* = \frac{1}{3}\sum_n h_n A_n$$

where: h_n is a pyramid height and A_n is surface of the corresponding crystal face.

Substituting for V_c^*, and h_n using Eq $\Delta\mu = \frac{2\gamma_n v_c}{h_n}$ gives:

$$\Delta G^* = -\frac{2\sum_n A_n\gamma_n}{3} + \sum_n A_n\gamma_n = \frac{1}{3}\sum_n A_n\gamma_n$$

The impingement rate W^*, is given by:

$$W^* = R^* S^* \tag{13}$$

where: R^* is the adsorption flux, i.e. the frequency with which condensing molecules reach unit area of critical nucleus, and S^* is the surface area of the nucleus.

Combining Eqns. (7), (8), and (13), the homogeneous nucleation rate can be written as:

$$J = R^* S^* n \exp\left[-\frac{\Delta G^*}{kT}\right]$$

or

$$J = \Omega \exp\left[-\frac{\Delta G^*}{kT}\right] \tag{14}$$

where: Ω is known as the pre-exponential factor.

Ω is not very dependent upon the supersaturation, compared with the exponential factor, and therefore one can consider Ω as nearly constant. Typical values of Ω are $\sim 10^{25} - 10^{35}\ \mathrm{cm}^{-3}\mathrm{s}^{-1}$.

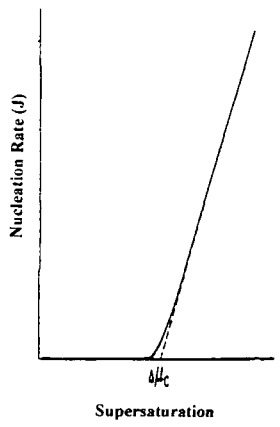

The form of Eq. 14 is such that J remains negligibly small until the supersaturation reaches a critical value, the Ostwald metastable limit, at which point J suddenly and dramatically increases.

Hence, this critical supersaturation *level* can be arbitrarily set as the rate at which $\ln J = 0$, i.e. the rate is 1 nucleus $cm^{-3}sec^{-1}$ (or any other suitable experimentally detectable limit) with little loss of accuracy.

1.3.5.1.2 Classical Heterogeneous Nucleation Theory:

In heterogeneous nucleation, impurity particles, ions, or foreign surfaces serve as an effective catalyst for nucleation. Hence the heterogeneous nucleation rate is greater than homogeneous nucleation.

$$J_{het} > J_{\text{hom}}$$

$$J_{\text{het}} = W^{*}_{\text{het}} n(i^{*})$$

Once more $n(i^*)$, the equilibrium concentration of critical nuclei, is given by a Boltzmann distribution

$$n(i^*) = n_0 \exp\left(-\frac{\Delta G^{*}_{het}}{kT}\right) \qquad (15)$$

Where: n_0 is the adatom concentration on the substrate and ΔG^{*}_{het} is the heterogeneous Gibbs free energy of formation of the critical nucleus.

Determination of ΔG^*, the Gibbs free energy of the critical nucleus:

The shape of the critical nucleus upon the substrate affects the heterogeneous Gibbs free energy change. The nuclei can be isotropic (cap-shaped) or anisotropic (disc-shaped / polygonal).

1.3.5.1.2a Cap-shaped nuclei:

The formal theory follows the outline above for homogeneous nucleation except that fewer atoms are needed to reach a particular surface curvature. It turns out that the spherical cap has a critical size that has the same radius as for the complete sphere, grown under homogeneous nucleation conditions.

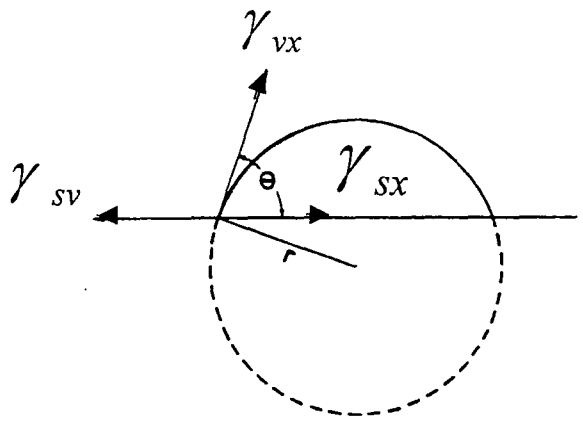

Fig. 1.5. A spherical cap on a substrate, showing the contact angle θ.

Young's equation may be used to determine the contact angle, θ:

$$\cos\theta = \frac{\gamma_{sv} - \gamma_{sx}}{\gamma_{vx}} \qquad (16)$$

where, γ is the surface tension and the subscripts s, v, and x refer to the substrate, vapour and nucleus, respectively.

Employing the classical technique of considering the cluster as bulk crystal with terms included accounting for its surface, gives:

$$\Delta G_i = -\frac{4}{3v_c}\pi r^3 \Delta\mu\left(\frac{2-3\cos\theta+\cos^3\theta}{4}\right)+4\left(\frac{1-\cos\theta}{2}\right)\pi r^2\gamma_{vx}+\pi r^2\sin^2\theta(\gamma_{sx}-\gamma_{sv})$$

Substituting for $(\gamma_{sx}-\gamma_{sv})$ using Young's Eq., this gives:

$$\Delta G_i = -\frac{4\pi r^3\Delta\mu}{3v_c}f(\theta)+4f(\theta)\pi r^2\gamma_{vx}$$

where: $f(\theta)=\left(\frac{2-3\cos\theta+\cos^3\theta}{4}\right)$.

Maximising ΔG_i with respect to r then leads to:

$$r^* = \frac{2\gamma v_c}{\Delta\mu}$$

i.e the Gibbs-Thomson equation. Substituting this into the expression for ΔG_i gives,

$$\Delta G^*_{het} = \frac{16\pi\gamma_{vx}^3 v_c^2}{3\Delta\mu^2}f(\theta)=\frac{\sum_n A_n\gamma_n}{3}=\Delta G^*_{\text{hom}}\frac{V^*_{het}}{V^*_{\text{hom}}} \qquad (17)$$

where: ΔG_{hom} is the Gibbs free energy of formation for homogeneous nucleation of this system and, V^*_{het} and V^*_{hom} are the volumes of the heterogeneous and corresponding homogeneous critical nuclei, respectively.

We find that for θ = 180°, the homogeneous value of ΔG^* is obtained, since heterogeneous nucleation does not occur as the crystallising species does not adsorb onto the foreign substrate.

If θ = 0°, complete wetting occurs and this model then predicts no nucleation barrier. For θ = 0°, though, the critical nucleus will be a 2-D monolayer disc and so Eq. (17) will not be applicable for such cases of very strong adsorption of adatoms onto the substrate.

1.3.5.1.2b Disc-shaped nuclei:

Disc shapes occur if adatom adsorption on the substrate is very strong, producing a monolayer 2D disc, or if the nucleus is 3D and anisotropic.

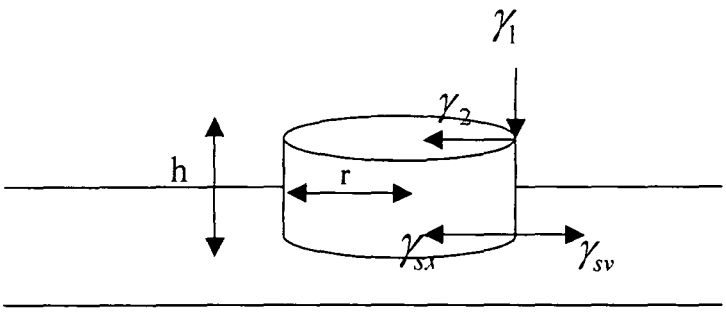

The Gibbs free energy of formation for either shape will be:

$$\Delta G_i = -(\pi r^2 h \Delta\mu / v_c) + \pi r^2 (\gamma_{sx} + \gamma_2 - \gamma_{sv}) + 2\pi r h \gamma_1 \qquad (18)$$

For the monolayer disc, h is a constant equal to the height of the atom perpendicular to the substrate surface, whilst for the anisotropic, less strongly adsorbed nucleus, h will be determined according to the Gibbs-Wulff law.

1.3.5.1.2c Monolayer discs:

Maximising ΔG_i in equation 18 with respect to r leads to:

$$r^* = \frac{\gamma_1}{(\Delta\mu / v_c) - [(\gamma_{sx} + \gamma_2 - \gamma_{sv})/h]} \tag{19}$$

and

$$\Delta G_{het}{}^* = \frac{\pi h \gamma_1{}^2}{(\Delta\mu / v_c) - [(\gamma_{sx} + \gamma_2 - \gamma_{sv})/h]} = \pi r^* h \gamma_1 \tag{20}$$

In this case, $\Delta G_{het}{}^*$ is equal to half the edge free energy terms, since the critical nucleus is a 2D, as opposed to a 3D, equilibrium shape. Any other 2D critical nucleus equilibrium shape will also have $\Delta G_{het}{}^*$ equal to half the edge free energy terms.

1.3.5.1.2d Anisotropic 3-dimensional nuclei:

From Eq. (18), i.e.

$$\Delta G_i = -(\pi r^2 h \Delta\mu / v_c) + \pi r^2 (\gamma_{sx} + \gamma_2 \_ \gamma_{sv}) + 2\pi r h \gamma_1$$

h can be determined from the Gibbs-Wulff law:

$$\frac{\gamma_n}{h_n} = \text{constant} \tag{21}$$

where: γ_n is the surface tension of face n, and h_n is the distance of the face from the Wulff point.

$$\frac{h}{\sum\gamma} = \frac{r}{\gamma_1} \longrightarrow h = \frac{r\sum\gamma}{\gamma_1} \tag{22}$$

substuting Eq. (22) into Eq. (18) gives:

$$\Delta G_i = -\frac{\pi r^3 \Delta\mu \sum\gamma}{\gamma_1 v_c} + \pi r^2 \sum\gamma + 2\pi r^2 \sum\gamma$$

$$= -\frac{\pi r^3 \Delta\mu \sum\gamma}{\gamma_1} + 3\pi r^2 \sum\gamma \qquad (23)$$

Differentiating ΔG_i and setting to zero gives ΔG_i^* and r^*:

$$\frac{d\Delta G_i}{dr} = -\frac{3\pi r^2 \Delta\mu \sum\gamma}{\gamma_1 v_c} + 6\pi r \sum\gamma = 0$$

As expected, this gives the Gibbs-Thomson law:

$$r^* = \frac{2\gamma v_c}{\Delta\mu} \qquad (24)$$

Substuting Eq. (24) into Eq. (23) gives:

$$\Delta G^* = \frac{-8\pi\gamma_1^2 \sum\gamma v_c^2}{\Delta\mu^2} + \frac{12\pi\gamma_1^2 \sum\gamma v_c^2}{\Delta\mu^2}$$

$$\Delta G^* = \frac{4\pi\gamma_1^2 \sum\gamma v_c^2}{\Delta\mu^2} = \pi (r^*)^2 \sum\gamma \qquad (25)$$

i.e. $\Delta G_i^* = 1/3$ of the surface area term.

The overall classical heterogeneous nucleation rate becomes:

$$J_{het} = W^* n_s \exp\left(-\frac{\Delta G_{het}^*}{kT}\right)$$

$$J_{het} = \Omega_{het} \exp\left(-\frac{\Delta G^{*}_{het}}{kT}\right) \qquad (26)$$

where: Ω_{het} is the pre-exponential factor. Typical values of Ω_{het} are $\sim 10^{17} - 10^{22}\,\mathrm{cm}^{-2}\,\mathrm{sec}^{-1}$.

1.3.5.2 Crystal Growth:

Crystal growth methods are generally classified into three categories: growth from the melt, growth from solution, and growth from the vapour phase. In this project the crystal were grown from solution.

In general by studying the structure of the crystal surface we can determine the mechanism of crystal growth.

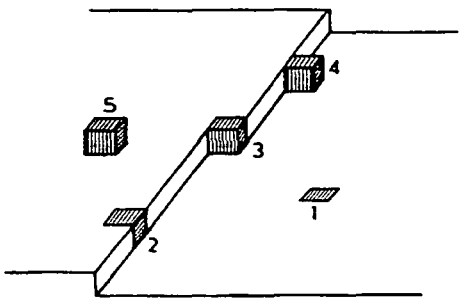

Fig.1.6. The most important sites an atom can occupy on a crystal surface:

1- embedded into the outermost crystal atom plane,
2- atom embedded into the step edge,
3- atom in half-crystal (kink) position,
4- atom adsorbed at the step, and
5- atom adsorbed on the crystal face.

Crystal faces can be divided into three types of faces, K (Kinked) faces, S (Stepped) faces, and F (Flat) faces. K faces are not parallel to any dense atomic rows, S faces are parallel to one dense atomic row, and F faces are parallel to at least two dense atomic rows. Depending on their positions the atoms are differently bound to the crystal surface, and also the detachment of these atoms leads to a change in the number of the unsaturated dangling bonds (or change in the surface energy), except for the atom in position (3), which has an equal number of saturated bonds and unsaturated bonds. That means no change in the surface energy will take place when the latter is detached from

this peculiar position. This position is called the half crystal, or kink position, because this position is bound to a half-atomic row, half-crystal plane and half-crystal block.

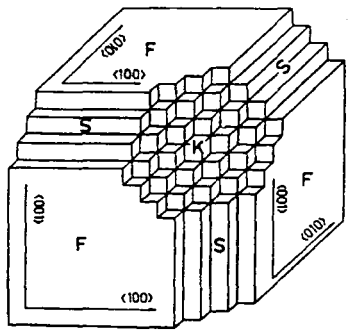

Fig. 1.7. A schematic representation of a Kossel crystal[13].

In a supersaturated solution, crystal growth is always favourable at kink sites. Therefore if a crystal face has a high density of kink sites the face can grow continuously.

1.3.5.2.1. Crystal Growth Mechanisms:

1.3.5.2.1a Continual growth mechanism for atomically rough faces:

In fact, S and K faces offer sufficient kink sites for continuous growth since they are atomically rough. F faces are atomically flat at low temperatures, however at temperatures above T_r, the roughening temperature, they become atomically rough, because entropy effects become more important at higher temperatures. Hence it will be favourable for the atomically flat face to become rough above T_r. Since the F faces are smooth below T_r, their growth requires formation of 2D nuclei or the presence of screw dislocations to ensure steps with kink sites along them.

K faces grow faster than S and F faces because the K faces offer kink sites with much greater density than S and F faces. However, the F faces of perfect crystals do not offer any kink sites at all. The rate of growth will be highest for K faces so they should disappear first. S faces will disappear next because of their smaller rate of growth

compared to K faces, F faces grow the slowest and so the crystal will be enclosed during the growth by F faces only. The crystal will cease to grow at all at small enough supersaturations.

For S, K, and F faces above their roughening transition, the rate of crystal growth is given by:

$$R = \lambda \Delta \mu \qquad (27)$$

where: λ is the kinetic coefficient. Typical values of R are $\sim 10^{-4} - 10^{-1} cm/\sec$.

The growth is continuous for these crystal faces because they have a sufficient density of kink sites. Crystals tend to have rounded morphologies if they grow by the continuous growth mechanism, because all faces grow at the same rate. But F faces cannot grow by this mechanism, because F faces at temperature below T_r (the roughening temperature) are atomically flat.

1.3.5.2.1b Layer growth of flat faces

Consider an atomically flat crystal belonging to a perfect defectless crystal. A single adatom on such a face is bound more weakly than an adatom in a cluster of adatoms on the surface. As a result, there is an energy barrier to the formation of each new crystal layer. This is the 2D analogue of homogeneous nucleation, and for this reason the rate of growth of this face will be determined by the formation of 2D critical nuclei.

Similarly to the 3D nucleation case, the rate of 2D nucleation is given by:

$$R = \Omega_{2D} \exp(-\Delta G^*_{2D} / kT) \qquad (28)$$

where: Ω_{2D} is the pre-exponential factor for 2D nucleation and ΔG^*_{2D} is the Gibbs free energy for formation of the 2D critical nucleus.

If the F crystal face is not perfect, and in particular if screw dislocation are present, then these screw dislocations represent a non-vanishing source of steps which alleviate the necessity of a 2D nucleation growth mechanism. Instead the rate of crystal growth is determined by the rate of the lateral movement of the steps.

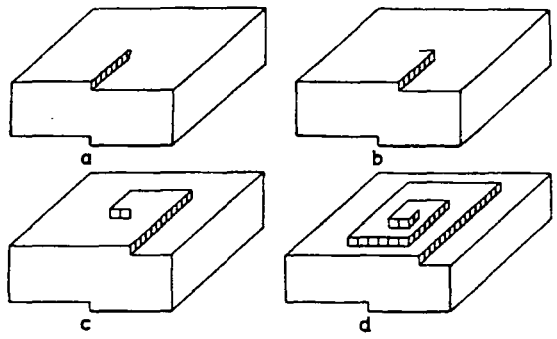

Burton, Cabrera and Frank (BCF) developed the theory of screw dislocation crystal growth and found that:

$$R = C(\sigma^2 / \sigma_c)\tanh(\sigma_c / \sigma) \qquad (29)$$

where: σ is the supersaturation parameter $\Delta\mu/kT$, σ_c is the characteristic supersaturation of the system and C is a rate constant.

Crystals growing by these layer-by-layer sarface-controlled mechanisms will be facetted. Typical values of R for growth by a layer by layer mechanism are $10^{-9} - 10^{-5}$ cm sec $^{-1}$.

1.3.5.2.2. Crystal Morphology:

1.3.5.2.2a Equilibrium Crystals and Macroscopic Crystals:

The equilibrium form of a crystal is controlled by:

$$\sum_n \gamma_n dA_n = 0 \qquad \text{i.e. the Gibbs-Wulff law.}$$

However the equilibrium shape is only likely to occur for sub-microscopic crystals.

When the crystals' surface area to volume ratio decreases the difference in surface energy of various forms becomes less significant. Consequently the relative growth rates of the different crystal faces control the macroscopic crystal morphology.

1.3.5.2.2b Predicting Crystal Morphologies:

The interaction energy per molecule between a slice (hkl) and the crystal face (hkl) is called the attachment energy, E_{att}. It is defined[14] as the energy released on the attachment of a growth slice to a growing crystal surface.

$$E_{att} = E_{latt} - E_{slice} \qquad (30)$$

where: E_{latt} is the lattice energy of the crystal, and E_{slice} is the energy of a growth slice of thickness d_{hkl}.

It is found[15] that the relative growth rate R of a face always increases with increasing E_{att}, although the exact form of the function $R(E_{att})$ depends on the growth mechanism and on various variables such as supersaturation, temperature, and solid-fluid interaction.

1.4. Monolayer Films:

1.4.1. Description

Only certain types of molecules are proficient at forming insoluble monolayers. An insoluble amphiphile consists of a polar (hydrophilic) and nonpolar (hydrophobic) portion which will naturally position itself at an air-water interface so that its hydrophilic portion will be adsorbed in the aqueous phase whilst the hydrophobic portion will remain in the air. Generally amphiphiles are known as surfactants. They normally contain a long hydrocarbon tail and a polar headgroup. As the length of the hydrocarbon chain is increased, the water solubility decreases.

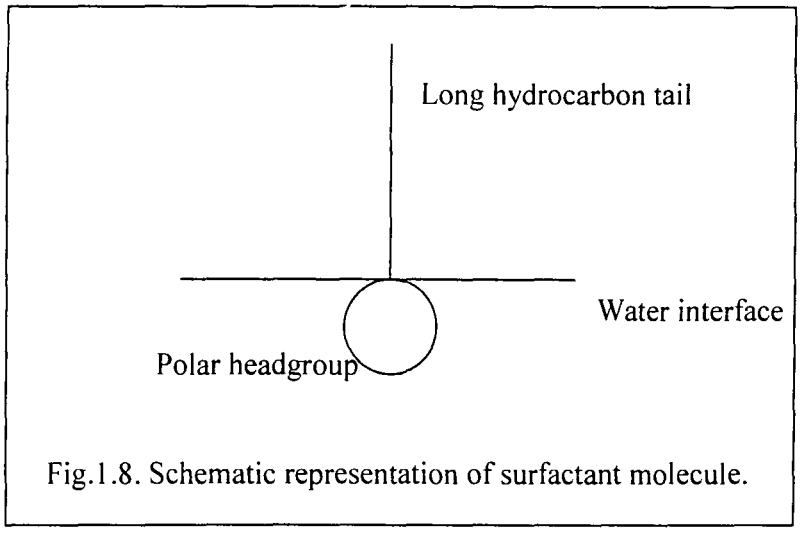

Fig.1.8. Schematic representation of surfactant molecule.

The surface pressure, π, is equal to the reduction of the pure water surface tension by the film-covered surface:

$$\pi = \gamma_0 - \gamma \qquad (31)$$

where: γ_0 is the surface tension of pure water, and γ is the interfacial tension of the water-film-air system. The magnitude of surface pressure, π, depends on the properties of area and temperature and the intermolecular forces present in the surfactant. Therefore at constant temperature, the surface pressure is altered by changing the surface area, A, accessible to each film molecule and a plot of surface pressure against area is then termed a π-A isotherm. These π-A curves provide invaluable information about the state of the monolayer system concerned. (see fig.1.9)

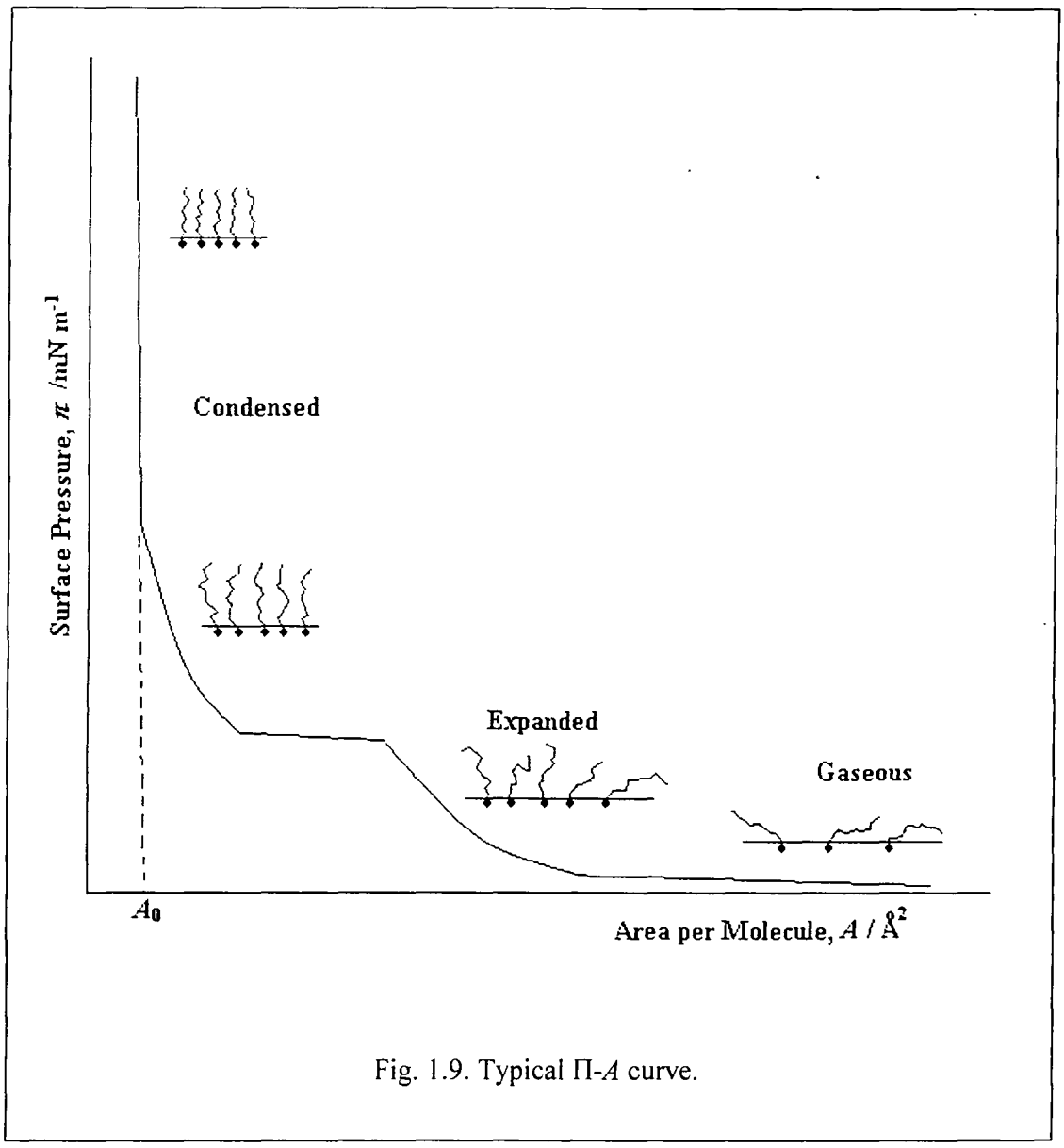

Fig. 1.9. Typical Π-*A* curve.

1.4.2. Monolayer States:

Monolayer films can exist in different states, and by analogy with 3-dimensioal systems these states are considered to be either gaseous, expanded, or condensed. The state which occurs under a given temperature and surface pressure depends upon the magnitude of the intermolecular forces present.

1.4.2.1. Gaseous Monolayer:

In gaseous monolayers, the film molecules are widely separated and apply comparatively little force on one another. The viscosity of gaseous monolayers is very low ($\approx 10^{-5} - 10^{-4}$ surface poises)[16], whilst its compressibility is extremely high ($> 10^{-1}$ m mN^{-1}) [17] and the surface pressure approaches zero asymptotically as the area available to the film is increased.

The π-A behaviour of gaseous monolayers is conventionally followed by a two-dimensional kinetic analysis corresponding to the three-dimensional ideal gas theory. Hence the subphase liquid molecules are ignored. This leads to an ideal two-dimensional gas equation:

$$\pi A = kT \tag{32}$$

where: A is the area per surfactant molecule.

The agreement between this relationship and experiment is not good, however, and various corrections[16] have been applied to account for the finite size of, and possible interactions between film molecules, leading to Schofield and Rideal[18] to propose an equation of the form:

$$\pi (A - A_0') = c' kT \tag{33}$$

where: A_0' is the incompressible area of the film upon the surface and $c' \approx 0.7$, typically.

For any molecule, the weight of evidence suggests that the average configuration in a gaseous monolayer is more nearly flat than vertically extended.

1.4.2.2. Expanded Monolayer:

The expanded monolayer is in a state between that of a gaseous and condensed film. The surface viscosity of expanded monolayers is low ($\approx 10^{-3}$ sp)[16], and the compressibility high ($\approx 10^{-1}$ m mN^{-1})[17]. The π-A diagram for expanded films show

considerable curvature, although they approach the π =0 axis at a fairly steep angle, more than for gaseous monolayer films. The molecular area is normally two or three times as large as the molecular cross section. Hence, at greater areas the tailgroups are too far apart to interact, whilst at smaller values their close proximity force the tailgroups into a regular, ordered arrangement, as in the condensed film. Balancing these contributions of the tailgroups interactions to the spreading pressure of the film leads to the equation:

$$(\pi - \pi_0)(A - A_0') = kT \qquad (34)$$

where: A_0' is the incompressible area of the headgroup and π_0 is the surface tension of the liquid hydrocarbon tail.

1.4.2.3. Condensed Monolayers:

In condensed monolayers, the molecules are nearly in their closest possible packing. The π-A curves for condensed films are nearly straight and very steep, showing low compressibility ($\approx 10^{-3}$ m mN^{-1})[17], and high surface viscosity ($\approx 10^{-2}$ sp)[16].
If the curve is extrapolated to the π =0 axis, then the area A_0 (known as the film's limiting area per molecule), at which the axis is cut, is typically the same order as the molecular cross-section of the film's headgroup.

1.4.3. Monolayer Stability:

When a monolayer is spread upon a subphase it may not be at equilibrium with its surroundings. Different processes like evaporation, dissolution, collapse, or fracture are all possible, producing film loss from the surface. These processes may occur in order to attain this equilibrium. These processes can determine whether the monolayer may be considered stable on the time-scale of the experiment. As π-A runs are repeated, unstable monolayer films will show continuing shifts to lower area per molecule values, which means that during each run significant film loss has occurred. (see Fig. 1.10).

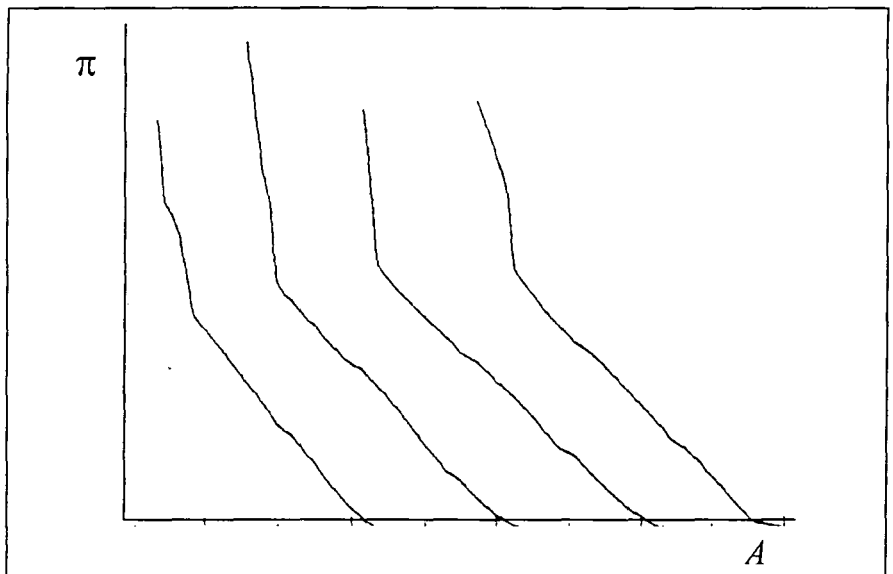

Fig.1.10. Unstable monolayer film

1.4.3.1. Evaporation:

Evaporation for long hydrocarbon chain (> C12) monolayers, will not normally be significant until temperature in excess of 40 °C are reached. At such temperatures, it is found[19] that the rate depends proportionally upon the surface pressure of the film.

1.4.3.2. Solution:

Film loss by dissolution typically occurs more than the other processes, especially for ionic films. There are two factors for the increased solubility of ionic films:

- the increased attraction of the headgroups to water, and
- the lowering of the system's free energy by removal of film molecules from a region of high electrical potential.

1.4.3.3. Collapse and Fracture:

The π-A curve displays a spike or plateau of maximum π, π_f, (see fig. 1.11), when the film has been over compressed and fractures. π_f, depends markedly upon the rate

of compression[20], and the fractured material is readily seen as a streak on the subphase surface, parallel to the advancing barrier.

If a film is compressed very slowly, film loss may occur at constant surface pressure due to the film collapsing[20] to form its stable bulk phase and the pressure at which it begins is known as the collapse pressure, π_c. π_e is the equilibrium spreading pressure[16]. π_e of a film is the pressure at which the monolayer is in equilibrium with this bulk phase.

When the film is compressed rapidly, there may be insufficient time for nucleation to occur and hence, surface pressures far greater than the collapse point may be obtained before the film finally fractures, i.e. $\pi_e << \pi_c << \pi_f$. For a film whose bulk phase is a liquid of low viscosity, however, collapse will always occur at $\pi \approx \pi_e$[16,20].

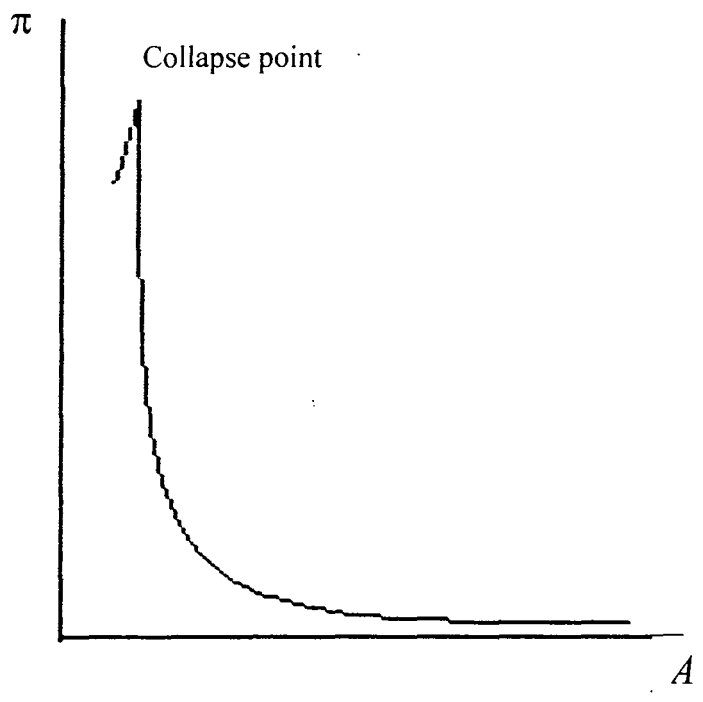

Fig 1.11. Π-*A* curve showing fracture pressure

1.4.4. Factors Determining Film Behaviour:

1.4.4.1. Solute:

The pressure applied may be insufficient to expel the solute, if the interaction between large solute molecules and the film is great enough, and for this reason the π-A curve will remain condensed, but will be shifted to larger area per molecule values when the attached solute is large[21], reflecting the presence of the stable film-solute complex at all surface pressures.

1.4.4.2. Impurities:

Impurities may affect the film's π-A curve[16] and also lead to hysteresis[22], if impurity is forced into solution at high surface pressures, whilst soluble impurities, especially divalent ions in even trace amounts, may adsorb onto the film and also change its properties greatly.

1.4.4.3. Vibration:

The importance of vibration-free troughs for producing monolayer experiments has been clearly proved. In particular, vibrations on inflexible monolayers held at pressure, π, where: $\pi_e < \pi_c < \pi_f$, will lead to an increased rate of film collapse and/or dissolution.

1.5. External Reflection FT-IR Spectroscopy:

In 1985, Dluhy[23] first showed that it was possible to perform external reflection FTIR upon a monolayer film at the air-water interface, and to observe peaks due to the film. External reflection, FT-IR at the air-water interface is now regarded[24] as a sensitive spectroscopic technique that can directly measures the molecular-level structure of the monolayer in *situ* at this interface. Subsequent studies and analysis[24-27] has shown that peaks due to groups vibrating parallel to the liquid surface dominate the spectra, due to the surface selection rules for external reflection off water.

CHAPTER 2

EXPERIMENTAL METHODS AND π-A ISTHERMS

2.1. Introduction:

Initial experiments in this work focused upon producing reproducible π-A curves for the film over pure water and saturated dl-aspartic acid, and then comparing these with the isotherms in the literature. The purpose of this chapter is, therefore, to demonstrate the appropriateness of both the equipment and materials to producing π-A curves and to the following study of nucleation beneath monolayer films.

2.2. Equipment:

All experiments regarding the monolayer film were performed on automated Langmuir troughs. The films were spread on dl-aspartic acid subphase surfaces in the PTFE trough between PTFE barriers. These barrier could then be moved under computer control, therefore changing the surface pressure, π, and area per molecule, A, of the films. The equipment used is shown in fig. 2.1. and its important items are as follows.

2.2.1. PTFE Langmuir Trough and Barriers:

Two troughs were used in this project; the first one was used for the initial experiments, to study the π-A curves and the ability of the films to crystallise dl-aspartic acid. It had dimensions of $\approx$30x 20x 0.5cm^3, so contained $\approx$ 400cm^3 of solution when filled with a meniscus. It was too big to be attached to an optical microscope for studying the crystals growth and shape *in situ*, so for this I used the smaller trough. This trough had dimensions $\approx$15x 7x 0.5cm^3, so it contained$\approx$90cm^3 of solution when filled. Both troughs were covered with plastic sheets to reduce the possibility of any impurity entering the system.

(a)

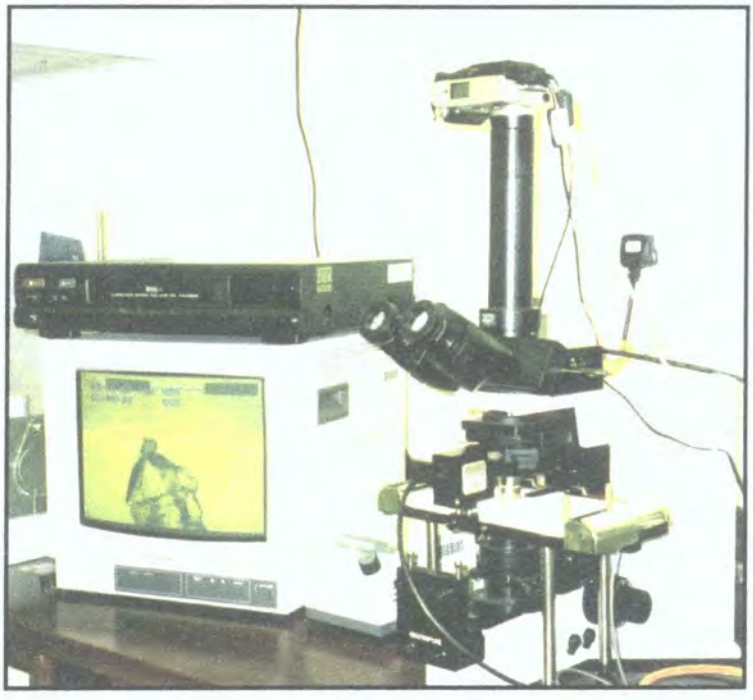

(b)

Fig. 2.1 photograph of a) large trough, and b) small trough.

2.2.2. Wilhelmy Plate Balance:

The Wilhelmy plate measured the surface pressure of the film and was made of either a piece of filter paper or thin platinum strip of set width (1 cm). The plate was dipped into the trough solution and was connected, via a light metal hook, to a microbalance. If it is assumed that the contact angle, θ, between the Wilhelmy plate and the liquid phase in the trough is zero, i.e. complete wetting of the plate occurs, then it is possible to relate the weight measured on the microbalance to the surface pressure, π.

2.2.3. Evaporation from the Troughs:

During the ~20 hr nucleation experiments, water evaporation from the trough solution occurred which increased the dl-aspartic acid supersaturation, and eventually caused the Wilhelmy plate to come out of the solution. This was a particular problem for the small trough, where up to 30% of the solution could be lost over 20 hours. This problem was greatly reduced by placing large dishes filled with hot water under the plastic sheets covering the trough.

2.3. Ensuring a Contamination Free Environment:

The quantity of film used in monolayer experiments is very small. << 1 mole are being measured, and so serious effects may occur if any impurities are in the system. For this reason, great care was taken to ensure that the trough and barriers were clean and the entire chemicals used were as pure as possible.

2.3.1. Trough Cleaning Procedure:

Before every monolayer experiment, the PTFE trough and barrier were cleaned using the following procedure.

1. Before starting with the cleaning procedure, disposable powder free plastic gloves were used to prevent any grease impurity from the hand entering the trough.
2. De-ionised ultra pure Milli-Q water was used to rinse both the trough and barriers.
3. The trough and barriers were both cleaned, using a special surfactant-free tissue soaked in chloroform.
4. The last step was to re-rinse both the trough and barrier using Milli-Q water.

Only after following the above four steps, were both the trough and barriers ready to use.

2.3.2. Wilhelmy Plate Cleaning:

When a piece of filter paper was used as a Wilhelmy plate, a fresh plate was used for every new experiment. When the Wilhelmy plate was made of a thin platinum strip, the platinum plate was dipped into hydrochloric acid solution and then flamed at the beginning of each experiment to clean it.

2.3.3. Purity of Chemicals Used:

The dl-aspartic acid was bought in its purest available form, 99%, from Sigma. Both in preparing the dl-aspartic acid solution and in the π-A runs, ultra pure Milli-Q water was used which had a resistivity of 18 MΩcm. The chloroform used to spread each film material was a 99.9% HPLC grade which was bought from Aldrich.

2.3.4. Criteria for a Clean Subphase Surface:

Before spreading any of the film upon the subphase solution, the surface was checked for any impurities by following this procedure.

1. The barriers were at their maximum area position, when the subphase was placed in the trough.
2. The surface pressure of the subphase was taken to be zero.
3. The surface pressure of the subphase was checked after the barriers were compressed to the minimum area.
4. If the surface pressure was higher than zero, the subphase surface was cleaned by using a clean pipette attached to a water pump. This procedure was repeated until a clean surface was obtained.

2.4. Film Spreading:

The solvent will be suitable for spreading film material under these conditions.

- It should be immiscible with the aqueous subphase and there must be no finite angle, θ, between the solvent and the subphase solution.
- To allow the uniform deposition of monolayer film, the solvent should spread quickly across the aqueous solution.
- It should evaporate rapidly and completely.

Because of these factors, ultra-pure chloroform was chosen as a suitable spreading solvent. Therefore, all the film solutions were made up as $\approx 1 \times 10^{-3}$ M solution of the film material in chloroform. But the nylon 6 6 was issufficiently soluble in chloroform alone and so its spreading solution also contained ≈ 70% trifluoroacetic acid (TFA). Since trifluoroacetic acid is a very strong acid, an alternative spreading solution containing 3:1 toluene: phenol was also used in later experiments. In this spreading solvent, the phenol will not evaporate like the toluene, but will dissolve in the subphase,

however the tiny quantity involved ~0.01% of the total trough solution, will not have a significant effect on the subsequent dl-aspartic acid crystallisation.

2.5. Experimental Details:

2.5.1. Preparation of Supersaturated Solutions:

The first step was to add the appropriate amount of dl-aspartic acid subphase material to 500 cm^3 of Milli-Q water. The mixture was then heated until all the crystalline material had dissolved. Next, using the heated filtering apparatus shown in figure 2.3 the solution was filtered. This step was conducted under normal atmospheric pressure, since raising the pressure beyond the normal pressure usually caused the 0.22μm filters that were used to tear. The reason behind using such fine filters was to eliminate the dust particles in the solution. This was then followed by filtering the solution into a conical flask, which was heated on a hot plate. The next step was to cover the solution and maintain it at a temperature of at least 10^0 C above its saturation temperature for two hours. Therefore, any microscopic crystal nuclei that could have passed through the filter were dissolved. Finally, the solution was left overnight. If the solution contained crystals the next day, it was not used; this happened only rarely. Otherwise, the majority of the solution was poured into a clean PTFE trough and a film was then spread upon it. The remainder of the solution was used as a control to check that no crystals nucleated in it during the course of the monolayer experiments.

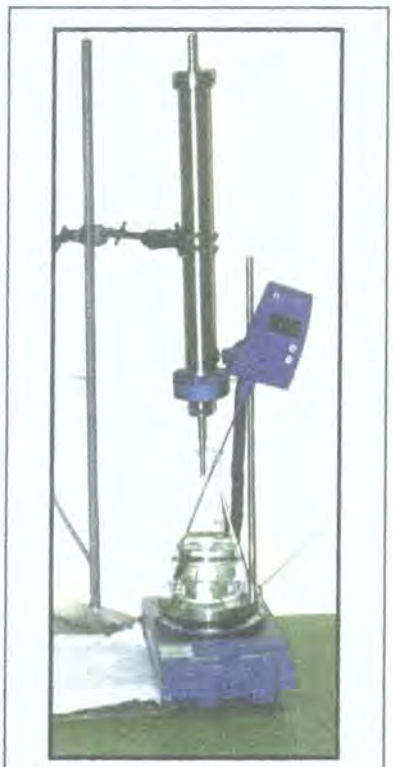

Fig. 2.3. filtering apparatus.

2.5.2. Nucleation Experiments:

The film was added drop-wise to a clean subphase surface using a micro syringe, which can measure 1μl quantities of the film solution. The distance between the needle and the subphase surface was kept as small as possible without touching the subphase surface to avoid any film solution sinking to the trough bottom. The solvent was allowed to evaporate between every addition by waiting 10 seconds before the next drop was added. After spreading the film, the solvent was allowed to evaporate by waiting 1 min. before the initial surface pressure reading was taken. Then the barriers were moved so as to compress the film. The barriers were stopped at the required surface pressure. The Nima isotherm program then recorded the pressure/area of the subphase every 10 min, for the 20-24 hour long experiments.

2.5.3. Removal of Surface Crystals:

The crystals that I got on the surface for all experiments were quite small (< 1 mm in length), and therefore it was not easy to remove the crystals from the surface, unless I used strips of filter paper to make it easier. The filter paper strip was dipped into the solution close to the surface and picked up as quickly as possible, so that the filter paper soaked the solution and the crystals then stick on the edge of the strip.

2.5.4. Analytical Techniques:

2.5.4.1. Optical Microscopy:

The small trough used for the nucleation experiments was fitted with an optical microscope, which was attached to a digital camera and connected to TV screen. This system allowed pictures of the solution surface to be taken whilst the crystal were still growing. The microscope and the digital camera zoom viewed the crystals on the surface with magnifications of x100 and x500. Photographs were taken to illustrate the typical crystal density and morphologies found for each experiment. The large trough was attached to a digital video camera and connected to a TV screen and video recorder. This video camera was not very helpful in recording the crystals growing, because the crystals were very tiny (<< 1 mm).

2.5.4.2. FTIR Spectroscopy:

A very tiny trough was fixed to the FTIR spectrometer with dimensions 9.5x 2.2x 0.5 cm^3. This allowed external reflection FTIR spectra to be taken of the subphase surface throughout the monolayer nucleation experiments. The spectra were taken to study the nucleation of dl-aspartic acid under each film material. These spectra were compared with spectra taken for all the films on pure water.

Fig. 2.4. FTIR spectrometer with tiny trough.

2.6. π-A Curve Results:

This results section shows the π-A curves of each of the seven films used in the nucleation experiments with pure water and with saturated dl-aspartic acid. These results are compared with literature π-A curves. However, it was not easy to get results exactly the same as the literature results, because of different conditions such as the surrounding temperature[16].

2.6.1. π-A Curves of Stearic Acid over Pure Water and dl-Aspartic Acid Subphases:

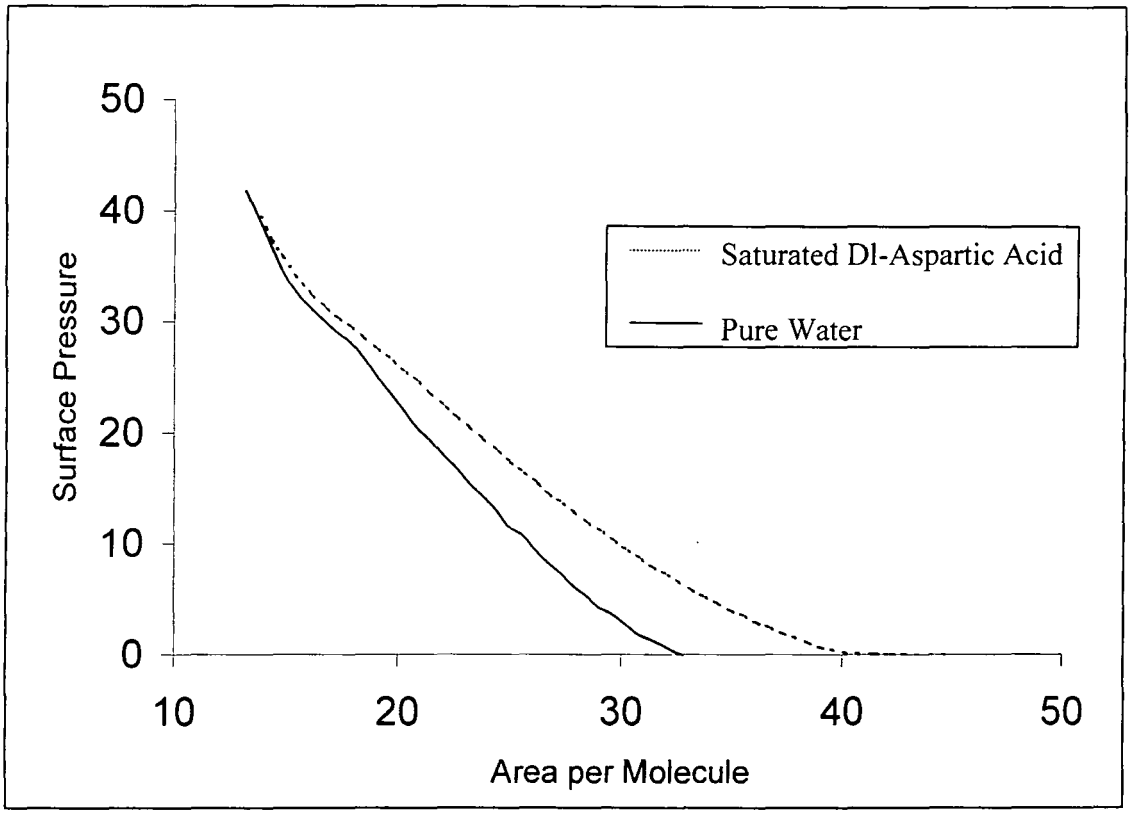

The π-A curve of stearic acid over pure water and saturated dl-aspartic shows that at π =0, the area per molecule of the film over water is ~32 and over dl-aspartic is ~39 $Å^2$. At high surface pressures the limiting area per molecule of ~20 $Å^2$ over pure water is obtained. The same result is obtained over saturated dl-aspartic acid. The curve is expanded over dl-aspartic acid solution at low pressures due to adsorption of dl-aspartic zwitterions between the film molecules[8]. The limiting area per molecule reported in the literature[28,29] is ~21 $Å^2$.

2.6.2. π-A Curves of Methyl Stearate over Pure Water and Dl-Aspartic Acid Subphases:

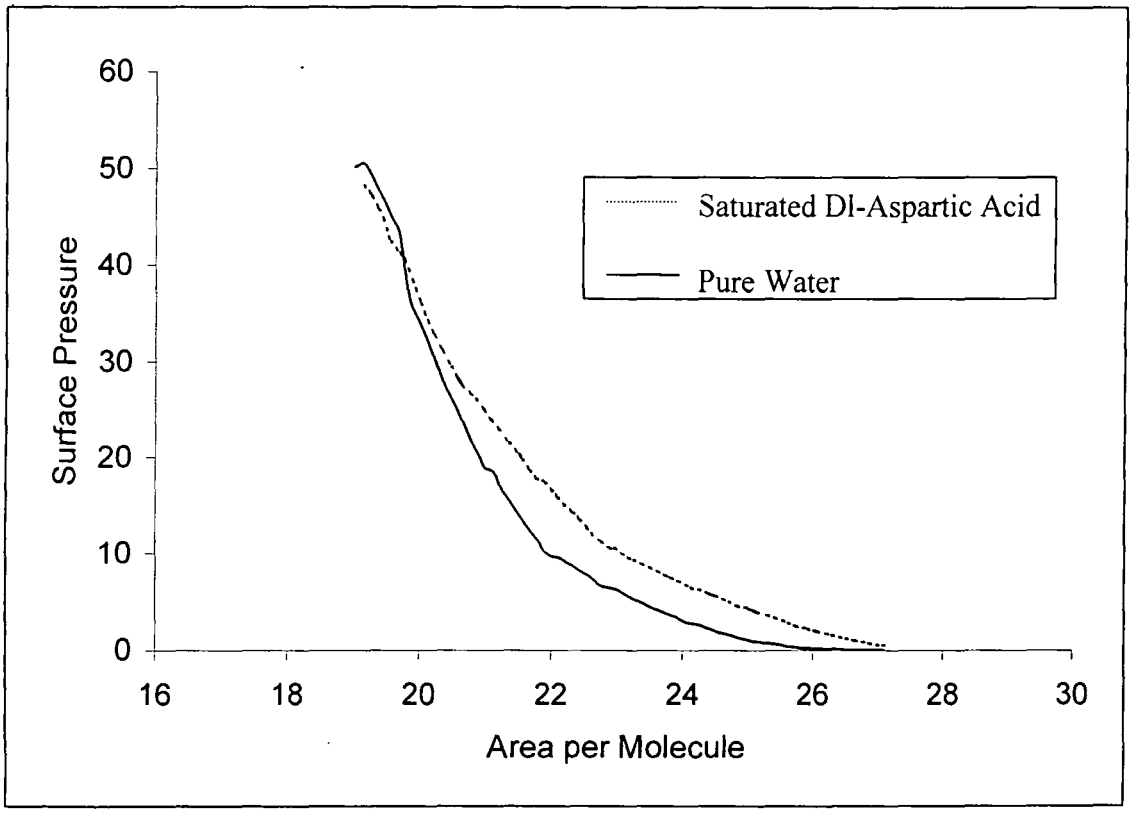

The π-A curves of methyl stearate over pure water and saturated dl-aspartic shows that the curve over dl-aspartic acid solution is more expanded, due to dl-aspartic aid adsorption between the film molecules. The limiting area per molecule for both is almost the same at ~22 $Å^2$, compared with the literature[30] value of ~20 $Å^2$.

2.6.3. π-A Curves of L-tyrosine-O-Octadeylcarbonyl Hydrochloride Methyl Ester over Pure Water and Dl-Aspartic Acid Subphases:

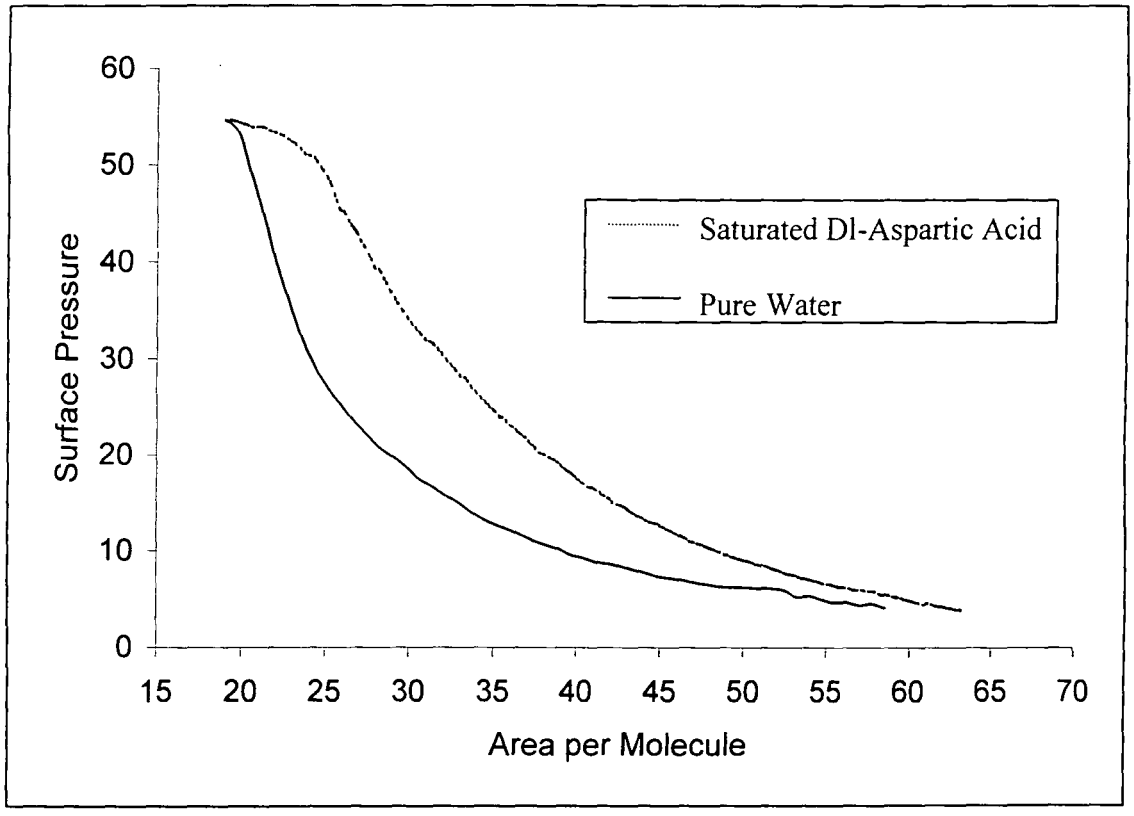

The π-A curves of l-tyrosine over pure water shows that the limiting area per molecule of the film is ~30 $Å^2$, the same as that reported in the literature[31,32]. Over dl-aspartic acid A_o~40 $Å^2$. The pressure of collapse for both is the same at ~55 mN/m. In this figure the curve over dl-aspartic acid solution is again more expanded, because of the adsorption of the acid zwitterions between the film molecules.

2.6.4. π-A Curves of Polycaprolactone over Pure Water and Dl-Aspartic Acid Subphases:

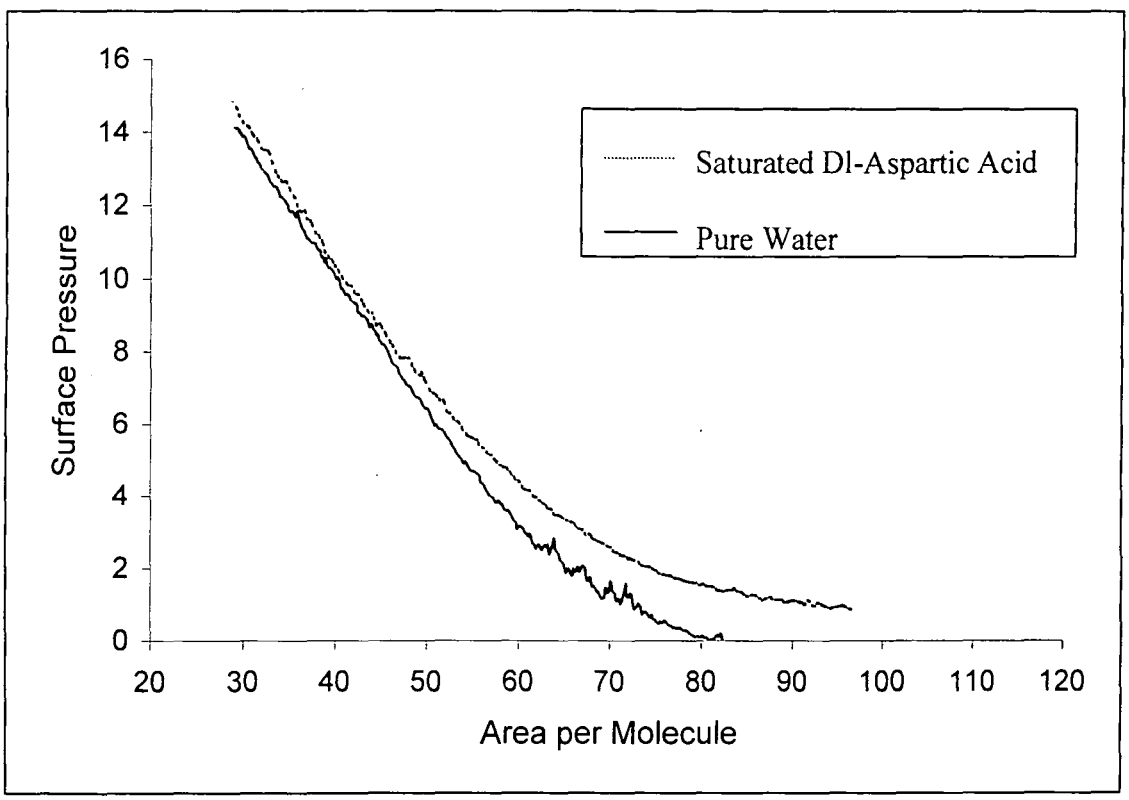

The π-A curve of polycaprolactone over pure water and saturated dl-aspartic shows that the limiting area per molecule for both are almost the same at ~65 $Å^2$. Again, adsorption of dl-aspartic acid between the film molecules causes the curve to be more expanded over dl-aspartic acid solution. The literature[33] value is 60 $Å^2$ for A_o.

2.6.5. π-A Curves of Poly-L-Isoleucine over Pure Water and Dl-Aspartic Acid Subphases:

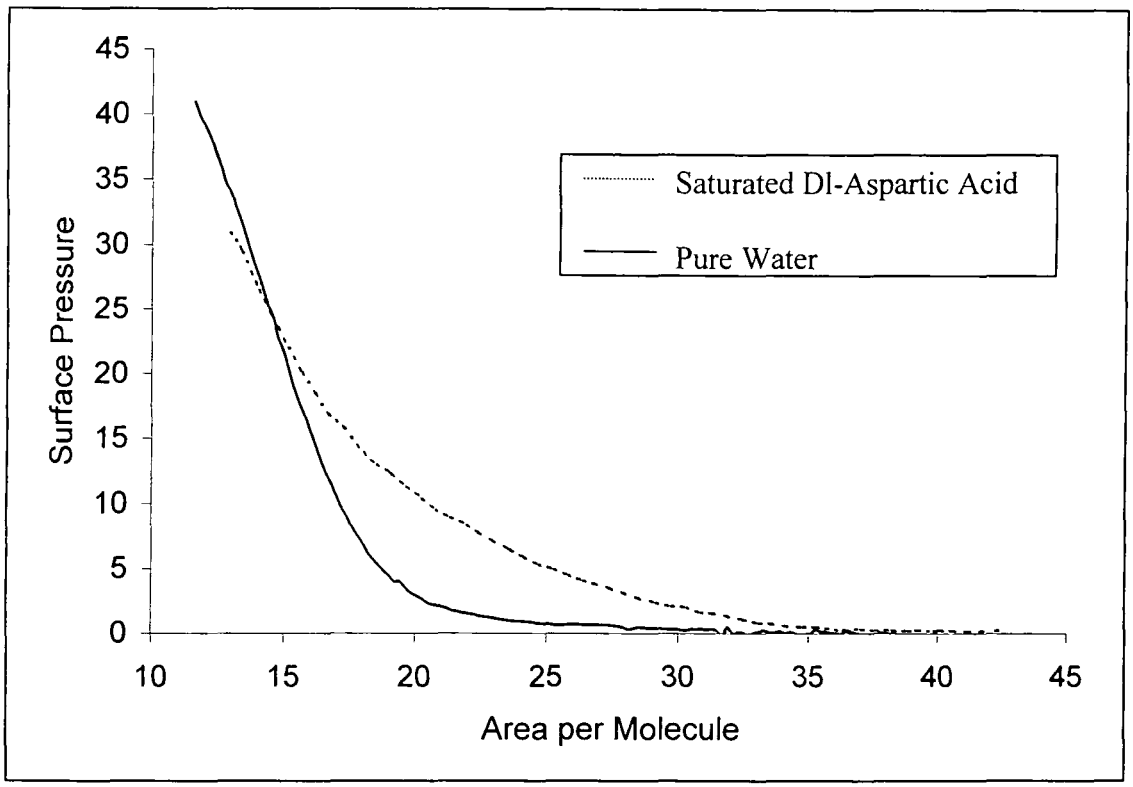

The π-A curves of poly-l-isoleucine over pure water and saturated dl-aspartic shows, that the curve is more expanded over dl-aspartic acid solution than over water, due to the adsorption of the acid between the film molecules. The limiting area per molecule for both is almost the same at ~19 $Å^2$. (No literature value could be found for this film.)

2.6.6. π-A Curves of Poly-γ-Benzyl-L-Glutamate over Pure Water and Dl-Aspartic Acid Subphases:

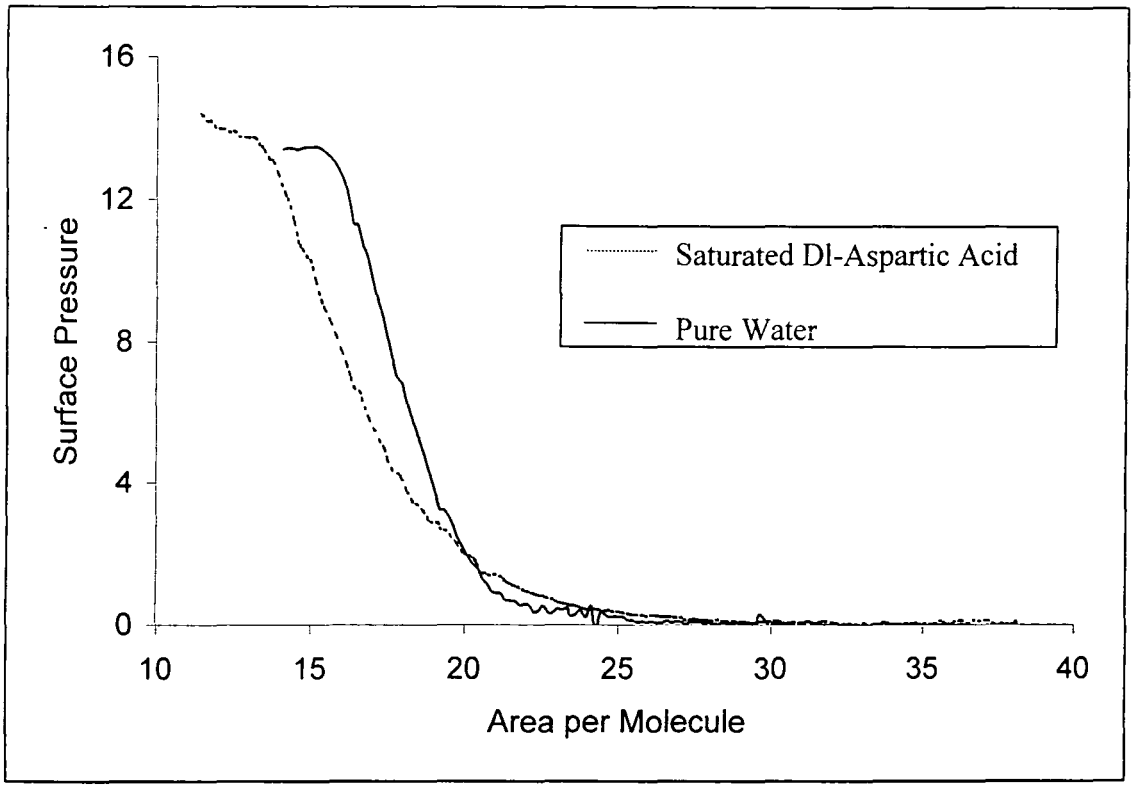

The π-A curve of poly-γ-benzyl-l-glutamate over pure water and saturated dl-aspartic shows that the area per molecule for both at π =0 is 30 $Å^2$. The limiting area A_o, is ~21 $Å^2$ over pure water and ~19 $Å^2$ over the acid. These values can be compared with the literature[34] value of~20 $Å^2$. The collapse pressures are ~14mN/m.

2.6.7. π-A Curves of Nylon 6 6 over Pure Water and Dl-Aspartic Acid Subphases:

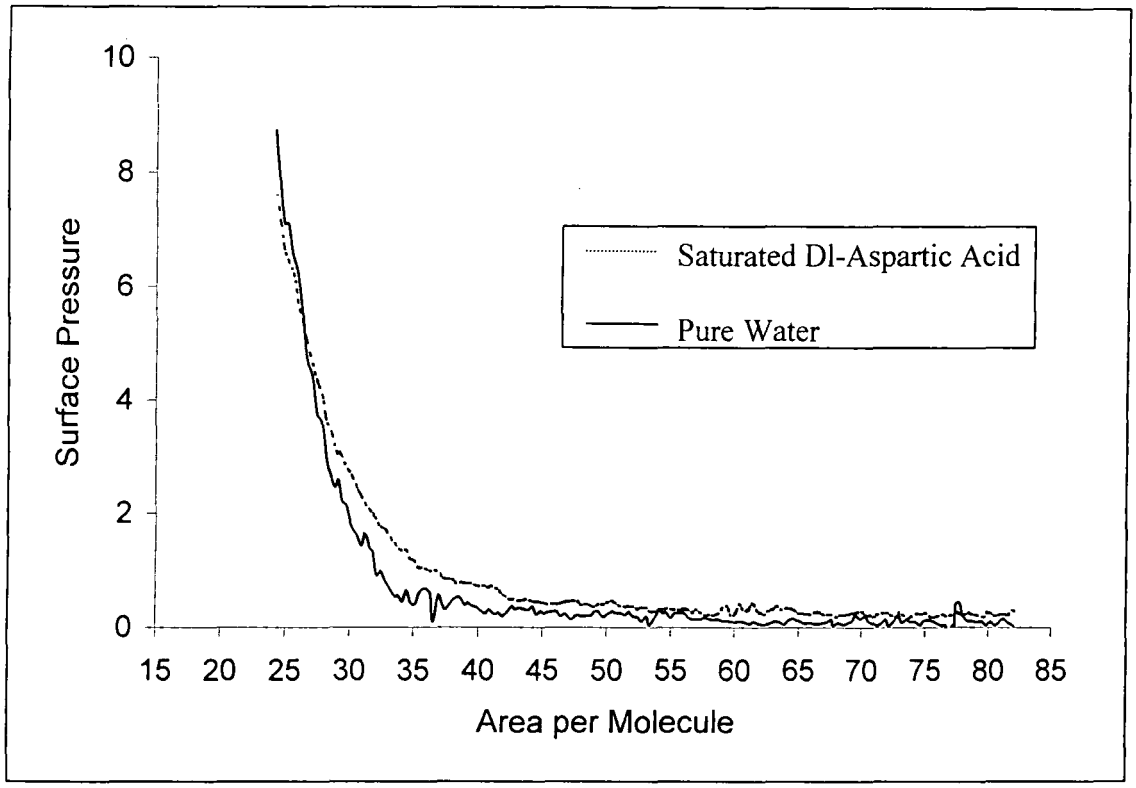

The π-A curve of nylon 6 6 over pure water and saturated dl-aspartic shows a limiting area per molecule, A_o, of ~30 $Å^2$. The value in the literature[35] is~35 $Å^2$. The adsorption of dl-aspartic acid between the film molecules caused the curve to be slightly more expanded than over pure water as seen in this figure.

CHAPTER 3

RESULTS AND DISCUSSION OF THE NUCLEATION EXPERIMENTS

3.1. Introduction:

This chapter shows the results of the nucleation experiments of dl-aspartic acid ($NH_3^+ - CH(CH_2CO_2H) - CO_2^-$). Over 110 experiments were used for studying the crystallisation of dl- aspartic acid and seven monolayer films were used upon different degrees of supersaturated dl-aspartic acid solutions.

The solubility data for dl-aspartic acid[36] are shown in table 3.1 and fig 3.1. From these the percentage supersaturation, α%, of the system may be determined, using:

$$\alpha\% = \frac{S - S_{sat}}{S_{sat}} \times 100\% \qquad (35)$$

where: s is the amount dissolved in solution (see table 3.2) and s_{sat} is the amount dissolved in saturated solution.

Temperatures (^{o} C)	0	10	20	30	40	50	60
Weight of Dl-aspartic acid dissolved in water (g/kg)	2.62	4.12	6.33	9.50	14.0	20.0	28.0

Table 3.1

Table 3.2 shows the range of percentage supersaturations, α %, used for temperature changes in the laboratory between 20 - 25^o C. The required mass of dl-aspartic acid dissolved in 500g of pure water to produce these supersaturations is also shown. The supersaturations given in the subsequent sections refer to a temperature of 20^o C.

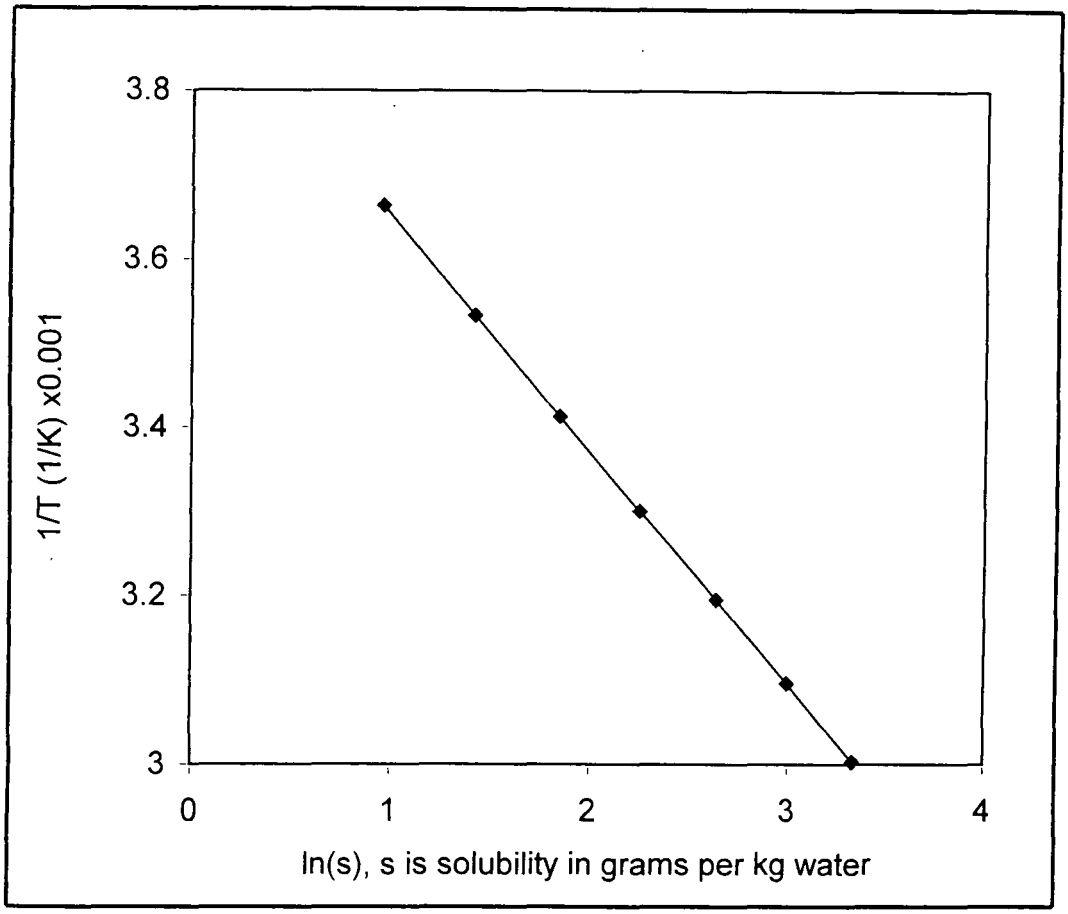

Fig. 3.1. Solubility graph for dl-aspartic acid crystals.

Percentage Supersaturation (α %)		Weight of Dl-aspartic Acid Dissolved in 500g of Water
At 20 ^{0}C	At 25 ^{0}C	
150%	105%	7.91g
120%	80%	6.96g
100%	64%	6.33g
90%	56%	6.01g
80%	47.5%	5.70g
75%	43%	5.54g
70%	39%	5.38g
60%	31%	5.06g
50%	23%	4.75g
40%	15%	4.43g
30%	6%	4.11g

Table 3.2

3.2. The Monolayer Films Used:

The monolayer films used were:

1. Stearic acid,

$$CH_3(CH_2)_{16}CO_2H$$

2. Methyl stearate,

$$CH_3(CH_2)_{16}CO_2CH_3$$

3. O-Octadeyl carbonyl-l-tyrosine methyl ester hydrochloride denoted the l-tyrosine for short.

$$CH_3-(CH_2)_{17}-NH-CO_2-C_6H_4-CH_2-\underset{\displaystyle CO_2CH_3}{\underset{|}{CH}}-NH_3^+Cl^-$$

4. Polycaprolactone, molecular weight=2000

$$[-CO(CH_2)_5O-]_n$$

5. Poly-l-isoleucine, molecular weight=8500

$$[\text{-NH-}\underset{\displaystyle (CH_2)_2CO_2CH_2C_6H_5}{\underset{|}{CH}}\text{-CO-}]_n$$

6. Poly-γ-benzyl-l-Glutamate, molecular weight=22000

$$[\text{-NH-}\underset{\displaystyle CH(CH_3)\text{-}CH_2\text{-}CH_3}{\underset{|}{CH}}\text{-CO-}]_n$$

7. Nylon 6 6, obtained from Aldrich did not have quoted molecular weight, but had a relative viscosity of 230 to 280 is a high viscosity grade, and so the molecular weight is much larger than 10,000.

$$[-NH(CH_2)_6NH-CO(CH_2)_4CO-]_n$$

These particular film materials were chosen, because we want to compare between small molecule and polymeric film behaviour. These film materials were also readily available without the need for any synthesis.

3.3. Nucleation Experiments:

Initial experiments were performed to choose the best degree of supersaturation for crystallising dl-aspartic acid. Experiments were started with 90% of saturated dl-aspartic acid; the results were not very good, because the crystals growing beneath the films were typically very few and too small. The second step of the project was to increase the supersaturation of the solution up to 150%. The quantity and the size of crystals were not bad, but at this high supersaturation there were crystals outside the barriers and a lot of them in the bottom of the trough. The next step was to decrease the supersaturation to 120%; the results were best for all of the films. Finally, to determine the lowest possible supersaturation, which still produced crystallisation, we used supersaturation levels of 100%, 80%, 75%, 70%, 60%, 50%, 40%, and 30%.

It was not possible to count the total number of crystals nucleating beneath the films, because may of the crystals were too small ($\wedge$ 0.1 mm) to be seen easily by eye. Instead the singe range of the crystals observed in the optical microscope, and the relative quantity of crystals seen by eye or quoted in the nucleation experiments.

3.4. The Effects of Film Surface Pressure upon Crystallisation:

In this section, I will discus the effect of compression surface pressure in the crystallisation process for each monolayer film; also, I will discus the quantities and the sizes of the crystals that grow between the barriers. Sometimes there were crystals grown outside the barriers. Since the left over, "control" supersaturated solution contained no crystals, it was unlikely that pre-existing nuclei were present in the trough solution before the films were added. Hence crystals outside the barriers probably occurred because of one of two reasons.

1) Film molecules had dissolved into the subphase solution and then reappeared at the surface outside the barriers. These film molecules then caused nucleation. This process tended to happen particularly when the film were compressed to high surface pressures, as was evident from the subsequent relatively large drop in surface pressure that occurred with time (see the stearic acid section), or
2) dust or impurities causing the crystallisation. The latter was more likely at high supersaturations. However, the number of crystals outside the barriers was always far less than those inside.

In the following tables, under the initial supersaturation and surface pressure condition, the small trough data typically gave a slightly higher crystallisation rate. This was because of the greater water evaporation that occurred in the small trough, which raised the supersaturation of the solution. The analysis has been made in terms of the compression surface pressure. However it should be remembered that nucleation will typically occur hours after the film has been spread (see FTIR data in chapter 4). Hence, the nucleation surface pressure will be less than the compression surface pressure, particularly for films compressed to high surface pressure, where film dissolution tended to occur. This is why I also provide in the subsequent tables the value of the surface pressure at the latest time of which the Wilhelmy plate was still in the solution.

Seven different monolayer films were used to find the best catalyst to nucleate dl-aspartic acid. Two different troughs were used as detailed in chapter 2; a large trough was used for studying the ability of the films to nucleate the dl-aspartic acid and a small trough was very helpful to study the crystals growing and their morphology because it was attached to a microscope and digital camera.

3.4.1. Stearic Acid:

Table 3.4 for the large trough data shows the effect of surface pressure on dl-aspartic acid nucleation beneath stearic acid on supersaturated solutions of 120%, 100% and 80%, respectively. The results using 120% supersaturated solution of dl-aspartic acid show that when a medium compression pressure was used eg. 16.4mN/m in exp. no.2, quite a few crystals with average length 0.47mm were obtained. In exp. no. 1 a high compression pressure of 33.5mN/m was used and this gives crystals with average length 0.6mm but less crystals than for exp. no. 2. In exp. no. 3 a low pressure of 9mN/m was used; the results were a few very tiny crystals. These results together with those using the 100% supersaturated solution show that a medium pressure is the best for nucleating the crystals. For example, in exps. no. 6-8 compression surface pressure of 18.5mN/m-21.3mN/m were used, which give the best results of lots of large crystals compared with the other experiments in this table using 100% supersaturated dl-aspartic acid. At high compression pressures, i.e. 31.5mN/m as in exp. no.4 lots of crystals were produced but less than exps. no. 6-8, and some crystals outside the barriers were also observed. These probably occurred due to crystallisation under film molecules that had dissolved in the solution, and then resurfaced outside the barriers, as

is evident from the relatively large surface pressure drop initially observed in this system, see fig 3.4 in table 3.3. At a low compression surface pressure of 10mN/m as in exp. no. 9, the crystals were very tiny difficult to see by eye. In 80% saturated solution system the stearic acid film was not effective at nucleating dl-aspartic acid. Hence these experiments show that the compression surface pressure in the range ~16mN/m-30mN/m were best at nucleating dl-aspartic acid.

Table 3.5 shows the small trough data. In exp. no. 11, at 120% supersaturated solution, and a surface pressure of 16mN/m, the result was a few small crystals with length ~0.1mm-0.2mm, see fig. 3.4a. In exp. no. 12, the supersaturation was 100%, and a surface pressure of 16.8mN/m was used. As expected, the result was less crystals than in exp. no. 11 and they were smaller with length 0.02mm-0.04mm, see fig. 3.4b.

3.4.2. Methyl Stearate:

Table 3.6 for the large trough data shows the effect of surface pressure on dl-aspartic acid nucleation beneath methyl stearate on supersaturated solutions of 150%, 120%, 100%, 90% and 80%, respectively. The result using compression pressures around 20mN/m is the best to give lots of crystals as in exp. no. 3. In this experiment, a surface compression pressure of 22mN/m was used under 120% supersaturated solution and this gave lots of large crystals with average length 0.67mm. Also in exp. no. 10 a compression surface pressure of 21.8mN/m was used under 100% supersaturated solution and this also give lots of crystals with average length 0.40mm. Using low pressures as in exp. no. 4, 5, 6 and 8, gives a few tiny crystals except for exp. no. 7, which gave a lot of tiny crystals at a low pressure of 7.5mN/m. This results may have been because of abnormally high water evaporation from the solution. The film was powerful at nucleating dl-aspartic acid in 120% supersaturated solution and at compression surface pressures around 20mN/m; the film was less effective in 150%, 100% and 90% supersaturated systems and not effective in 80% supersaturated solution. At compression pressures higher than 25mN/m, nucleation started outside the barriers, due to film dissolution.

Table 3.7 shows the small trough data. In exp. no. 14, the supersaturation was 120%, the surface pressure was 17.1mN/m and the result was many small crystals, with average length 0.1mm-0.2mm, see fig.3.5.

	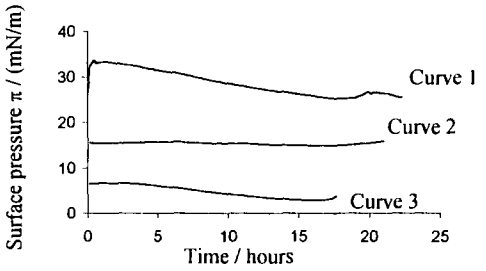			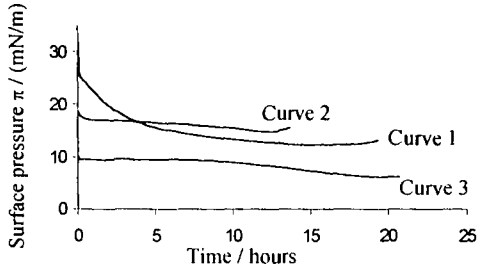		
Figures	Figure 3.2			Figure 3.3		
Supersaturation of dl-aspartic acid	120%			100%		
Curves no.	1	2	3	1	2	3
Compression surface pressure (mN/m)	33.5	16.4	9	31.5	18.8	10
Relative quantities of crystals observed	**	***	*	**	***	*
Crystals observed outside the barriers	no	no	no	yes	no	no

Table 3.3

*** meant lots of crystals on the surface of the solution (most)
** meant less crystals on the surface of the solution (many)
* meant fewer crystals on the surface of the solution (least)

Tables (3.4) and (3.5): Results of nucleation experiments under stearic acid monolayer film in different conditions:

Large trough data:

Experiments. No.	*Degree of super-saturation*	*Compressing Pressure (mN/m)*	*Final Pressure (mN/m) at given time*	*Note*
1	120%	33.5	26.3at 19.7hrs	Some tiny crystals with average length 0.6mm.
2	120%	16.4	14.96 at 16.3hrs	More crystals than in exp. no.1 but the crystals were smaller with average length 0.47mm.
3	120%	9	2.86 at 16hrs	Fewer crystals than exp. no.1 & 2 and the crystals were smaller.
4	100%	31.5	12.2 at 15hrs	Some tiny crystals but less than in exp. no.7 / out*.
5	100%	27	9.44 at 24hrs	Many crystals but less than in exp. no.6 & 7 / few out**.
6	100%	21.3	15.6 at 15hrs	Same as exp. no.7 results / few out**.
7	100%	18.5	14.75 at 12.7hrs	Quite a few crystals between the barriers with average length 0.6mm / out*.
8	100%	18.5	13.44 at 19.5hrs	Quite a few crystals but smaller than in exp. No.7.
9	100%	10	6.16 at 20.7 hrs	Very tiny crystals, difficult to see by eye / out*.
10	80%	30.6	15.28 at 16.7hrs	No crystal.

Table 3.4

* out means crystals also observed outside the barrier, but always less than inside.

** few out means only a few crystals observed outside the barriers.

Computer software failure prevented the measurement of subsequent π values.

Small trough:

Experiment No.	*Degree of super-saturation*	*Compressing Pressure (mN/m)*	*Final Pressure (mN/m) at given time*	*Note*
11	120%	16	1.2 at 17hrs	Quite a few tiny crystals, see fig.3.4a.
12	100%	16.8	4.3 at 16hrs	Quite a few tiny crystals but less than in exp. no. 11, see fig.3.4b.

Table 3.5

Tables (3.6) and (3.7): Results of nucleation experiments under methyl stearate monolayer film in different conditions:

Large trough data:

Experiment No.	*Degree of super-saturation*	*Compressing Pressure (mN/m)*	*Final Pressure (mN/m) at given time*	*Note*
1	150%	33	#	A few tiny crystals / out*.
2	150%	20	#	A few tiny crystals.
3	120%	22	10.49 at 7.3hrs	More crystals than exp. no.8 but smaller with average length 0.67mm.
4	120%	8.6	#	Less crystals and smaller than exp. no.3 with average length 0.47mm / few out**.
5	120%	8.4	#	A few tiny crystals.
6	120%	8.3	6.6 at 1.7hrs	A few tiny crystals.
7	120%	7.5	7.25 at 2hrs	Lots of tiny crystals / high water evaporation
8	120%	1.3		A few crystals with average length 0.85mm.
9	100%	29.4	0.04 at 21.7hrs	Less crystals than in exp. no. 10 &11 / one little crystal out.
10	100%	21.8	0.952 at 14.5hrs	More crystals than in exp. no. 11 with average length 0.40mm.
11	100%	8.8	0 at 14.8hrs	Lots of small crystals.
12	90%	20	#	Very tiny crystals / out*.
13	80%	12.7	3.13 at 21.7hrs	No crystals at all.

Table 3.6

* out means crystals also observed outside the barrier, but always less than inside.

** few out means only a few crystals observed outside the barriers.

Computer software failure prevented the measurement of subsequent π values.

Small trough data:

Experiment No.	*Degree of super-saturation*	*Compressing Pressure (mN/m)*	*Pressure (mN/m) at given time*	*Note*
14	120%	17.1	3.6 at 10hrs	Lots of small crystals, see fig.3.5a, b, c, d, e and f.

Table 3.7

3.4.3. l-tyrosine:

Table 3.8 for the large trough data shows the effect of surface pressure on dl-aspartic acid nucleation beneath l-tyrosine at supersaturation of 150%, 120%, 100% and 80%, respectively. At 150% supersaturation using a compression surface pressure of 8 mN/m, the result was a few crystals with average length 0.50 mm and some crystals outside the barriers also observed; this may be because of the high supersaturation of the solution. At 120%, the result of exp. no. 5 was very good with the film under a compression surface pressure of 12mN/m and many crystals produced with average length 0.66mm. When high surface pressures were used eg. 25mN/m in exp. no. 3, fewer smaller crystals were observed inside the barriers and some crystals outside the barriers were also observed. In exp. no.6 the surface pressure was 6mN/m, and there were less crystals than in exp. no. 5. The crystals were also smaller with average length 0.55mm, however the crystals were larger than the crystals observed in exp. no. 3 in which the compression surface pressure was 25mN/m. Hence these experiments suggest that medium compression surface pressures were best for nucleating dl-aspartic acid.

In experiments using 100% supersaturated solution at a compression surface pressure of 19mN/m as in exp. no. 9, the result was lots of small crystals inside the barriers and there were a few crystals outside the barriers that may have occurred because of dust or impurity. At a high compression pressure of 32.3mN/m as in exp. no. 8, the result was lots of small crystals but less than in exp. no. 9, which used a surface pressure of 19mN/m. Using low surface pressure as in exp. no. 10, the result was a few small crystals inside the barriers and also some outside which may have crystallised on dust or impurity. Hence medium surface pressures in the range ~12mN/m – 25mN/m were best for nucleating dl-aspartic acid.

Table 3.9 shows the small trough data. In exp. no. 12, the supersaturation solution was 120%, and a compression surface pressure was used of 13.7mN/m. The result was many small crystals with average length 0.2mm-0.3mm, see fig.3.6.

Tables (3.8) and (3.9): Results of nucleation experiments under l-tyrosine monolayer film in different conditions:

Large trough data:

Experiment No.	*Degree of super-saturation*	*Compressing Pressure (mN/m)*	*Pressure (mN/m) at given time*	*Note*
1	150%	8	#	A few crystals with average length 0.50mm / out*.
2	120%	25	#	Lots of crystals but less than in exp. no.1 / out*.
3	120%	25	17.8 at 20.8	Lots of small crystals.
4	120%	12.5	8.6 at 23.6hrs	More crystals than in exp. no.1 & 2 / high evaporation.
5	120%	12	0 at 8.6hrs	More crystals than in exp. no. 2 & 4 with average length 0.66mm.
6	120%	6	0 at 11.3hrs	Few crystals but larger than in exp. no. 3 with average length 0.55mm.
7	120%	3.2	#	Few crystals & small with average length 0.40mm.
8	100%	32.3	16.98 at 20.5hrs	Lots of small crystal but less than exp. no.9 / out*.
9	100%	19	6.62 at 15.3hrs	Lots of small crystals / few out**.
10	100%	6.9	#	A few small crystals / out*.
11	80%	12	7.65 at 18hrs	No crystals at all.

Table 3.7

* out means crystals also observed outside the barrier, but always less than inside.

** few out means only a few crystals observed outside the barriers.

Computer software failure prevented the measurement of subsequent π values.

Small trough data:

Experiment No.	*Degree of super-saturation*	*Compressing Pressure (mN/m)*	*Pressure (mN/m) at given time*	*Note*
12	120%	13.7	#	Many small crystals, see fig. 3.6a, b, c, d, e and f.

Table 3.9

3.4.4. Polycaprolactone:

Table 3.10 for the large trough data shows the effect of medium compression surface pressures on dl-aspartic acid nucleation beneath polycaprolactone at supersaturations of 150%, 120%, 100%, 90% and 80%. Time constraints prevented further experiments at higher or lower surface pressure, so experiments were concentrated on the medium surface pressure range, because the previous films studied suggested these pressures were optimum for 14.4mN/m – 16mN/m was used and in all cases, a few crystals nucleated between the barriers, typically growing in groups or lines and many crystals nucleated on the trough base. At 120% supersaturation, fewer crystals were observed on the base, and many crystals nucleated between the barriers for medium compression pressures, see exps no. 6 and 7 in table 3. 10. At 100% supersaturation, exp. no. 10 used a low compression surface pressure of 10mN/m, the result was lots of small crystals, but also a few crystals were observed outside the barriers; this may be because dust or other impurity. In exps. no. 8 and 9, a compression surface pressures in the range 15.2mN/m – 17.8mN/m were used and, the results were less crystals than in exp. no. 10. At 90% and 80% supersaturation, only a few crystals nucleated because of the low supersaturation.

Table 3.11 shows the small trough data. In exp. no. 14, a compression surface pressure of 14.2mN/m was used under 120% supersaturated solution, and the result was lots of crystals grown in lines, with average length 0.13mm-0.40mm, see fig.3.7a and b. In experiments using low supersaturations, only a few crystals nucleated because of the low supersaturation.

It was found in exp. no. 17, that the film had not spread very well on the subphase, even through by eye it had appeared that the film had spread fully. Under the optical microscope, the film was seen to be aggregated into spheres, which floated on the subphase surface like oil drops floating on water, as shown in fig. 3.9a. Consequently, the crystals that nucleated grew under clumps of film material, rather than a spread monolayer film, see fig. 3.9b. In all subsequent experiments eg. for polycaprolacton and all the other polymer film experiments, the microscope was used to check that the film had spread properly. Thus we were sure crystals nucleated on monolayer film and not just undispersed polymer material.

Tables (3.10) and (3.11): Results of nucleation experiments under polycaprolactone monolayer film in different conditions:

Large trough data:

Experiment No.	*Degree of super-saturation*	*Compressing Pressure (mN/m)*	*Final Pressure (mN/m) at given time*	*Note*
1	150%	very high pressure #	#	Small crystals grown in lines with average length 0.33mm / few out
2	150%	15.5	9.5 at 18.5hrs	A few small crystals
3	150%	16	#	A few small crystals
4	150%	16	#	A few small crystals but larger than in exp. no.3
5	150%	14.4	0.5 at 8.3 hrs	Small crystals with average length 0.27mm, grown in lines.
6	120%	14.5	0.9 at 24hrs	Lots of crystals grown in line with average length 0.52mm (best result)
7	120%	14	6.8 at 17.5hrs	Lots of crystals grown in line with average length 0.27mm (not as much as exp. no.6)
8	100%	17.8	17.29 at 10.8hrs	Less crystals than in exp. no.9
9	100%	15.2	11.8 at 11.5	Less crystals than in exp. no.10
10	100%	10	0.16 at 7hrs	Lots of crystals / few out
11	90%	16	#	Very few tiny crystals
12	80%	19.1	18.68 at 2hrs	Tiny crystals, difficult to see by eye
13	80%	12.7	7.55 at 17hrs	Very few tiny crystals, difficult to see by eye.

Table 3.10

* out means crystals also observed outside the barrier, but always less than inside.

** few out means only a few crystals observed outside the barriers.

. # Computer software failure prevented the measurement of subsequent π values

Small trough data:

Experiment No.	*Degree of super-saturation*	*Compressing Pressure (mN/m)*	*Final Pressure (mN/m) at given time*	*Note*
14	120%	14.2	5.9 at 17.5hrs	Lots of crystals grown in lines / see fig. 3.7a and b.
15	70%	20.5	#	A few small crystals/ see fig. 3.7c and d.
16	40%	19.7	13 at 10.6hrs	A few small crystals / few out**/see fig. 3.8a and b.
17	40%	19.3	14 at 119.8hrs	Lots of crystals / see fig. 3.9a and b.(the film not spread properly)
18	40%	12.7	2.2 at 20hrs	A few small crystals / see fig. 3.8c and d.
19	40%	7.5	1.8 at 18.8hrs	No crystals.
20	30%	14.5	3.3 at 16.8hrs	Very few very tiny crystals (countable).

Table 3.11

** few out means only a few crystals observed outside the barriers.

Computer software failure prevented the measurement of subsequent π values

3.4.5. Poly-l-isoleucine:

Table 3.12 for the large trough data shows all the nucleation experiments for dl-aspartic acid beneath poly-l-isoleucine monolayer film, using different compression surface pressures. The results were not consistent. This suggests that the nucleation of dl-aspartic acid beneath the poly-l-isoleucine film was not strongly affected by surface pressure. Ever at high compression surface pressure up to 30mN/m no crystals nucleated outside the barrier of the trough. Other, as yet unidentified factors, such as the concentration of the spreading solution, may have been a more dominant factor. For example in experiments 5 and 6 the compression surface pressure were very similar, but the spreading solution had different concentrations.

Table 3.13 shows the small trough data. In exp. no.24, the supersaturated solution used was 120%, and the surface pressure was 16.4mN/m. The result was lots of crystals, with average length range ~0.1mm-0.3mm, see fig. 3.10a and b. In exp. No.25, the supersaturated solution used was 50%, under a compression surface pressure of 13.6mN/m. The result was tiny crystals that grew in lines, with average length range ~0.04mm-0.1mm.

3.4.6. Poly-γ-benzyl-l-glutamate:

Table 3.14 for the large trough data shows the effect of surface pressure on dl-aspartic acid nucleation beneath poly-γ-benzyl-l-glutamate at supersaturations of 120%, 100% and 80%. At 120% supersaturation, exp. no.1 used a compression surface pressure of 19.2mN/m, and the result was lots of small crystals; more than in exp. no.2, which used a low compression surface pressure of 7.2mN/m. At 100% supersaturated solution, exp. no.6 used a compression surface pressure of 11.2mN/m, and the result was a few small crystals but more than in exp. no.5, which used a surface pressure of 16mN/m and also more than in exp. no. 3 and 4, which used surface pressures of 30.9mN/m and 26.2mN/m, respectively. In these two experiments, some crystals were observed outside the barriers because of enhanced film dissolution due to the high surface pressure. At 80% supersaturated solution, the poly-glutamate monolayer film was not active at nucleating the dl-aspartic acid. Hence, these experiments show that compression surface pressure around 10mN/m- 20mN/m were best at nucleating dl-aspartic acid.

Tables (3.12) and (3.13): Results of nucleation experiments under poly-l-isoleucine monolayer film in different conditions:

Large trough data:

Experiment No.	*Degree of super-saturation*	*Compressing Pressure (mN/m)*	*Final Pressure (mN/m) at given time*	*Note*
1	120%	27.9	11.3 at 17hrs	A few crystals with average length 0.56mm.
2	120%	26	6.37 at 14.7hrs	Lots of small crystals with average length 0.34mm / one large crystal out*.
3	120%	23.5	17.9 at 4.3hrs	No crystals.
4	120%	21	#	A few crystals with average length 0.55mm, and less crystals than in exp. no. 12.
5	120%	20.8	2.17 at 22.3hrs	A few crystals with average length 0.6mm.
6	120%	20	4.7 at 20.8hrs	Lots of crystals with average length 0.6mm.
7	120%	19.8	0.059 at 17.8	No crystals because of producing multi layer film while compressing the barriers.
8	120%	18.8	7.3 at 15.8hrs	Lots of crystals with average length 0.5mm.
9	120%	17.8	0.07 at 18.5	A few crystals with average length 0.55mm.
10	120%	15.2	5.32 at 22.5hrs	Lots of small crystals.
11	120%	14.9	8.77 at 14.3hrs	Lots of small crystals.
12	120%	12.3	0.04 at 16.5	A few crystals with average length 0.67mm.
13	120%	9	1.1 at 4hrs	Tiny crystals.
14	120%	7.2	2.92 at 22hrs	A few tiny crystals.
15	120%	2.4	0.85 at 23.8hrs	Lots of small crystals with average length 0.41mm, larger than in exp. no.13 & 17*.
16	120%	2	1 at 10.8hrs	No crystals.
17	120%	1.1	0.011 at 11.5hrs	Lots of small crystals.
18	120%	0.8	#	Tiny crystals were grown in a line.
19	120%	0.7	0.013 at 4hrs	More crystals than in exp. no.18 with average length 0.41mm

Table 3.12 (to be continued)

Continued large trough data:

Experiment No.	*Degree of super-saturation*	*Compressing Pressure (mN/m)*	*Final Pressure (mN/m) at given time*	*Note*
20	100%	31.8	11.6 at 18hrs	A few small crystals.
21	100%	21.3	7.58 at 18hrs	A few small crystals but less than exp. no. .22.
22	100%	13.7	2.69 at 18hrs	A few small crystals but less than exp. no. 20.
23	80%	19.2	6.15 at 18.7hrs	No crystals.

Table 3.12

* one large crystal out, means only one crystals also observed outside the barrier.

Computer software failure prevented the measurement of subsequent π values

Small trough data:

Experiment No.	*Degree of super-saturation*	*Compressing Pressure (mN/m)*	*Final Pressure (mN/m) at given time*	*Note*
24	120%	16.4	8.5 at 13.3hrs	Lots of crystals / see fig. 3.10a and b.
25	50%	13.6	6.1 at 13hrs	Tiny crystals grown in lines .

Table 3.13

Table 3.15 for the small trough data show that in exp. no.8, a compression surface pressure of 13.3mN/m was used with 120% supersaturated solution, and the result was many small crystals with average length range 0.1mm-0.2mm, see fig. 3.11a and b. In exp. no.9, the compression surface pressure was 13.5mN/m, and the supersaturation was 40%, and only a few tiny crystals grew, probably at a late stage when the supersaturation had rise due to water evaporation.

3.4.7. Nylon 6 6:

Table 3.16 for the large trough data shows the effect of relatively low surface pressures on dl-aspartic acid nucleation beneath nylon at supersaturation of 120%, 100%, 80%, 75%, 70%, 60%, 50% and 40%, respectively. Higher surface pressures were not obtained because the spreading solution needed to be very dilute in order to avoid the polymer aggregating and forming the spherical structures observed for polycaprolactone, see fig. 3.9a. In addition, a recent paper by Popouitz-Biro et al.[35] showed that a nylon 6 6 film tended to form an increasing number of ~2nm microfibils with increasing surface pressure, so that a monomolecular layer was no longer present at higher surface pressures.

Exp. no.1, used a compression surface pressure of 7.4 mN/m on 120% supersaturated solution. The result was lots of quite large crystals with average length 0.55mm. In exp. no.2 the surface pressure was 1.1mN/m, and the result was a few small crystals. At 100% supersaturated solution, and a compression surface pressure of 4.4mN/m, the result of exp. no.3 was lots of large crystals with average length 0.6mm. At low supersaturations eg. exps. no.4-10, the result was fewer, smaller crystals. At 40% supersaturated solution, the nylon monolayer film was not effective at nucleating dl-aspartic acid.

Table 3.17 shows the small trough data. The best nucleating result using this trough was in exp. no 12, which used 120% supersaturated solution, and a compression surface pressure of 5.8mN/m. The result was lots of crystals grown in lines with average length 0.1mm-0.26mm, see fig. 3.12a and b; some crystals were also observed outside the barriers, maybe because of dust or impurity. In the experiments using low supersaturation eg. in exp.no.13-20, the results were fewer smaller crystals, but more crystals than were observed in the large trough, because of the greater water

Tables (3.14) and (3.15): Results of nucleation experiments under poly-γ-benzyl-l-glutamate monolayer film in different conditions:

Large trough data:

Experiment No.	*Degree of super-saturation*	*Compressing Pressure (mN/m)*	*Final Pressure (mN/m) at given time*	*Note*
1	120%	19.2	2 at 21.3hrs	Lots of small crystals.
2	120%	7.2	0.09 at 4.3hrs	A few small crystals/ few out**.
3	100%	30.9	2.6 at 20.3hrs	Very few &very small crystals / some larger crystals out*.
4	100%	26.2	5.7 at 16.8hrs	Very few &very small crystals / some larger crystals out*.
5	100%	16	7 at 15.2hrs	Very few &very small crystals and less than in exp. no.6.
6	100%	11.2	0.12 at 6.5hrs	A few small crystals and less than in exp. no. 2.
7	80%	13	11.2 at 11.2hrs	No crystals.

Table 3.14

*some larger crystal out, means only a few crystals observed outside the barriers but larger than inside.

** few out means only a few crystals observed outside the barriers.

Small trough data:

Experiment No.	*Degree of super-saturation*	*Compressing Pressure (mN/m)*	*Final Pressure (mN/m) at given time*	*Note*
8	120%	13.3	3.1 at 11.8hrs	Many small crystals / see fig. 3.11a and b.
9	40%	13.5	10.6 at ~12hrs	A few small crystals.

Table 3.15

evaporation from the small trough. These experiments suggest that nylon is a very good catalyst for nucleating dl-aspartic acid, it can nucleate at very low surface pressures supersaturated solutions as low as ~40%.

Tables (3.16) and (3.17): Results of nucleation experiments under nylon monolayer film in different conditions:

Large trough data:

Experiment No.	*Degree of super-saturation*	*Compressing Pressure (mN/m)*	*Final Pressure (mN/m) at given time*	*Note*
1	120%	7.4	5.7 at 5.7hrs	Lots of larger crystals than in exp. no. 2 with average length 0.53mm.
2	120%	1.1	#	A few small crystals but larger than in exp. no. 7.
3	100%	4.4	0.03 at 11hrs	Lots of crystals with average length 0.6mm / out*.
4	80%	11.5	6.9 at 10.8hrs	A few very small crystals.
5	80%	11.5	2 at 19.3hrs	A few very small crystals less than exp. no. 6.
6	80%	7.8	4.97 at 13.3hrs	Lots of small crystals with average length 0.47mm, but less than in exp. no.1/one crystal out**.
7	80%	0.8	#	A few very small crystals with average length 0.27mm / few larger crystals out***.
8	75%	4	0.18 at 3hrs	A few very small crystals with average length 0.25mm and less than in exp. no. 5.
9	60%	9.8	7.2 at 5hrs	A few very tiny crystals (countable).
10	50%	9.3	1.03 at 15hrs	A few very tiny crystals (countable)
11	40%	4.5	1.5 at 19hrs	No crystals.

Table 3.16

* out means crystals also observed outside the barrier, but always less than inside.

** one crystal out, means only one crystal outside the barriers.

*** few larger crystal out, means only a few larger crystals than inside observed outside the barriers.

Computer software failure meant the subsequent π values weren't recorded.

Small trough data:

Experiment No.	*Degree of super-saturation*	*Compressing Pressure (mN/m)*	*Final Pressure (mN/m) at given time*	*Note*
12	120%	5.8	0.9 at 0.5hr	Lots of crystals grown in lines / see fig.3.12a & b.
13	70%	6	4.8 at 6.5hrs	Lots of quite large crystals / one group out* / see fig. 3.12c.
14	60%	6.5	5.6 at 8hrs	Lots of crystals but less & smaller than in exp. no.17 using polycaprolactone monolayer film / see fig. 3.12d.
15	50%	7.5	6.5 at 16hrs	Lots of crystals / one out**.
16	40%	13.6	0.9 at 22hrs	Large groups of tiny crystals/ one small group out*.
17	40%	10.3	8.7 at 2.5hrs	No crystals.
18	40%	5.5	0.9 at 16.3hrs	A few crystal / few out***/ see fig. 3.12e.
19	40%	4.2	#	Lots of very tiny crystals / see fig. 3.12f.
20	30%	15.3	2.3 at 7hrs	Very few tiny crystals (countable).

Table 3.17

*one group out, means only a few crystals grown in a group observed outside the barriers

** one out, means only one crystal outside the barriers.

*** few out means only a few crystals observed outside the barriers.

Computer software failure meant the subsequent π values weren't recorded.

3.5. Comparison of the Film's Ability to Crystallise Dl-aspartic Acid:

3.5.1. Stearic Acid:

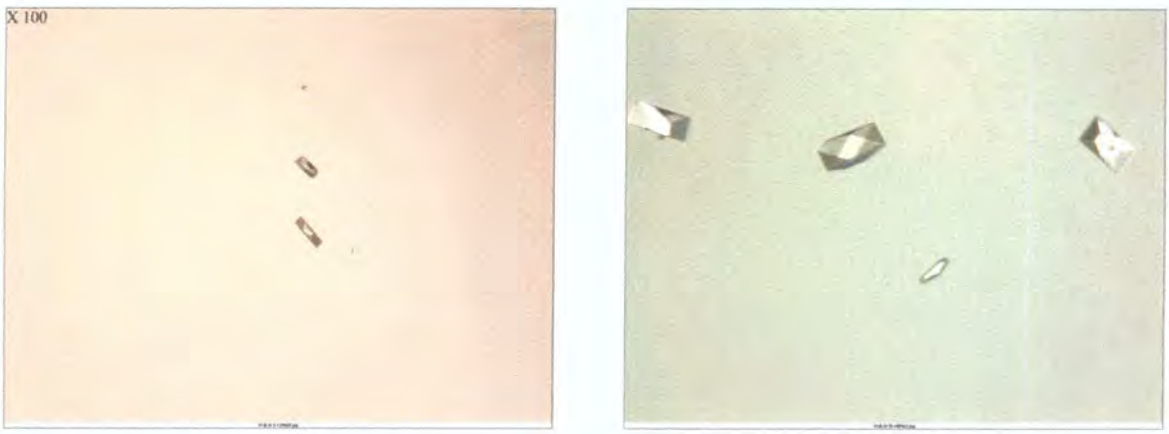

(a) (b)

Fig.3.4. Crystals of dl-aspartic acid beneath stearic acid monolayer film on the subphase surface of a) 120% supersaturated solution and π = 16mN/m (with a scale of 1mm=2.5x10^{-2} mm), and b) 100% supersaturated solution and π =16.8mN/m (with a scale of 1mm=5x10^{-3} mm), after 17-18hrs.

The stearic acid monolayer film is not a very good catalyst to crystallise dl-aspartic acid compared with the other films. Comparing the crystal quantity and size, the stearic acid nucleates very small and few crystals which were not easy to see by eye, unless using an optical microscope. The best compression surface pressure for nucleating the dl-aspartic acid beneath stearic acid is in the range of ~16mN/m to 30mN/m. N.B. In table 3.3 the sizes of the crystals using the large trough were larger than the small trough (table 3.4) even if under the same supersaturation condition. This was because the age of the crystals from the large trough was more than 24hrs in order to make it easy to pick them up from the surface.

3.5.2. Methyl stearate:

The methyl stearate monolayer film was best at nucleating the dl-aspartic acid at compression surface pressures around 22mN/m. The results of this film proved that it is better than stearic acid at nucleating dl-aspartic acid, see tables 3.5 and 5.6.

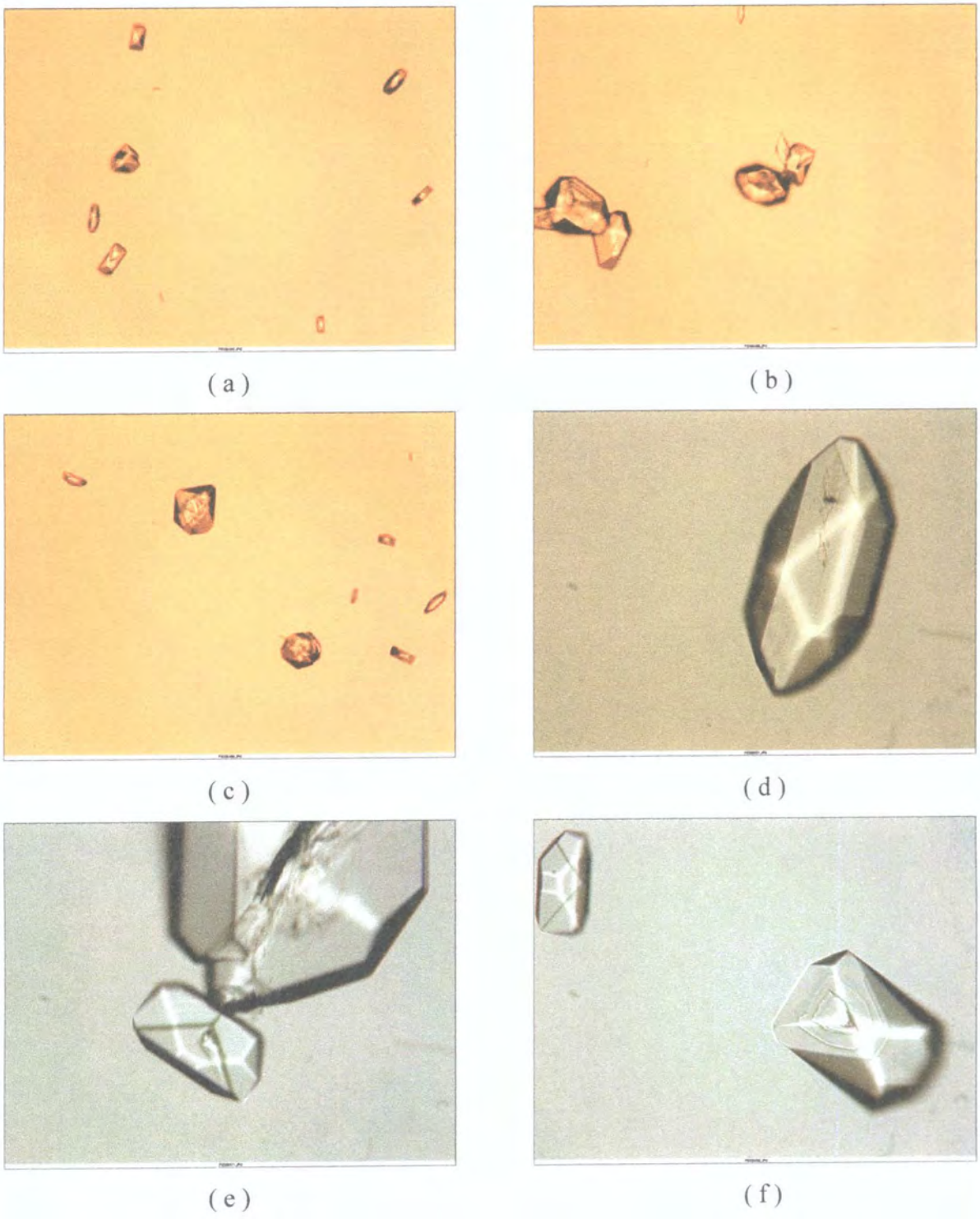

Fig. 3.5 Crystals of dl-aspartic acid beneath methyl stearate monolayer film on the subphase surface of 120% supersaturated solution and π = 17.5mN/m a), b), and c) with a scale of 1mm= 2.5×10^{-2} mm, and d), e), and f) with a scale of 1mm= 5×10^{-3} mm , after ~16hrs.

3.5.3. O-octadeyl carbonyl-l-tyrosine methyl ester hydrochloride:

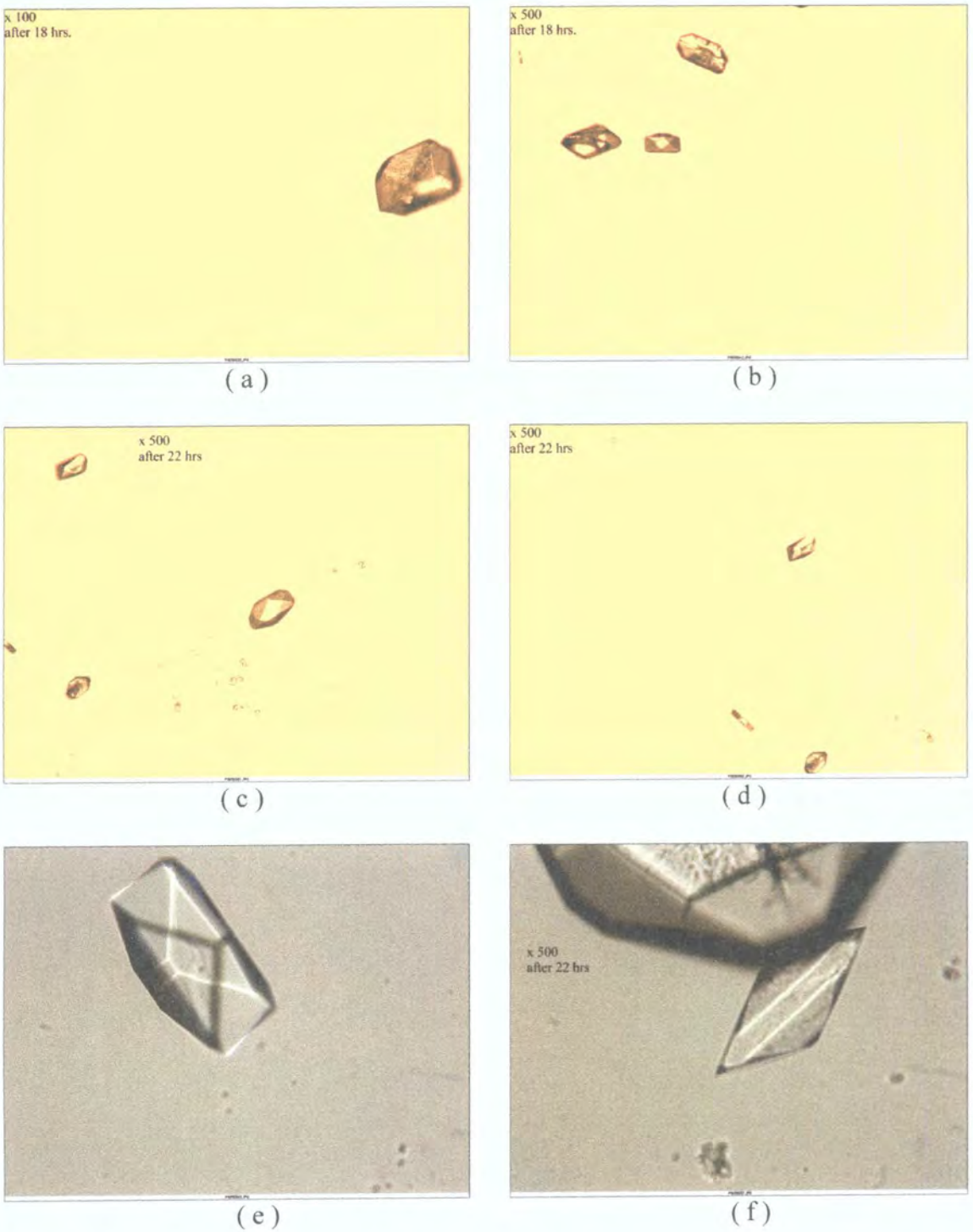

Fig. 3.6. Crystals of dl-aspartic acid beneath l-tyrosine monolayer film on the subphase surface of 120% supersaturated solution and π = 13.7mN/m a), b),c) and d) with a scale of 1mm=2.5x10^{-2} mm and e) and f) with a scale of 1mm=5x10^{-3} mm, after 18-22hrs.

The l-tyrosine monolayer film nucleates few crystals but they are larger than those from the stearic acid and methyl stearate monolayer films. After 18 hours from spreading, the film had crystallised a few large crystals on the subphase (see fig.3.4. a and b), and after 22 hours new tiny crystals started to grow (see fig3.4. c and d); that was why we saw different size ranges at the same time. The best compression surface pressure for nucleating dl-aspartic acid is in the range of ~12mN/m – 25mN/m.

3.5.4. Polycaprolactone:

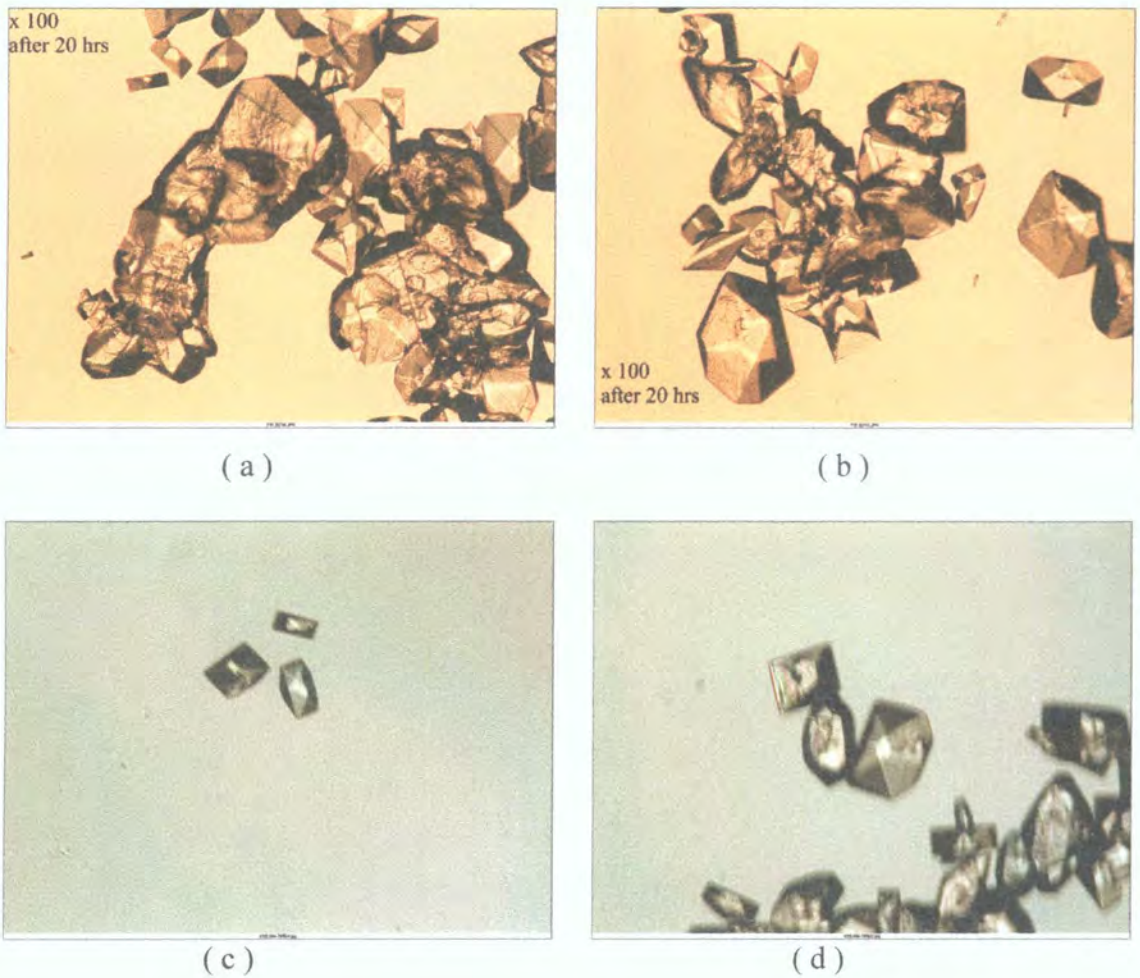

Fig. 3.7. Crystals of dl-aspartic acid beneath polycaprolactone monolayer film on the subphase surface of a) and b) 120% supersaturated solution for π= 13.7mN/m (with a scale of 1mm=2.5x10^{-2} mm), c) and d) 70% supersaturated solution for π=20.5mN/m, (with a scale of 1mm=5x10^{-3} mm), after ~20hrs .

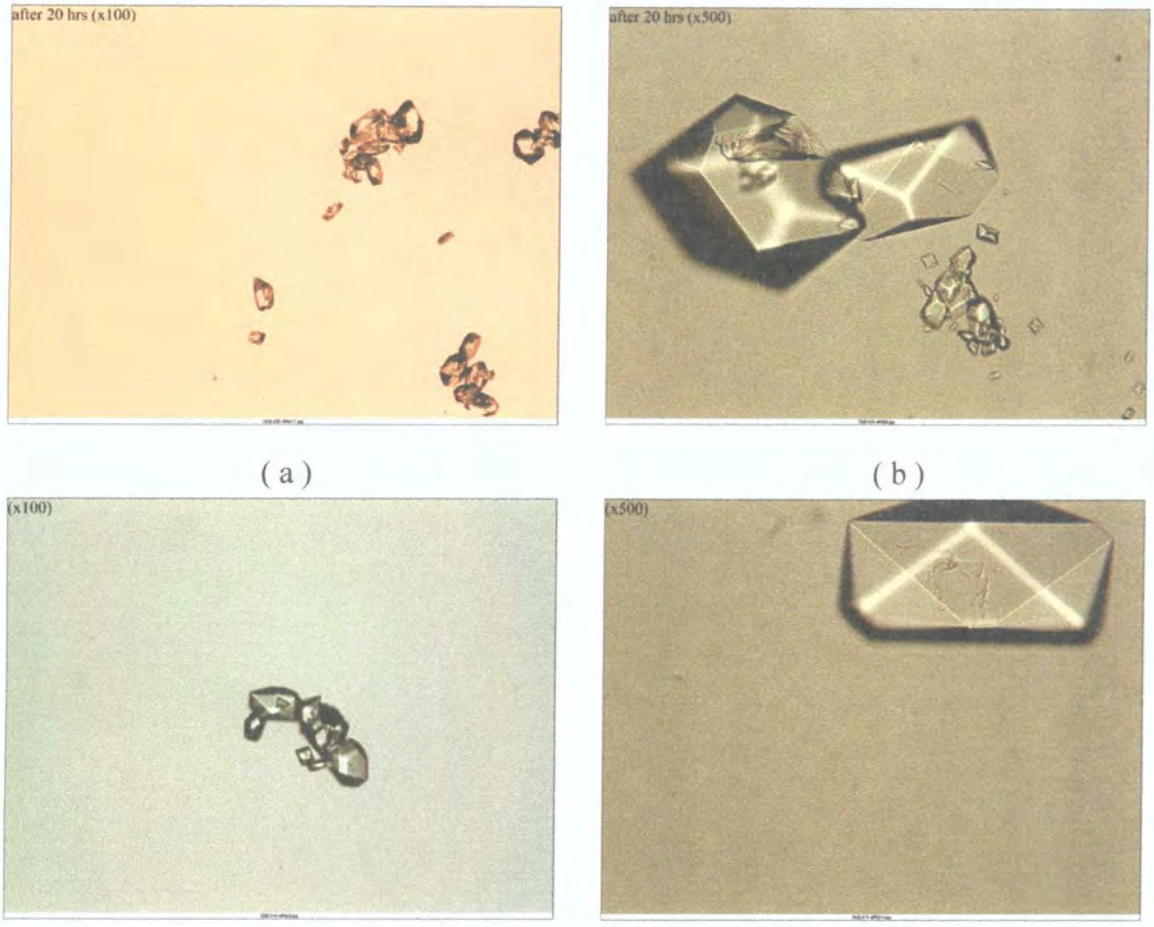

(a) (b)

(c) (d)

Fig. 3.8. Crystals of dl-aspartic acid beneath polycaprolactone monolayer film, on the subphase surface of a) and b) 40% supersaturated solution for π= 19.7mN/m a) with a scale of 1mm= $2.5x10^{-2}$ mm, and b) with a scale of 1mm= $5x10^{-3}$ mm ,c) and d) 40% supersaturated solution for π=12.7mN/m, c) with a scale of 1mm= $2.5x10^{-2}$ mm, d) with a scale of 1mm= $5x10^{-3}$ mm, after ~20hrs. #

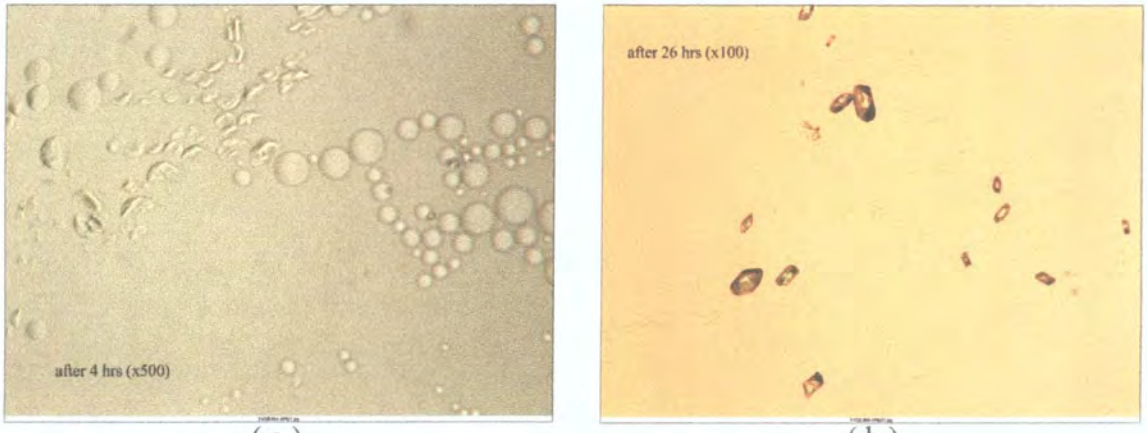

(a) (b)

Fig. 3.9 Crystals of dl-aspartic acid beneath polycaprolactone monolayer film, on the subphase surface of a) and b) 40% supersaturated solution for π= 19.3mN/m a) with a scale of 1mm= $5x10^{-3}$ mm (show the drops of the film, not spreading very well), after ~4hrs, and b) with a scale of 1mm= $2.5x10^{-2}$ mm (show the result after 26 hrs, where there are lots of small crystals), after ~26hrs.#

meant any micrograph pic. magnify x100 with a scale of 1mm= $2.5x10^{-2}$ mm and any micrograph pic. magnify x500 with a scale of 1mm= $5x10^{-3}$ mm

The polycaprolactone monolayer film is a very good catalyst to nucleate dl-aspartic acid in compression surface pressure ranges of 14mN/m-16mN/m. This film nucleated lots of large crystals compared to the other films and the crystals grew in a group or line typically (see fig.3.9 a & b). This film was a good catalyst down to ~40% supersaturated solutions but the best results were under 120% supersaturated solution.

3.5.5. Poly-l-isoleucine:

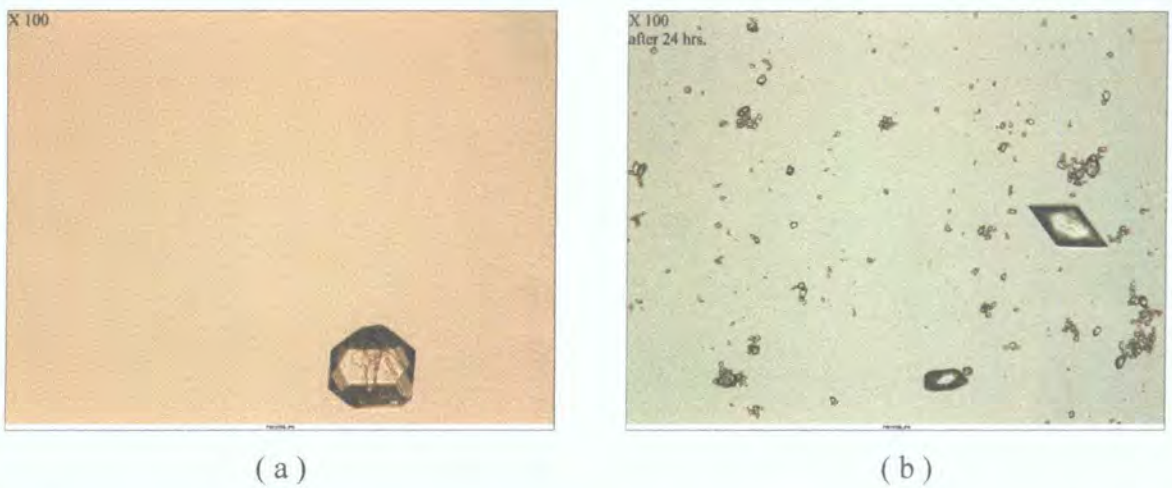

(a) (b)

Fig. 3.10. Crystals of dl-aspartic acid on the subphase surface of 120% supersaturated solution and π = 16.2mN/m a) the subphase after 16 hrs from the spreading, b)the subphase after 24 hrs showing the new tiny crystal with some large crystals nucleated earlier (with a scale of 1mm=2.5×10^{-2} mm).

The poly-l-isoleucine monolayer film was good at nucleating the dl-aspartic acid, but the compression surface pressures did not appear to have a strong effect in the nucleation process. The best result was obtained using 120% supersaturation. This film nucleated the dl-aspartic acid in the early stages as shown in fig. 3.10a, so that the crystal was large after 16 hrs. Then after 20-24hrs new tiny crystals grew beneath the film, as shown in fig. 3.10b.

3.5.6. Poly-γ-benzyl-l-glutamate:

The poly-γ-benzyl-l-glutamate monolayer film is best at nucleating the dl-aspartic acid at compression surface pressures around 10mN/m-20mN/m under 120% supersaturated

solution. The size of the crystals which grew beneath this film are typically smaller than the first larger crystals which nucleated beneath poly-l-isoleucine (see fig 3.8 &3.9).

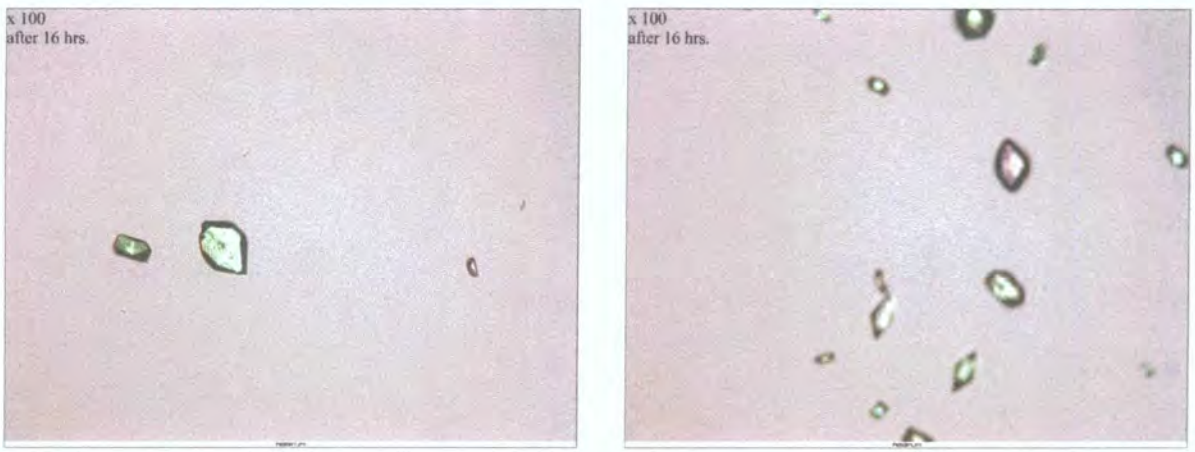

(a) (b)

Fig. 3.11. Crystals of dl-aspartic acid beneath poly-γ-benzyl-l-glutamate monolayer film on the subphase surface of 120% supersaturated solution and π = 13.8mN/m a) nd b) show the subphase after 16 hrs from the spreading (with a scale of 1mm=$2.5x10^{-2}$ mm), after ~16hrs.

3.5.7. Nylon 6 6:

The nylon monolayer film is a very good catalyst for nucleating dl-aspartic acid. It can nucleate at very low surface pressures in the range of 4mN/m-7mN/m and at low supersaturation down to ~40%. The crystals which grew under this film typically grew in groups or lines as in the polycaprolactone experiments. The difference between nylon and polycaprolactone is that the crystals grown beneath nylon were smaller than those grown beneath polycaprolactone.

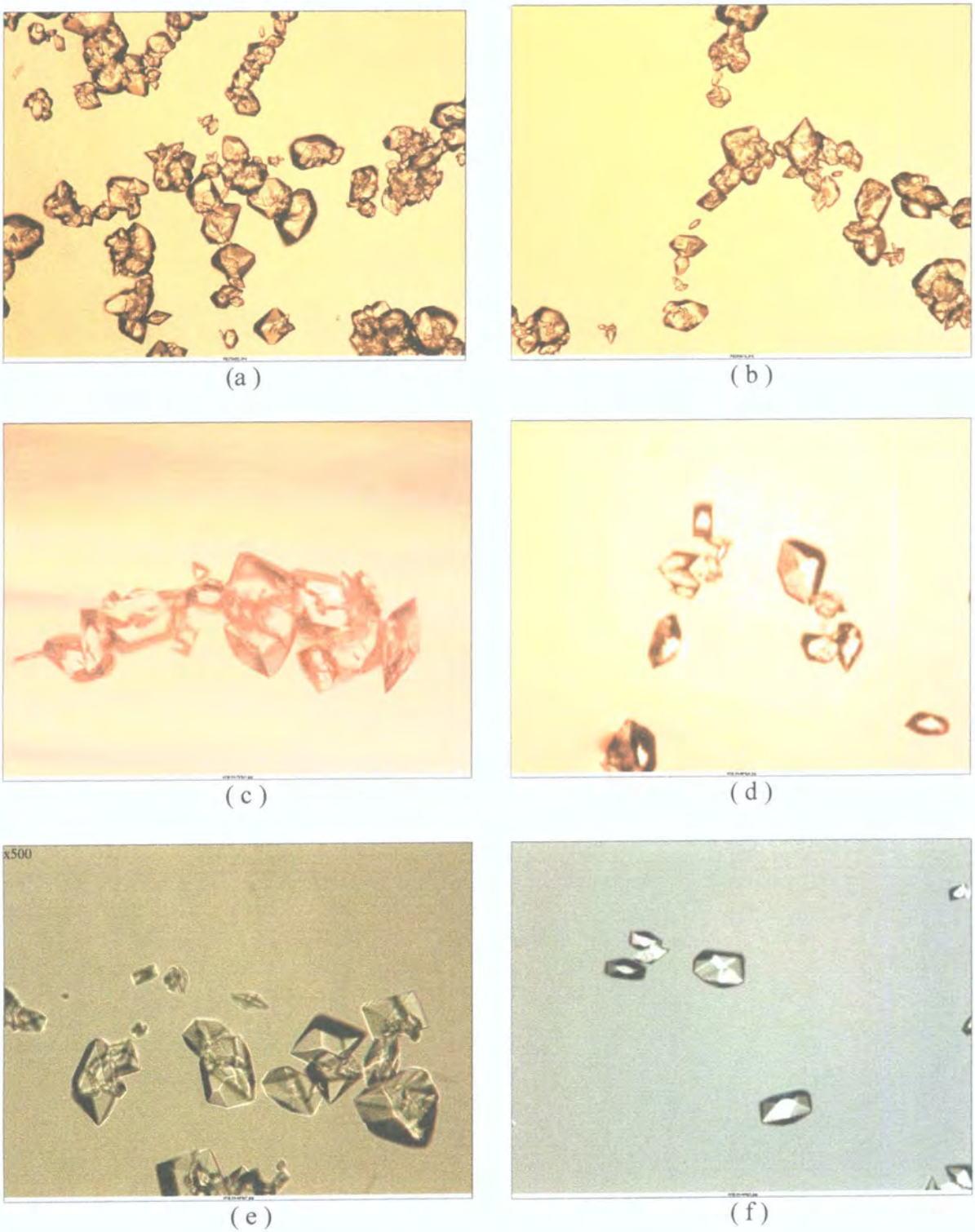

Fig. 3.12 a) and b) dl-aspartic crystals beneath nylon monolayer film on the subphase of 120% supersaturated dl-aspartic acid at π = 5.8mN/m, c) 70% supersaturated solution and at π = 6mN/m, d) 60% supersaturated solution and at π =6.5mN/m. (figs. a), b), c), and d) are with a scale of 1mm=2.5×10^{-2} mm), e) 40% supersaturated solution and at π = 5.5 mN/m, and f)40% supersaturated solution and at π =4.2 mN/m, after ~20hrs.(figs. e) and f) are with a scale of 1mm=5×10^{-3} mm).

3.6. Conclusion:

Nylon 6 6 and polycaprolactone were the best monolayer films at nucleating dl-aspartic acid; the results were many large crystals compared with the results of the other films, and typically the crystals grew in groups or lines (see figs. 3.7 , 3.8 and 3.12). Thy also induced crystallisation at lower supersaturations (down to ~40%) compared with the other films.
Stearic acid was the least effective monolayer film at nucleating dl-aspartic acid compared with the methyl stearate, l-tyrosine, poly-l-isoleucine and poly-γ-benzyl-l-glutamate films (see figs. 3.4, 3.5, 3.6, 3.10 and 3.11).

CHAPTER 4
MORPHOLOGY STUDIES AND FTIR RESULTS

4.1. Introduction:

In this chapter I will detail the crystal morphologies of dl-aspartic acid obtained from the nucleation experiments and I will show the results of external reflection FTIR spectra taken throughout the crystallisation process.

4.2. The Morphology:

It was always found that the crystal face growing beneath the film was larger than that found in the usual aqueous morphology. This is to be expected because the face is not in contact with the supersaturated solution, and hence it will grow the slowest, and have the largest area. In addition, this face also typically contained many surface irregularities, and was rough, not smooth. These irregularities probably arise from misfit dislocations, which occur because the film structure and dl-aspartic acid crystal structure differ[7,8].

4.2.1. Computational Modelling:

The Cerius morphology module from MSI (Molecular Simulations Incorporated) predicts the external morphology of the crystalline material from the internal crystal structure.

The morphology module supplies four methods:

1- The Bravais Friedel Donnay Harker (BFDH) method. This uses the crystal lattice dimensions and symmetry to generate a list of possible growth faces and their relative growth rates.
2- The Attachment Energy (AE) method for growth morphologies. This relies on the calculation of the energy released when a growth slice is added to a growing plane. This method can predict the shape of macroscopic/microscopic crystals more accurately because it takes the energetics of the system into account.
3- The Surface Energy (SE) method for equilibrium morphologies. This predicts the morphology, which minimizes the total surface energy of the crystal, by

determining the surface energy of the relevant faces. This is only valid for very small crystals (~nm size).

4- The Hartman-Perdok (HP) method. This uses a powerful algorithm for identifying stable growth planes by generating connected chains and nets of strong bonds in the crystal.

I used the BFDH and AE methods in this project. For the AE method, the force field COMPASS was used to calculate the crystal and attachment energies. In both the BFDH and AE methods, the morphologies obtained would be those expected in a vacuum, since no account is taken of the interaction of the crystal faces with the solvent, water.

The areas of the dl-aspartic acid crystals by using BFDH method:

Crystal Face	**Crystal Face Area**
$\{\bar{1}\ 1\ 1\}$	7.18
{1 1 0}	6.48
$\{\bar{2}\ 0\ 2\}$	4.22
{2 0 0}	16.68
$\{\bar{3}\ 1\ 1\}$	0.44

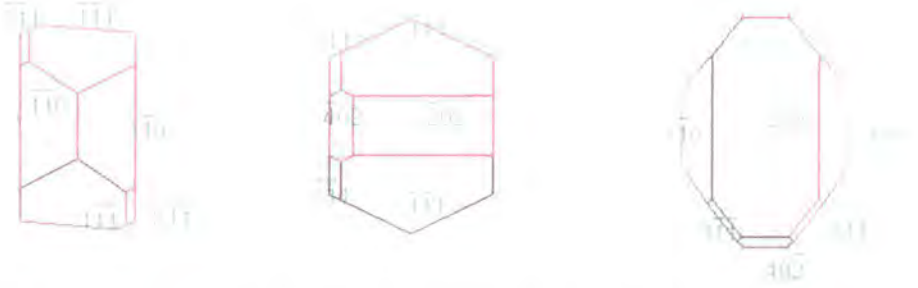

Fig. 4.1. Three perpendicular views of the crystal morphology predicted for dl-aspartic acid by BFDH method.

Table 4.1

The areas of the dl-aspartic acid crystals by using AE method:

Crystal Face	Crystal Face Area
$\{\bar{1}\ 1\ 1\}$	4.77
$\{1\ 1\ 0\}$	7.74
$\{\bar{2}\ 0\ 2\}$	12.95
$\{2\ 0\ 0\}$	11.60
$\{\bar{3}\ 1\ 1\}$	0.21

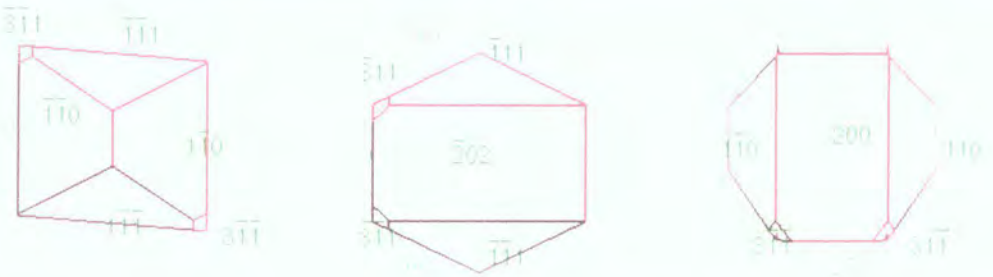

Fig. 4.2. Three perpendicular views of the crystal morphology predicted for dl-aspartic acid by AE method.

Table 4.2

4.2.2. Crystal Habit of Dl-aspartic Acid in Aqueous Solution:

A typical crystal revealed that the dominant crystal faces present when dl-aspartic acid is crystallised from aqueous solution were the $\{1\ 1\ 0\}$, and $\{\bar{1}\ 1\ 1\}$ faces, with the $\{\bar{2}\ 0\ 2\}$ face also sometimes present, see fig.4.3.

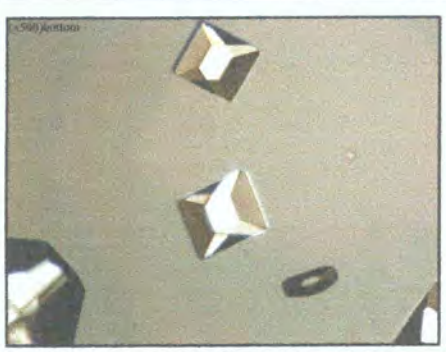

Fig..4.3. The typical crystal faces of dl-aspartic acid, which crystallised from aqueous solution. These crystals were taken from the bottom of the trough (with scale of $1mm=7x10^{-3}mm$.

Space group	C2/c (number 15)
Unit cell parameters	a=18.947 b=7.433 c=9.184 $\alpha = 90^0$ $\beta = 123.75^0$ $\gamma = 90^0$
Number of molecules per unit cell	8

Table 4.3

Comparing the typical aqueous morphology with the predicted vacuum morphologies obtained by the BFDH and AE methods, see figs. 4.1 & 4.2, it is clear that both the BFDH and AE methods overestimate the important of the $\{\bar{2}\,0\,2\}$, $\{2\,0\,0\}$ and $\{\bar{3}\,1\,1\}$ faces. Of the two, the AE method is slightly more accurate in producing the observed aqueous morphology, because the $\{2\,0\,0\}$ and $\{\bar{3}\,1\,1\}$ faces that are not seen in the aqueous morphologies, have smaller areas.

4.2.3. Investigation of Crystal Habit beneath Each Monolayer Film:

The following figures for crystal morphologies were produced from the Cerius software programme by varying the sizes of the crystal faces present. In particular, the face growing beneath the film was always made larger, as this was observed experimentally. The following figures 4.4 - 4.7 were used to help identify the crystal faces:

(1) (2) (3)

Fig. 4.4. Three different shaped $\{\bar{1}\ 1\ 1\}$ crystal faces (shaded). For an experimental morphology similar to (1) see e.g. fig. 4.12f, for (2) see e.g. fig. 4.10c, and for (3) see e.g. fig. 4.10a.

(1) (2)

Fig.4.5. Two different shaped {110} crystals faces (shaded). For an experimental morphology similar to (1) see e.g. fig. 4.12a, and for 2 see e.g. fig. 4.8.2.

(1) (2) (3)

Fig.4.6. Three different shaped $\{\bar{2}02\}$ crystals faces (shaded). For an experimental morphology similar to (1) see e.g fig. 4.12b, for (2) see e.g. fig. 4.9a3, and for (3) see fig. 4.10f.

(1) (2)

Fig. 4.7. Two different shaped {200} crystal faces (shaded). For an experimental morphology similar to (1) see e.g. fig.4.11c, and for (2) see e.g. fig. 4.14b.

4.2.3.1. Crystal Habits of Dl-aspartic Acid Grown beneath Stearic Acid Monolayer Film:

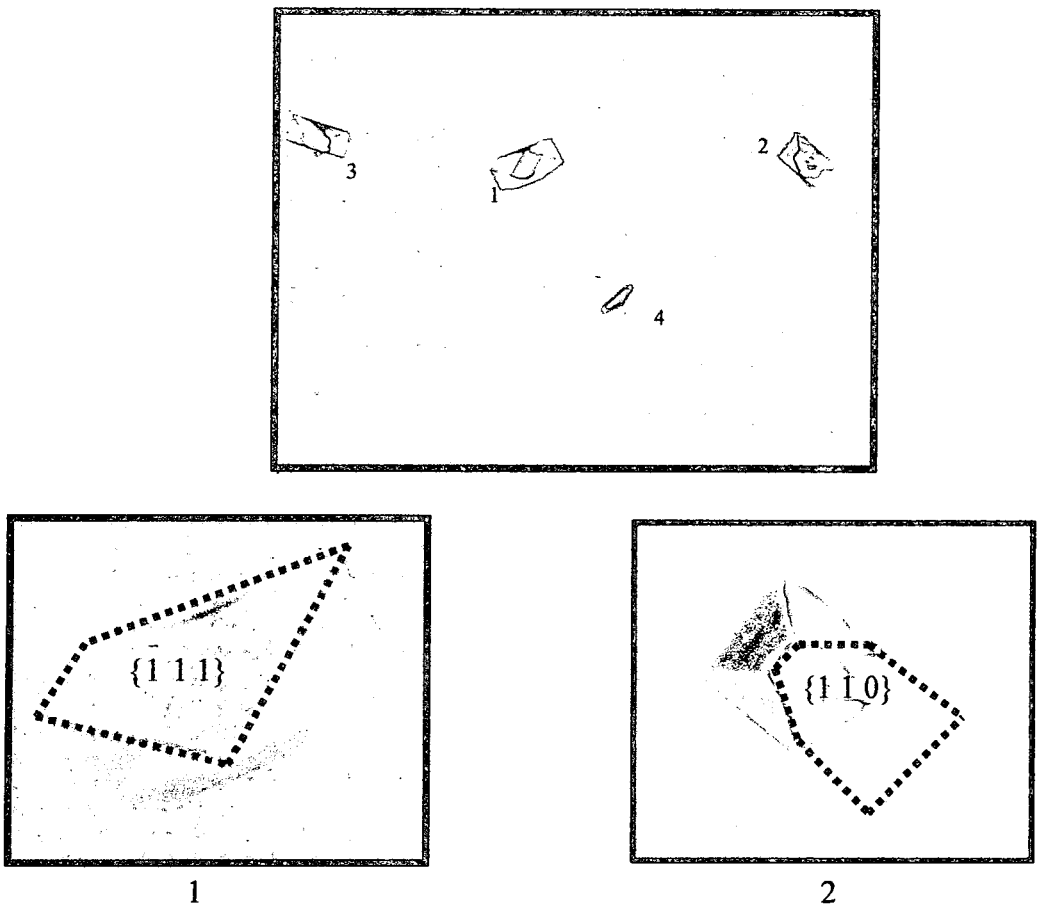

Fig. 4.8. Crystals of dl-aspartic acid grown beneath stearic acid monolayer film on a subphase surface of 120% supersaturated solution, under a compression π = 16mN/m.

From this figure, we can see that 1 and 4 have the {$\bar{1}$ 1 1} face grown beneath the film and 2 and 3 have the {1 1 0} face grown beneath the film. These were the typical faces that crystallised beneath stearic acid films.

4.2.3.2. Crystal Habits of Dl-aspartic Acid Grown beneath Methyl Stearate Monolayer Film:

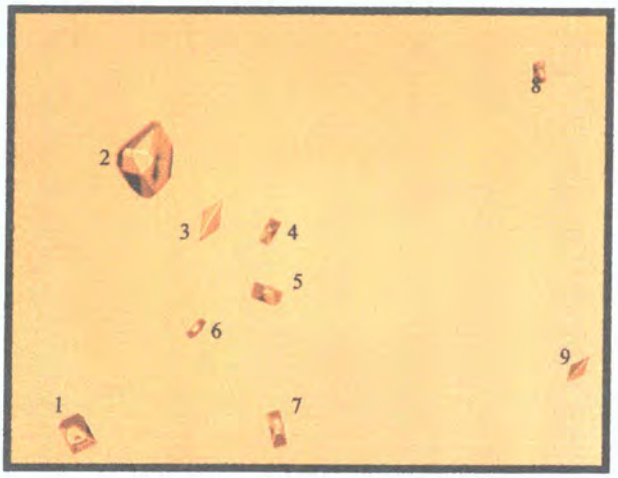

(a)

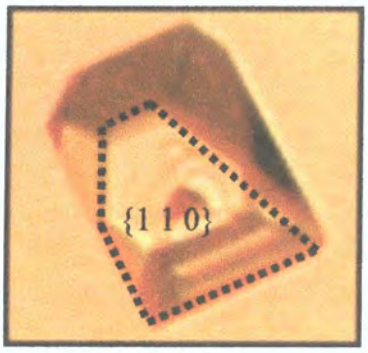

(a) 1

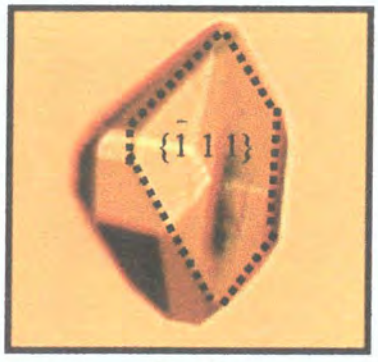

(a) 2

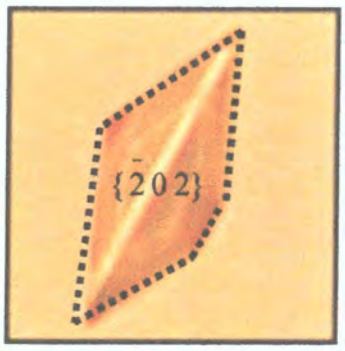

(a) 3

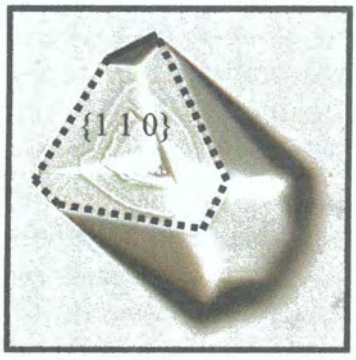

(b)

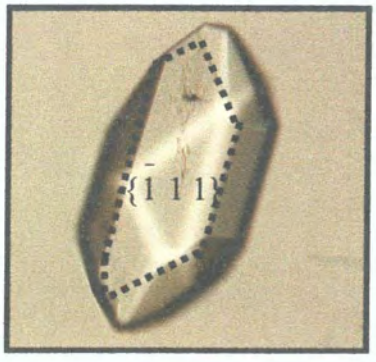

(c)

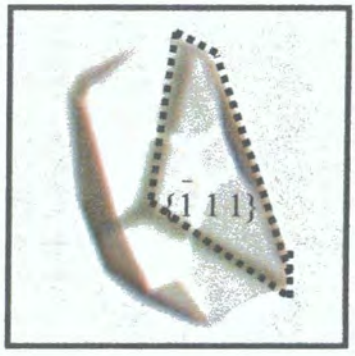

(d)

Figs. 4.9.a-d. Crystals of dl-aspartic acid beneath methyl stearate monolayer film on a subphase surface of 120% supersaturated solution, under a compression π = 17.1mN/m.

In fig. 4.9a, the faces growing beneath the film are as follows: {110} for crystals 1, 4, 7, and 8, $\{\bar{1}\ 1\ 1\}$ for crystals 2, 5, and 6, and $\{\bar{2}\ 0\ 2\}$ for crystals 3 and 9.
From the analysis of these and micrographs from other experiments it was found that the typical crystal faces grown beneath the methyl stearate films were mainly {1 1 0}, with some $\{\bar{1}\ 1\ 1\}$and a few $\{\bar{2}\ 0\ 2\}$ crystal faces.

4.2.3.3. Crystals Habit of Dl-aspartic Acid Grown beneath L-tyrosine Monolayer Film:

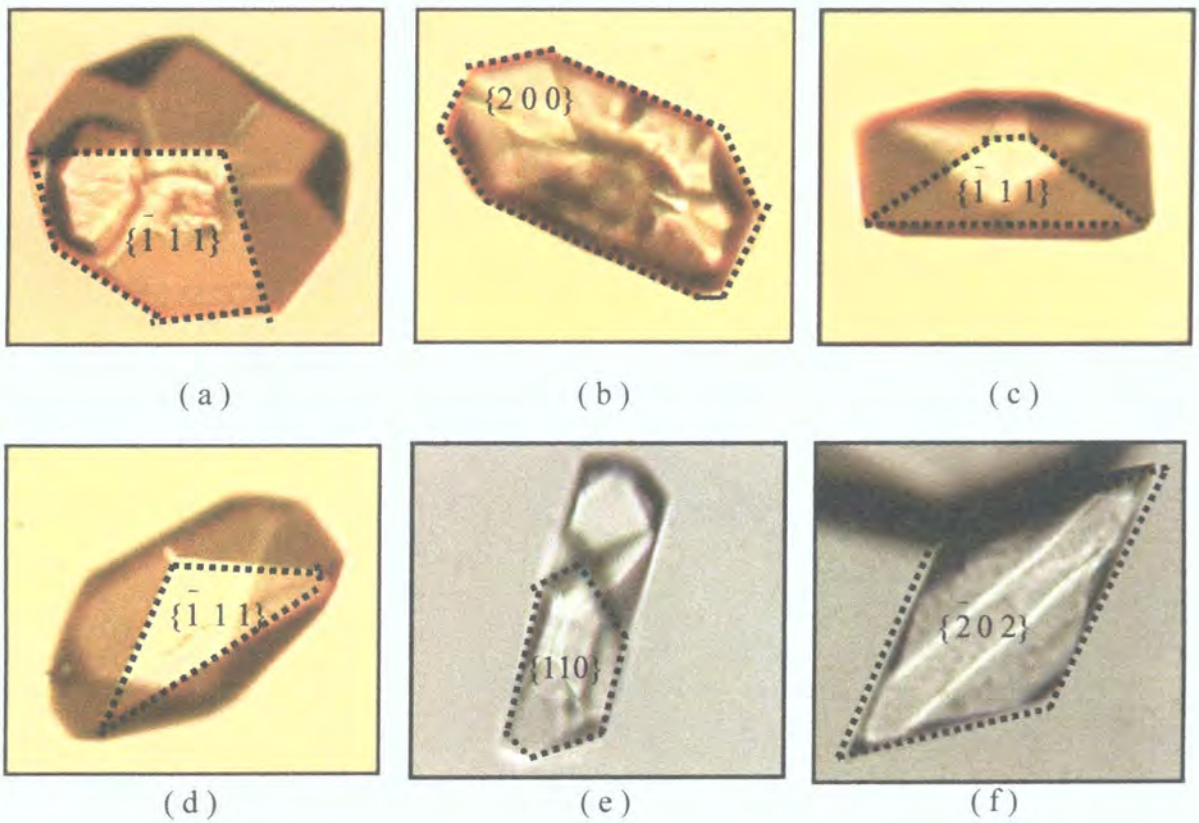

Fig.4.10.a-f. Crystals of dl-aspartic acid beneath l-tyrosine monolayer film on subphase surface of 120% supersaturated solution, under a compression π = 13.7mN/m. From the analysis of these figures and micrographs from other experiments, it was found that the typical crystal faces grown beneath the l-tyrosine monolayer film were mainly $\{\bar{1}\ 1\ 1\}$, with some {1 1 0}, and $\{\bar{2}\ 0\ 2\}$, and a few {2 0 0} crystal faces.

4.2.3.4. Crystal Habits of Dl-aspartic Acid Grown beneath Polycaprolactone Monolayer Film:

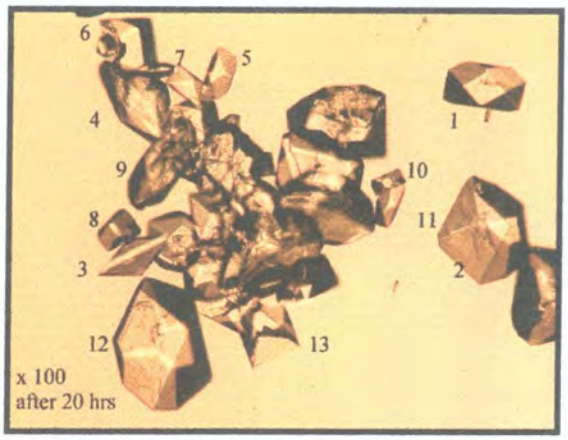

(a)

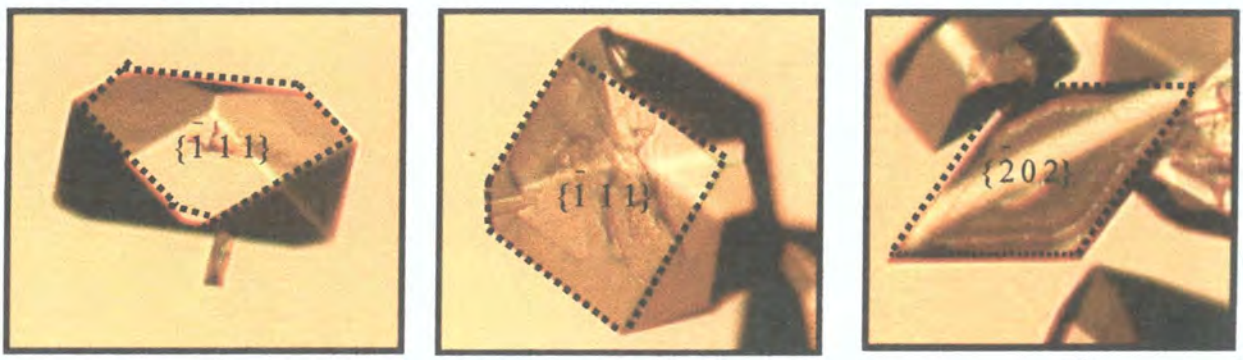

a 1 a 2 a 3

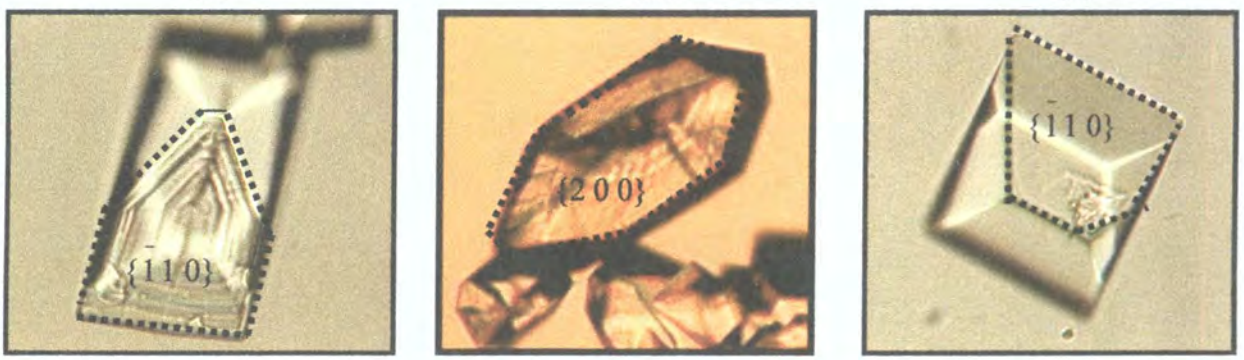

(b) (c) (d)

Fig. 4.11.a-d. Crystals of dl-aspartic acid beneath polycaprolactone monolayer film on a subphase surface of 120% supersaturated solution, under a compression π = 14.2mN/m.

In fig. 4.11a the faces growing beneath the film are as follows {$\bar{1}$ 1 1} for crystals 1, 2, 5, 7, 11, and 12, {1 1 0} for crystals 6, 8, 10, and 13, {2 0 0} for crystals 4 and 9, and {$\bar{2}$ 0 2} for crystal 3.

From the analysis of these figures and those from other experiments, it was found that the typical crystal faces grown beneath the polycaprolactone monolayer film were mainly {$\bar{1}$ 1 1}, with some {1 1 0}, and {$\bar{2}$ 0 2} and a few {2 0 0} crystal faces.

4.2.3.5. Crystals Habit of Dl-aspartic Acid beneath Poly-l-isoleucine Monolayer Film:

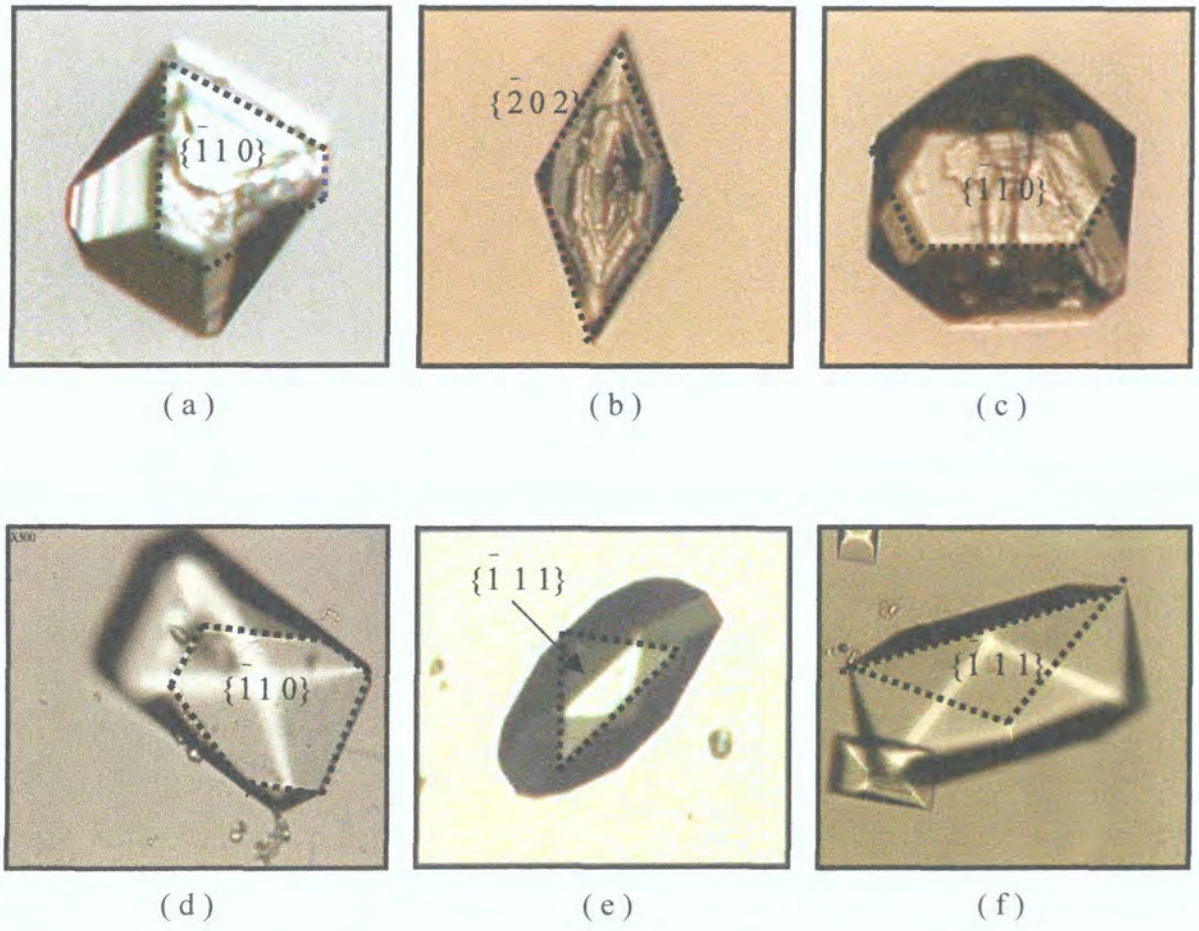

Fig. 4.12.a-e. Crystals of dl-aspartic acid beneath poly-l-isoleucine monolayer film on a subphase surface of 120% supersaturated solution, under a compression π = 16.4mN/m. Fig. 4.5.f is on a subphase surface of 50% supersaturated solution, with a compression π = 13.6mN/m.

From the analysis of these figures and those from other experiments, it was found that the typical crystal faces grown beneath the poly-l-isoleucine monolayer film were mainly {1 1 0}, with some {$\bar{1}$ 1 1} and a few {$\bar{2}$ 0 2} crystal faces.

4.2.3.6. Crystal Habits of Dl-aspartic Acid Grown beneath Poly-γ-benzyl-l-glutamate Monolayer Film:

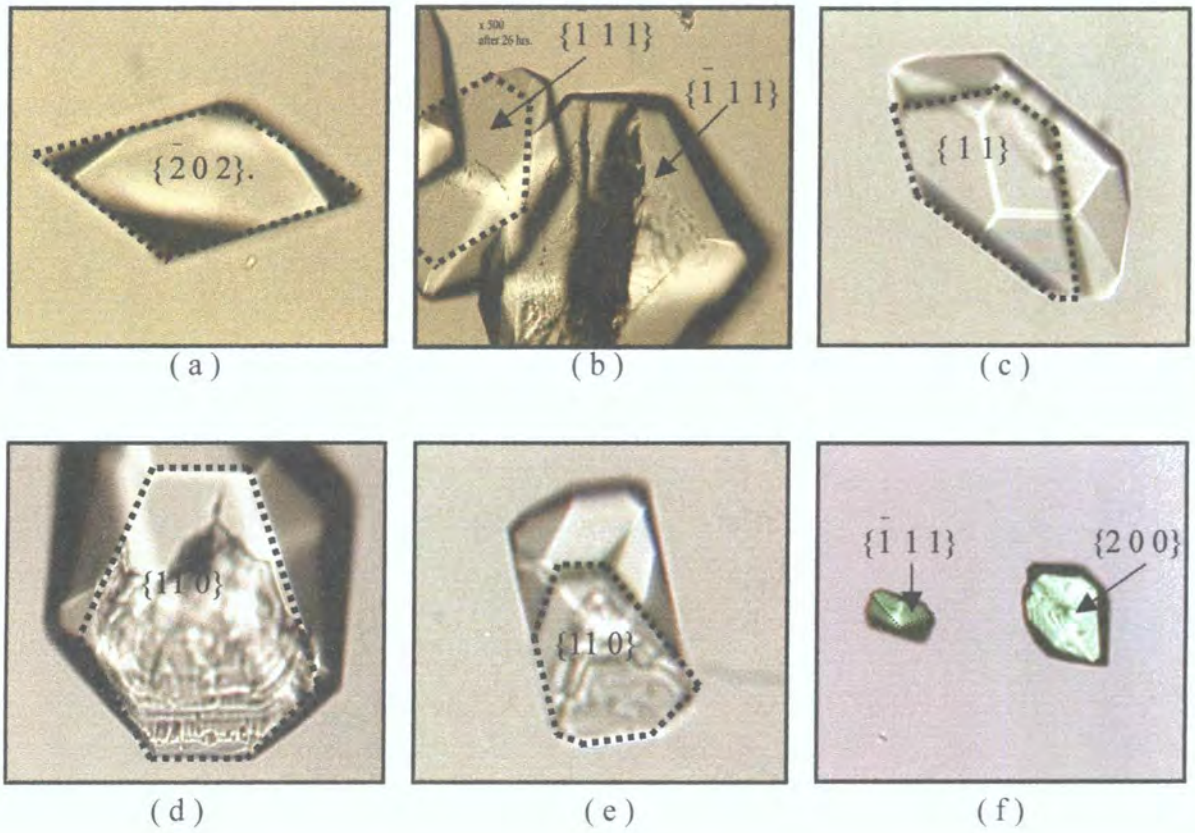

Fig.4.13.a-f. Crystals of dl-aspartic acid beneath poly-γ-benzyl-l-glutamate monolayer film on a subphase surface of 120% supersaturated solution, under a compression π = 13.3mN/m.

From the analysis of these figures and those from other experiments, it was found that the typical crystal faces grown beneath the poly-γ-benzyl-l-glutamate monolayer film were mainly {11 0} and {1 1 1}, with some {2 0 2} and a few {2 0 0} crystal faces.

4.2.3.7. Crystal Habits of Dl-aspartic Acid Grown beneath Nylon 6 6 Monolayer Film:

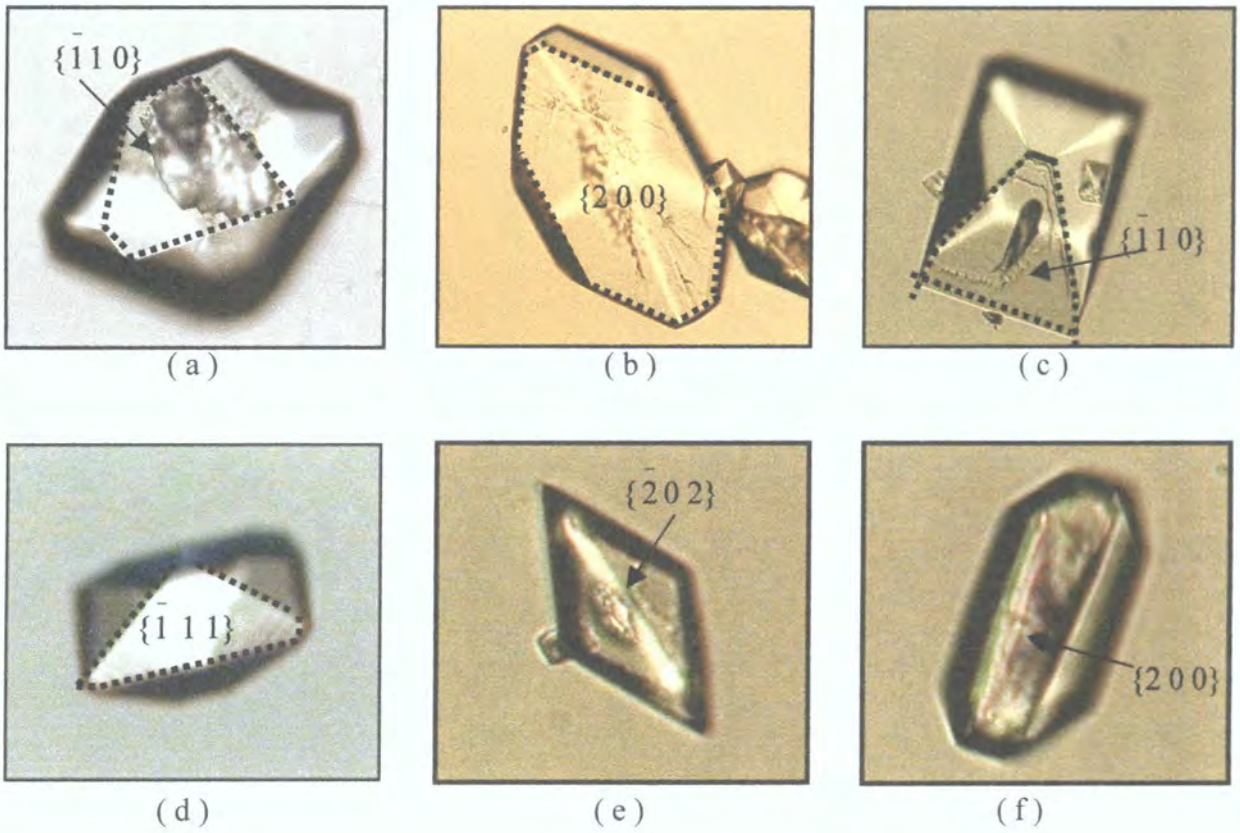

Fig.4.14.a and b. Crystals of dl-aspartic acid beneath nylon 6 6 monolayer film on a subphase surface of 120% supersaturated solution, under a compression π = 5.8mN/m. Fig.4.7.c, d, e and f, are on a subphase surface of 40% supersaturation under a compression π = 5.5mN/m.

From the analysis of these figures and those from other experiments, we found that the typical crystal faces grown beneath the nylon 6 6 monolayer film were mainly {1 1 0}, with some {$\bar{1}$ 1 1}, and {$\bar{2}$ 0 2} (but more {$\bar{2}$ 0 2} than for the other films) and a few {2 0 0} crystal faces.

4.3. The Results of External Reflection FTIR Spectroscopy:

The FTIR data for each of the seven films was collected every half an hour for 20 to 24 hours, by using a macro command file. Negative absorbance peaks are observed, due to the reflectivity properties of water[9,27], for both the film and dl-aspartic acid absorbing groups. In addition, positive peaks at 770 cm^{-1}(strong) and 1219 cm^{-1}(very weak) due to chloroform are observed in the first few spectra, together with broad positive liquid water peaks centred around 3580, 1660 and 900cm^{-1}. The CO_2 gas peaks occur at 2358 and 2335cm^{-1}. During the experiments peaks due to water vapour between ~1300-1900 cm^{-1} and above ~3400 cm^{-1} increased in intensity with time, due to water evaporation from the trough.

In the following tables, the main peaks observed for dl-aspartic acid crystals are tabulated, except for those which are obscured by the water vapour peaks, i.e. those between ~1300-1700 cm^{-1}, which include the CO_2 stretch and NH bending modes. In addition, any peaks due to the monolayer film are also tabulated. Peaks due to the dl-aspartic acid crystals are observed whenever the FTIR beam of size ~mm hits these crystals. During the course of the ~20 hrs experiment, the tiny crystals will move around the water surface slightly if there are any vibration. Hence, the intensity of the dl-aspartic acid crystalline peaks will increase with time as the crystals grow, provided the crystal density is high enough, that it is always likely that the beam will hit some crystals.

For each film case, four figures of FTIR spectra are shown. The first set show the entire spectral region from 4000-650 cm^{-1}. The second set show spectra in the region ~3000-2800 cm^{-1}, where the film peaks are expected. The third set show spectra from ~1220-800 cm^{-1} showing the main dl-aspartic acid crystalline peaks. The fourth set show spectra from ~1220-1000cm^{-1} for times just before and after dl-aspartic acid crystallisation began. The majority of the figures show raw spectra. Some spectra, notably the fourth set of spectra, were baseline corrected and offset, purely for ease of comparison. None of the spectra was smoothed.

4.3.1. Stearic Acid:

Table 4.4. Important peaks of the FTIR spectra (see figs. 4.15-4.17) from 4000-650cm^{-1} for stearic acid spread on 120% supersaturated solution of dl-aspartic acid at a compression surface pressure of 12 mN/m.

The Time of the Spectra Reading after Spreading the Film/(hour)							Assignment[37]
0	3	6	11.5	12	13.5	15	
				854	854	854	CH_2 rock for dl-aspartic acid
				893	894	894	CC stretch for dl-aspartic acid
				987	984	985	CC stretch for dl-aspartic acid
				1070	1071	1071	CN stretch for dl-aspartic acid
				1115	1115	1114	NH_3^+ rocking for dl-aspartic acid
				1141	1140	1140	NH_3^+ rocking for dl-aspartic acid
				1213	1213	1213	CH_2 twist for dl-aspartic acid
2850	2850	-	2850	2850	2850	2850	CH_2 symmetric stretch for stearic acid
2916	2916	-	2616	2916	2916	2916	CH_2 asymmetric stretch for stearic acid

Table 4.4

From the FTIR spectra (see figs 4.15 and 4.17) and table 4.4, we can see that peaks due to dl-aspartic acid crystals first appeared ~11-12 hrs after spreading the film. Interestingly at the same time at which the dl-aspartic acid crystalline peaks first appeared, we also saw a dramatic increase in intensity of the CH_2 symmetric and asymmetric stretches of the stearic acid film, see figs. 4.15 and 4.16. The intensity continued to increase for another few hours, as the dl-aspartic acid continued to crystallise. No such dramatic increase in intensity of these peaks was observed in the FTIR spectra of the control experiment of stearic acid on water, left for the same amount of time.

We tentatively attribute this dramatic intensity increase in the film peaks to a rearrangement of the film, so that the chains are more perpendicular to the surface. This would lead to the methylene groups being more parallel to the solution surface, and hence this would lead to an increased intensity peak, since groups vibrating parallel to the water surface have entranced absorption, compared to those vibrating perpendicular to the water surface[27]. We propose that the film re-orientates so as to minimise the structural mismatch between itself and the growing dl-aspartic acid crystals. A recent paper by Ahn *et. al.*[9] also demonstrated by external reflection FTIR that film reorganisation occurred for surfactant-induced crystallisation of calcium carbonate.

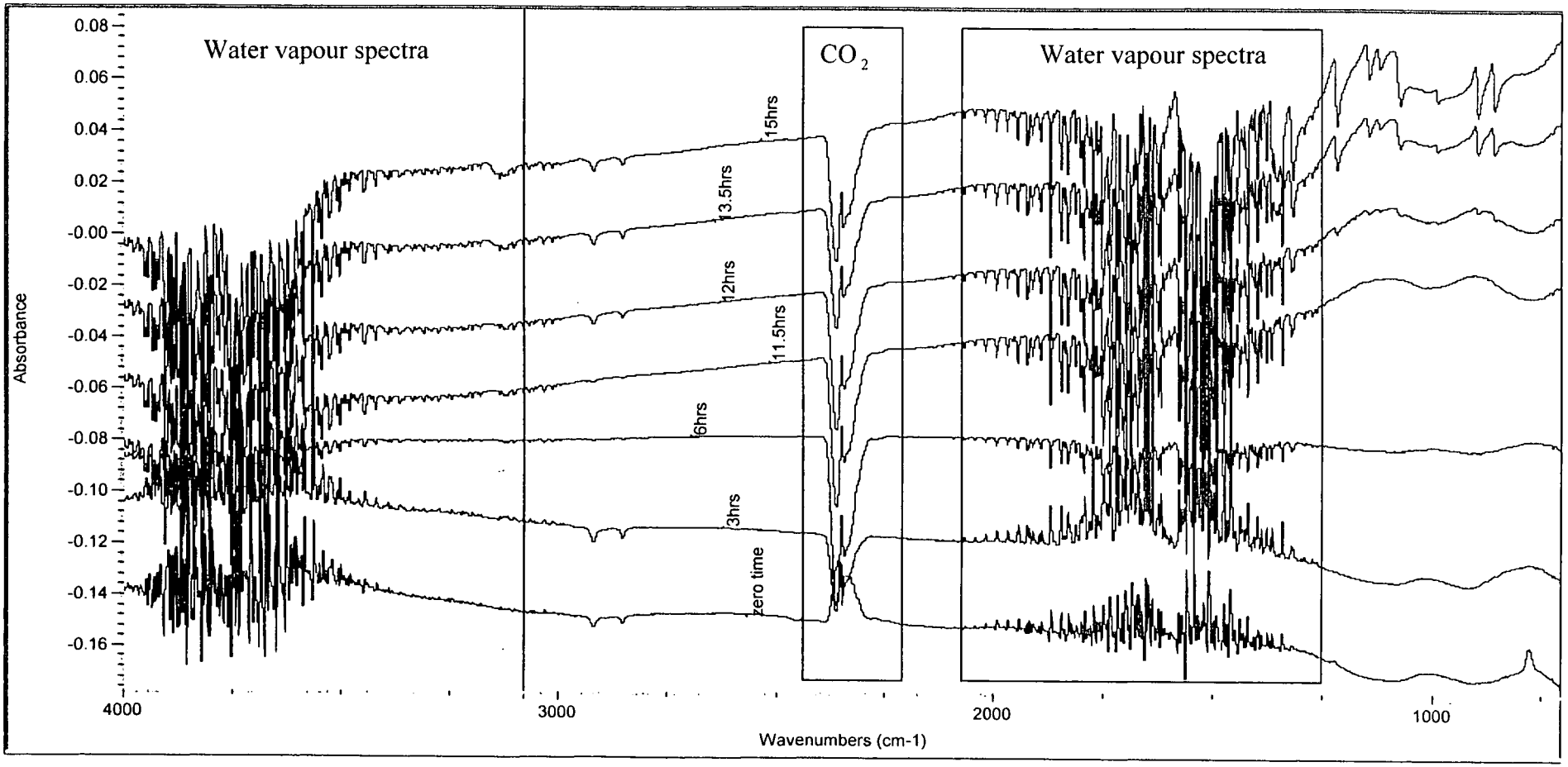

Fig.4.15. External reflection FTIR spectra from 4000-650cm^{-1} for stearic acid spread on a 120% supersaturated solution of dl-aspartic acid at a compression surface pressure of 12 mN/m.

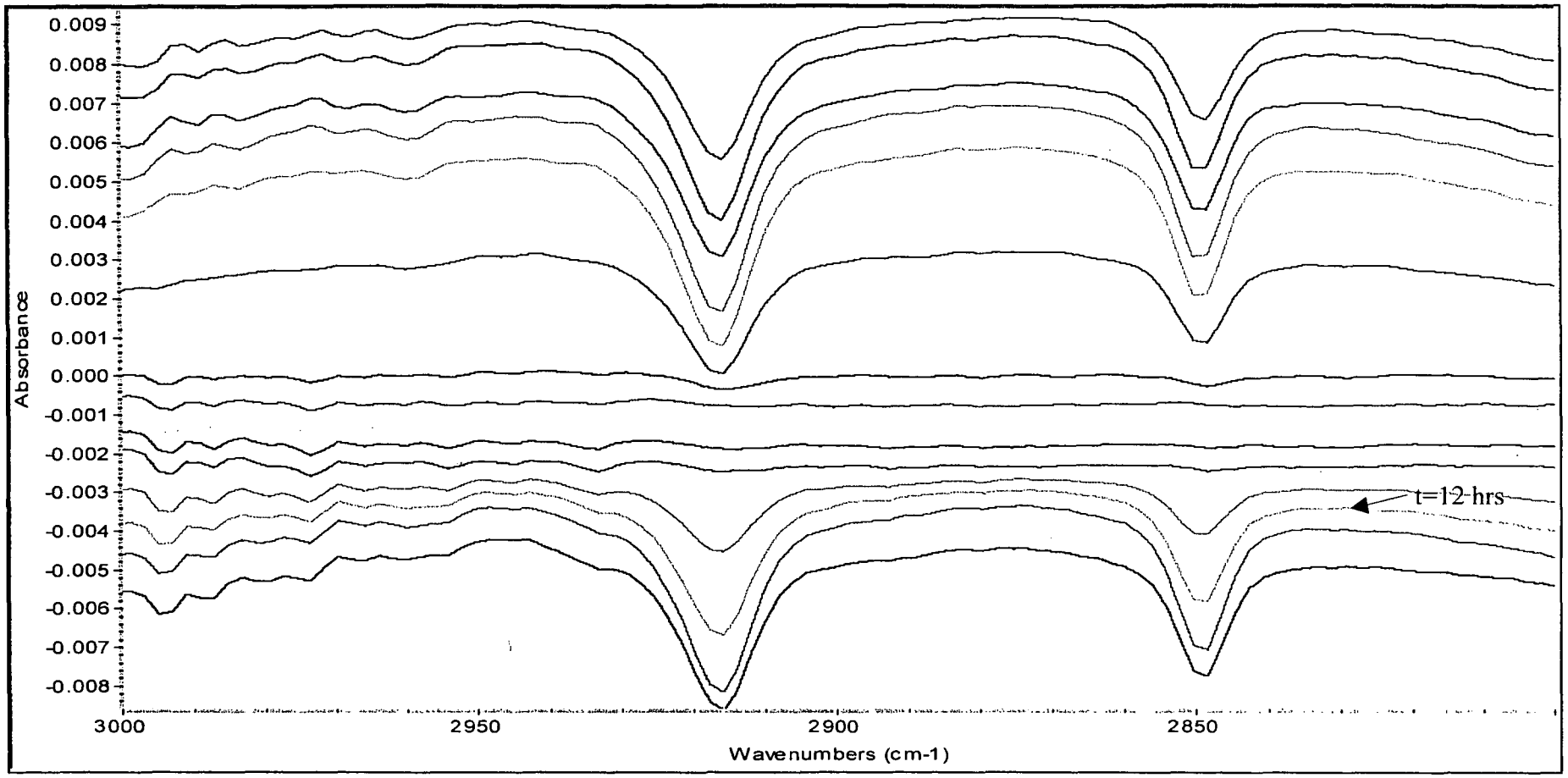

Fig.4.16. External reflection FTIR spectra from 3000-2800 cm^{-1} for stearic acid spread on a 120% supersaturated solution of dl-aspartic acid solution at a compression surface pressure of 12 mN/m. Note the spectra have been offset for ease of comparison. t=0-14 hrs. (t=0 at top).

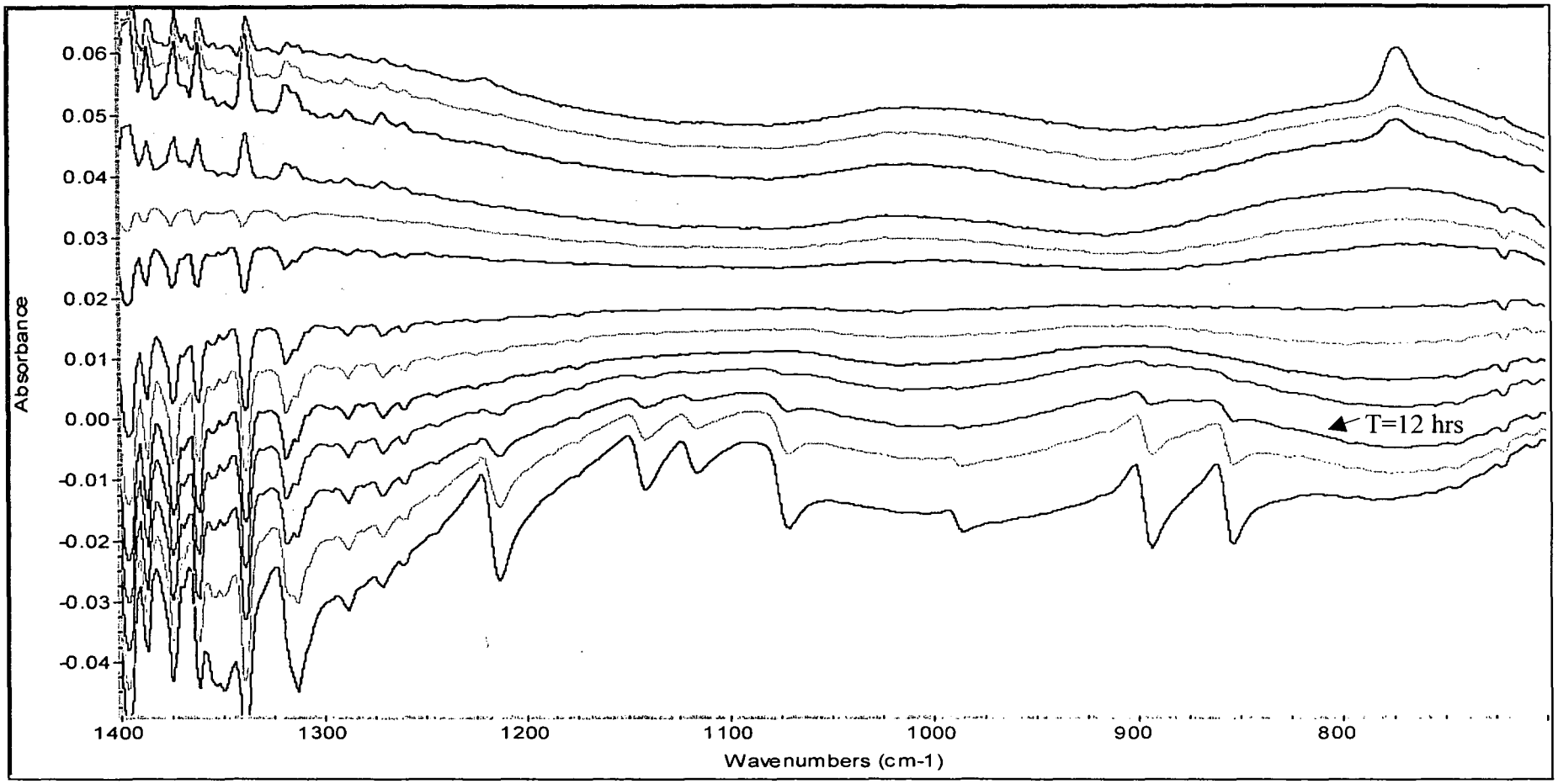

Fig. 4.17. External reflection FTIR spectra from 1400-700cm^{-1} for stearic acid spread on a 120% supersaturated dl-aspartic acid solution a compression surface pressure of 12 mN/m. Note the spectra have been offset for ease of comparison t=0-14hrs (t=0 at top).

4.3.2. Methyl Stearate :

Table 4.5. Important peaks of the FTIR spectra (see figs. 4.18 and 4.19) from 4000-650cm^{-1} for methyl stearate film spread on a 120% supersaturated solution of dl-aspartic acid at a compression surface pressure of 12.1 mN/m.

The Time of the Spectra Reading after Spreading the Film/(hour)							Assignment[37]
0	3	6	9.5	10	16	23	
				852	852	852	CH_2 rock for dl-aspartic acid
				892	892	892	CC stretch for dl-aspartic acid
				985	985	985	CC stretch for dl-aspartic acid
				1071	1071	1071	CN stretch for dl-aspartic acid
				1116	1116	1116	NH_3^+ rocking for dl-aspartic acid
				1141	1141	1142	NH_3^+ rocking for dl-aspartic acid
				1213	1213	1213	CH_2 twist for dl-aspartic acid
2850	2848	2851	2848	2847	2847	2848	CH_2 symmetric stretch for methyl stearate
2918	2917	2916	2916	2917	2916	2916	CH_2 asymmetric stretch for methyl stearate

Table 4.5

From the FTIR spectra (see fig. 4.18 and 4.19) and table 4.5 we can see that peaks due to dl-aspartic acid crystals first appeared ~10 hrs after spreading the film. Again from figs. 4.18, we can see an increase in intensity of the methylene stretches, which first occurs at ~ 10 hrs i.e. at the same time period at which the dl-aspartic acid crystalline peaks appear.

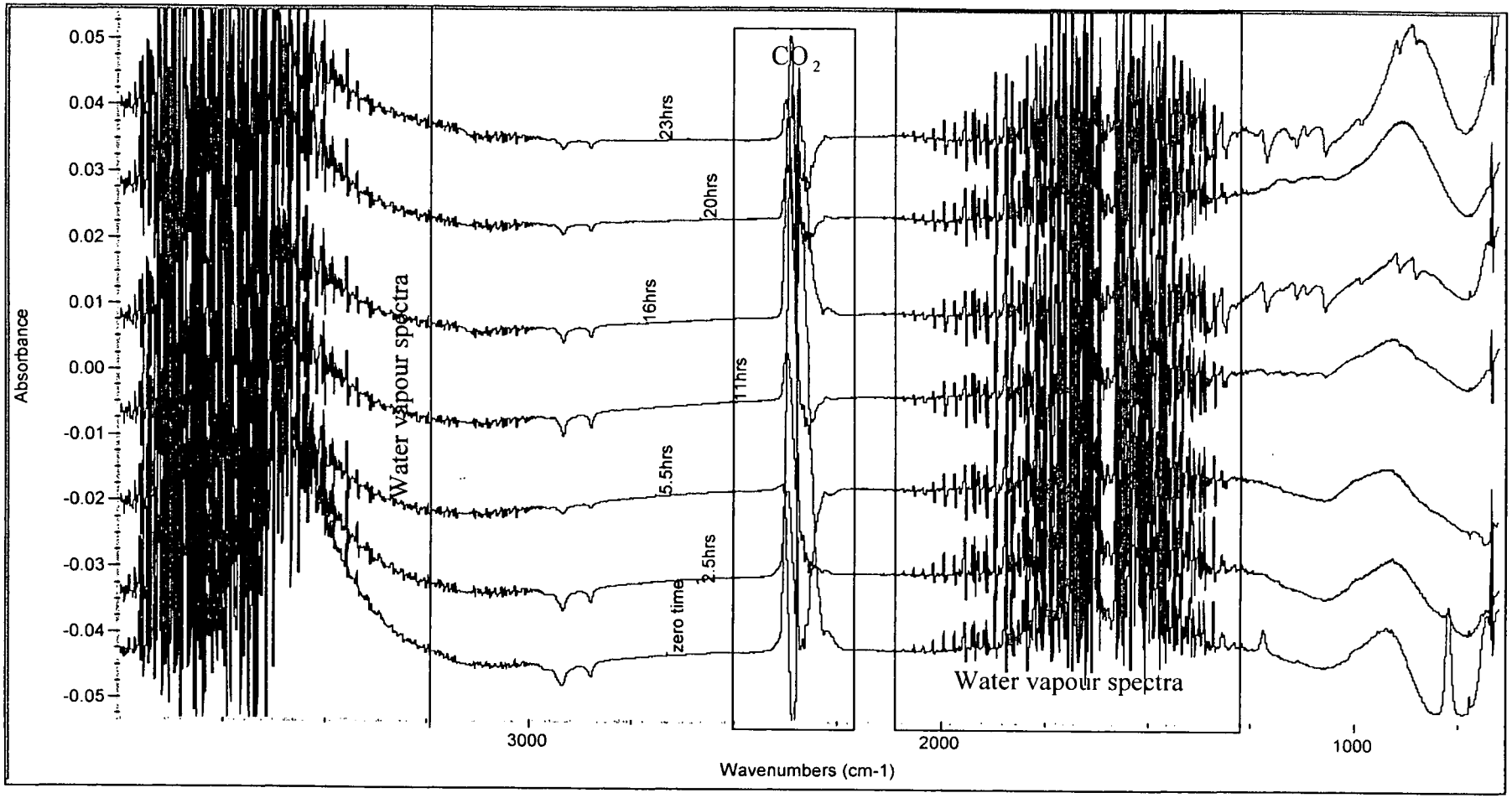

Fig. 4.18 External reflection FTIR spectra from 4000-650cm $^{-1}$ for methyl stearate spread on a 120% supersaturated solution of dl-aspartic acid solution at a compression surface pressure of 12.1 mN/m.

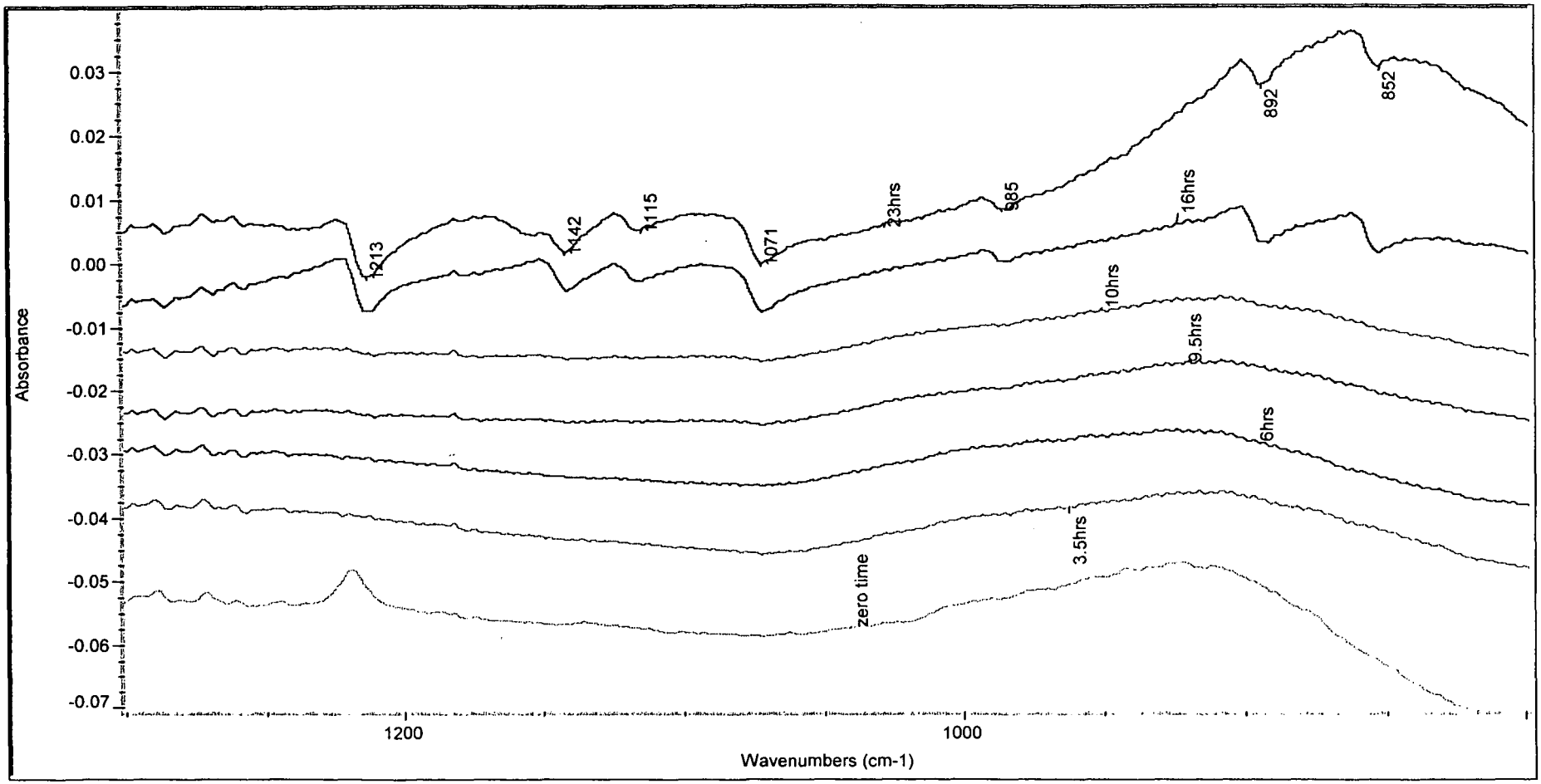

Fig. 4.19 External reflection FTIR spectra from 1300-800cm^{-1} for methyl stearate spread on a 120% supersaturated solution of dl-aspartic acid solution at a compression surface pressure of 12.1 mN/m.

3.3.3. l-tyrosine:

Table 4.6 Important peaks of the FTIR spectra (see figs. 4.20 and 4.21) from 4000-650cm^{-1} for l-tyrosine film spread on a 120% supersaturated solution of dl-aspartic acid at a compression surface pressure of 8.8 mN/m.

The Time of the Spectra Reading after Spreading the Film/(hour)						Assignment[37]
0	5.5	6	9	16	21.5	
		852	852	852	852	CH_2 rock for dl-aspartic acid
		894	894	894	894	CC stretch for dl-aspartic acid
		985	985	986	985	CC stretch for dl-aspartic acid
		1071	1071	1071	1071	CN stretch for dl-aspartic acid
		1115	1115	1115	1115	NH_3^+ rocking for dl-aspartic acid
		1141	1141	1141	1141	NH_3^+ rocking for dl-aspartic acid
		1213	1213	1213	1213	CH_2 twist for dl-aspartic acid
2850	2850	2850	2850	2850	2850	CH_2 symmetric stretch for l-tyrosine
2918	2918	2918	2918	2918	2918	CH_2 asymmetric stretch for l-tyrosine

Table 4.6

From the FTIR spectra (see figs. 4.20 and 4.21) and table 4.6 we can see that peaks due to dl-aspartic acid crystals first appeared ~6 hrs after spreading the film. However, it was noticed that the dl-aspartic acid peak intensities did not increase as much with time as for the other films, perhaps because the density of crystals was always small.

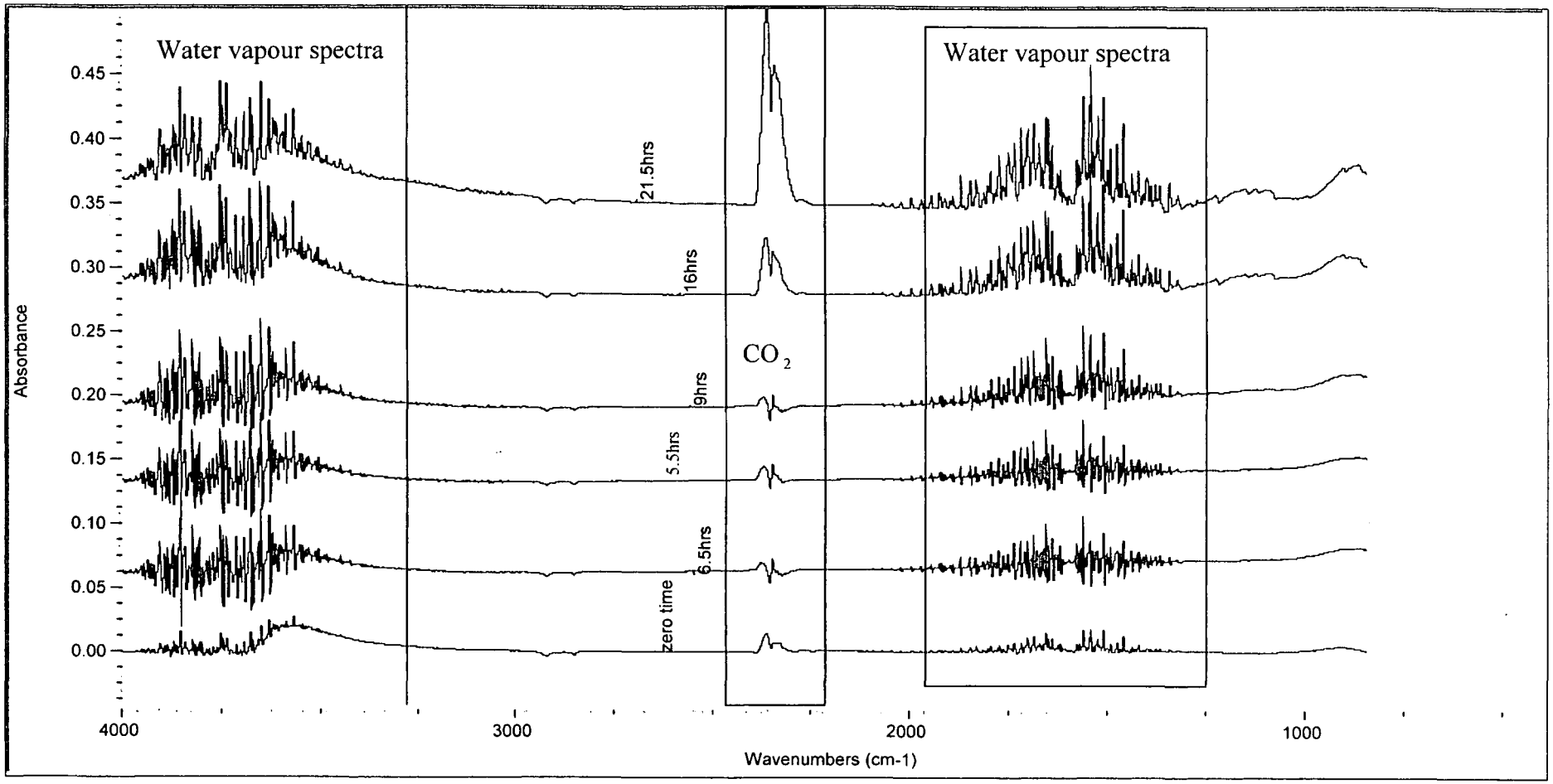

Fig.4.20 External reflection FTIR spectra from 4000-700cm^{-1} for l-tyrosine film on a 120% supersaturated solution of dl-aspartic acid at a compression surface pressure of 8.8 mN/m.

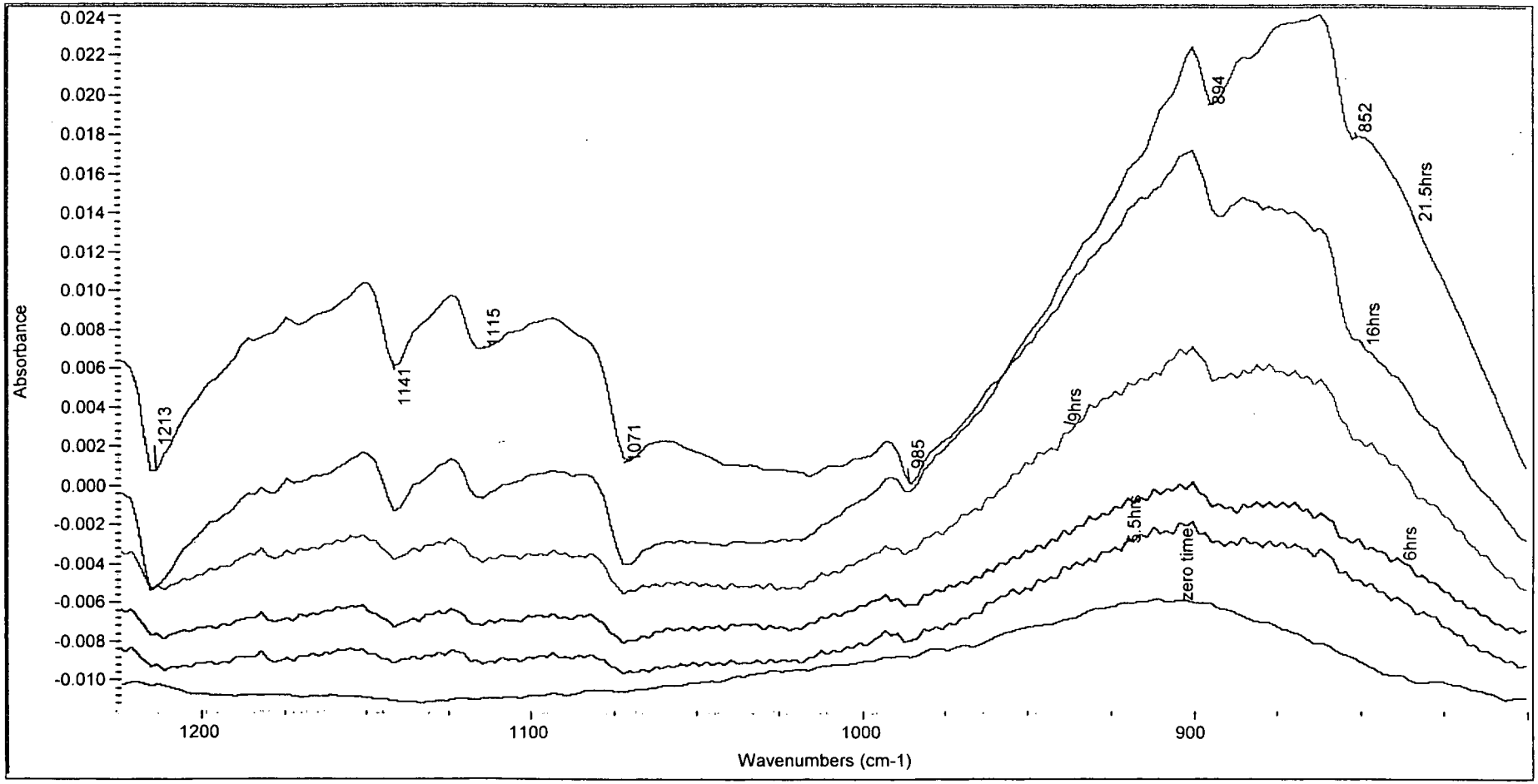

Fig. 4.21 External reflection FTIR spectra from 1220-800cm^{-1} for l-tyrosine film on a 120% supersaturated solution of dl-aspartic acid at a compression surface pressure of 8.8 mN/m.

4.3.4. Polycaprolactone:

Table 4.7. Important peaks of the FTIR spectra (see figs 4.22-4.24) from 4000-650cm^{-1} for polycaprolactone spread on a 120% supersaturated solution of dl- aspartic acid at a compression surface pressure of 15.4 mN/m.

The Time of Spectra Reading after Spreading the Film/(hour)						Assignment[37]
0	5	8	9	12	16	
			852	852	852	CH_2 rock for dl-aspartic acid
			892	892	892	CC stretch for dl-aspartic acid
			985	985	985	CC stretch for dl-aspartic acid
			1071	1071	1071	CN stretch for dl-aspartic acid
			1115	1115	1115	NH_3^+ rocking for dl-aspartic acid
			1141	1141	1141	NH_3^+ rocking for dl-aspartic acid
		1213	1213	1213	1213	CH_2 twist for dl-aspartic acid
2854	2854	2854	2854	2854	2854	CH_2 symmetric stretch for polycaprolactone (very weak)
2920	2920	2920	2920	2920	2920	CH_2 asymmetric stretch for polycaprolactone (very weak)
			3136	3136	3136	NH_3^+ asymmetric stretch for dl-aspartic acid

Table 4.7

From the FTIR spectra (see figs. 4.22 and 4.24) and table 4.7 we can see that peaks due to dl-aspartic acid crystals first appeared ~9 hrs after spreading the film. Unfortunately, peaks due to the monolayer film were very weak for polycaprolactone (see fig 4.23), so we couldn't observe changes when the dl-aspartic acid crystallised.

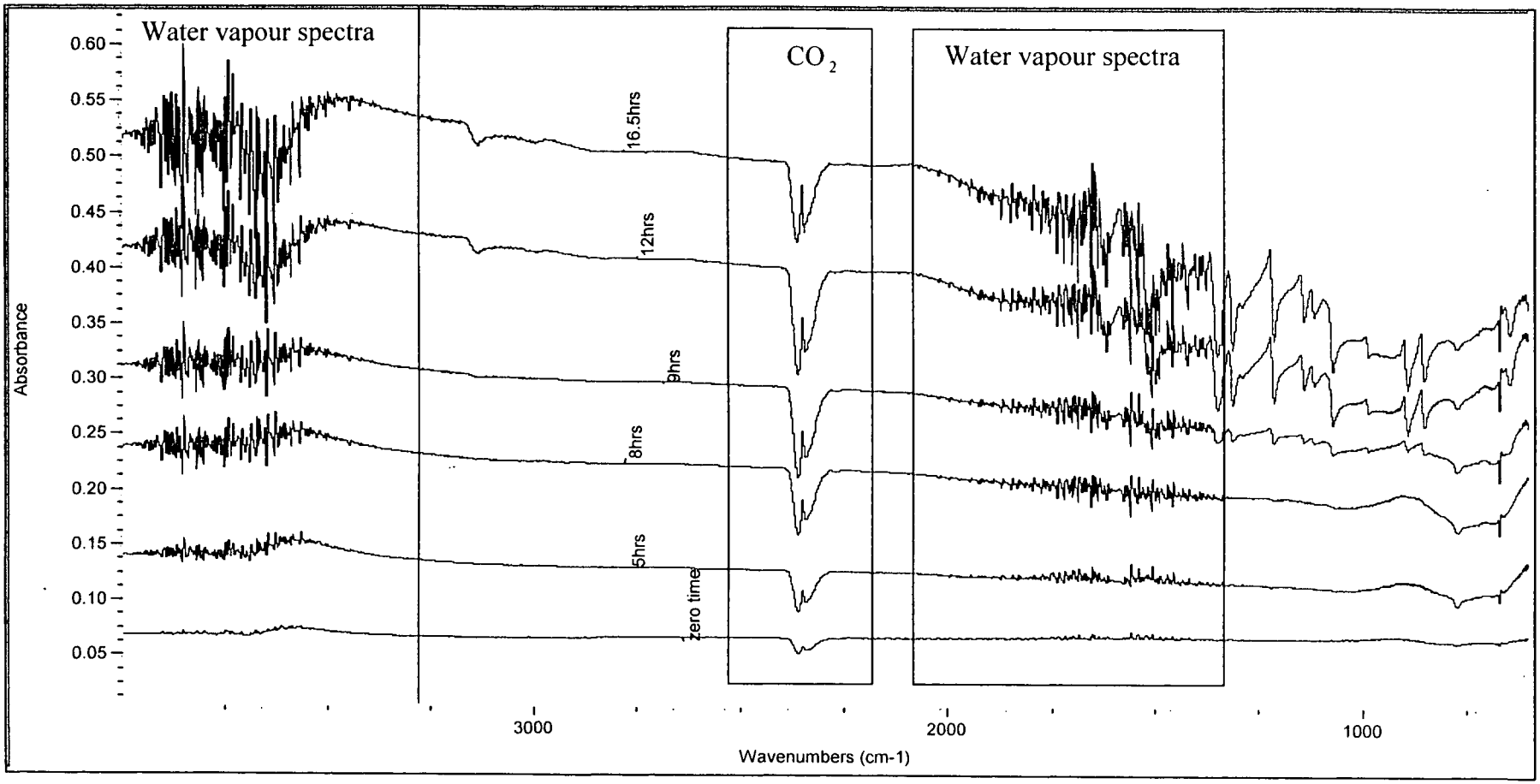

Fig. 4.22 External reflection FTIR spectra from 4000-650cm^{-1} for polycaprolactone spread on a 120% supersaturated solution of dl-aspartic acid at a compression surface pressure of 15.4 mN/m.

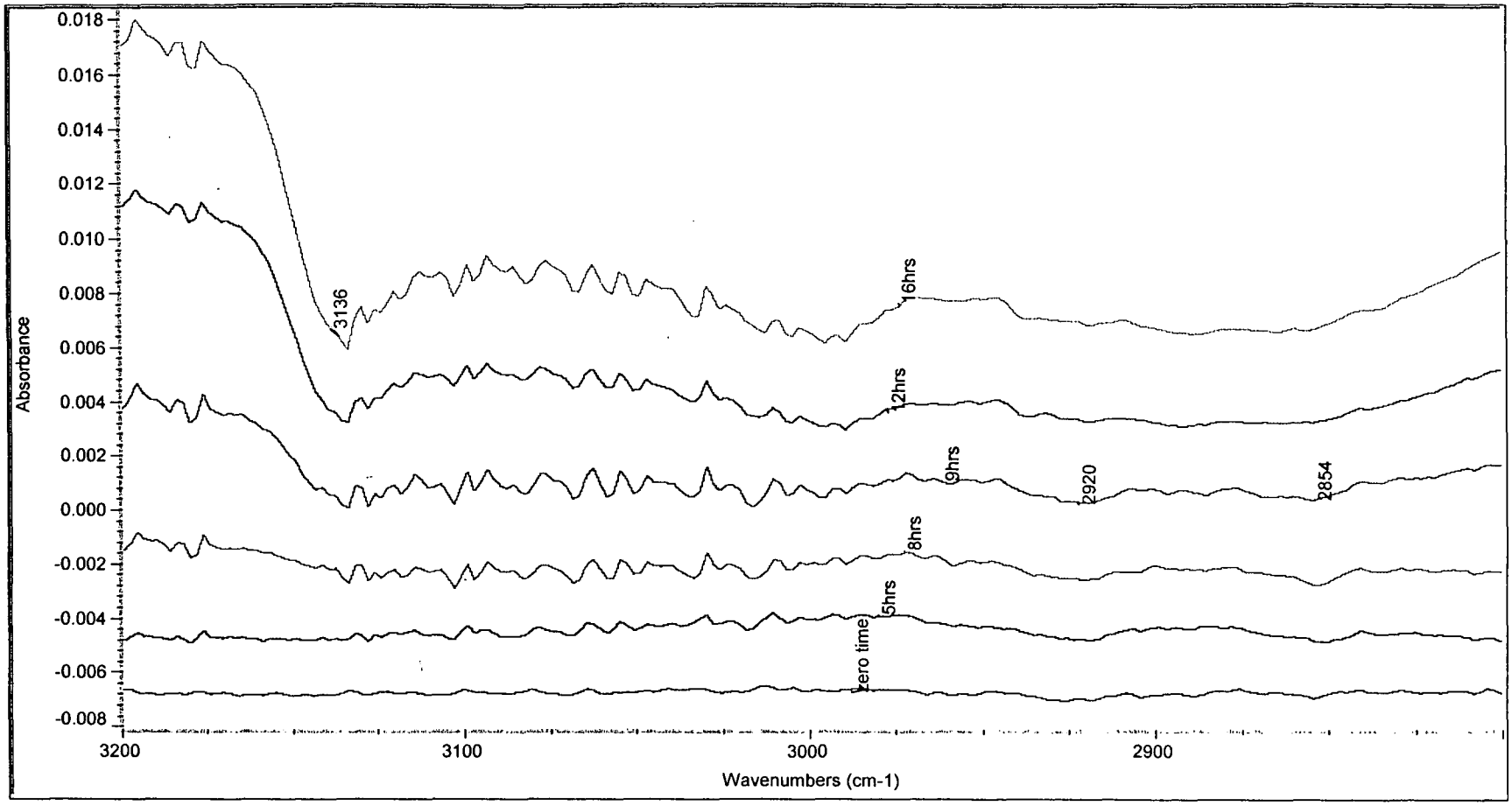

Fig. 4.23 External reflection FTIR spectra from 3200-2800cm^{-1} for polycaprolactone spread on a 120% supersaturated solution of dl-aspartic acid at a compression surface pressure of 15.4 mN/m.

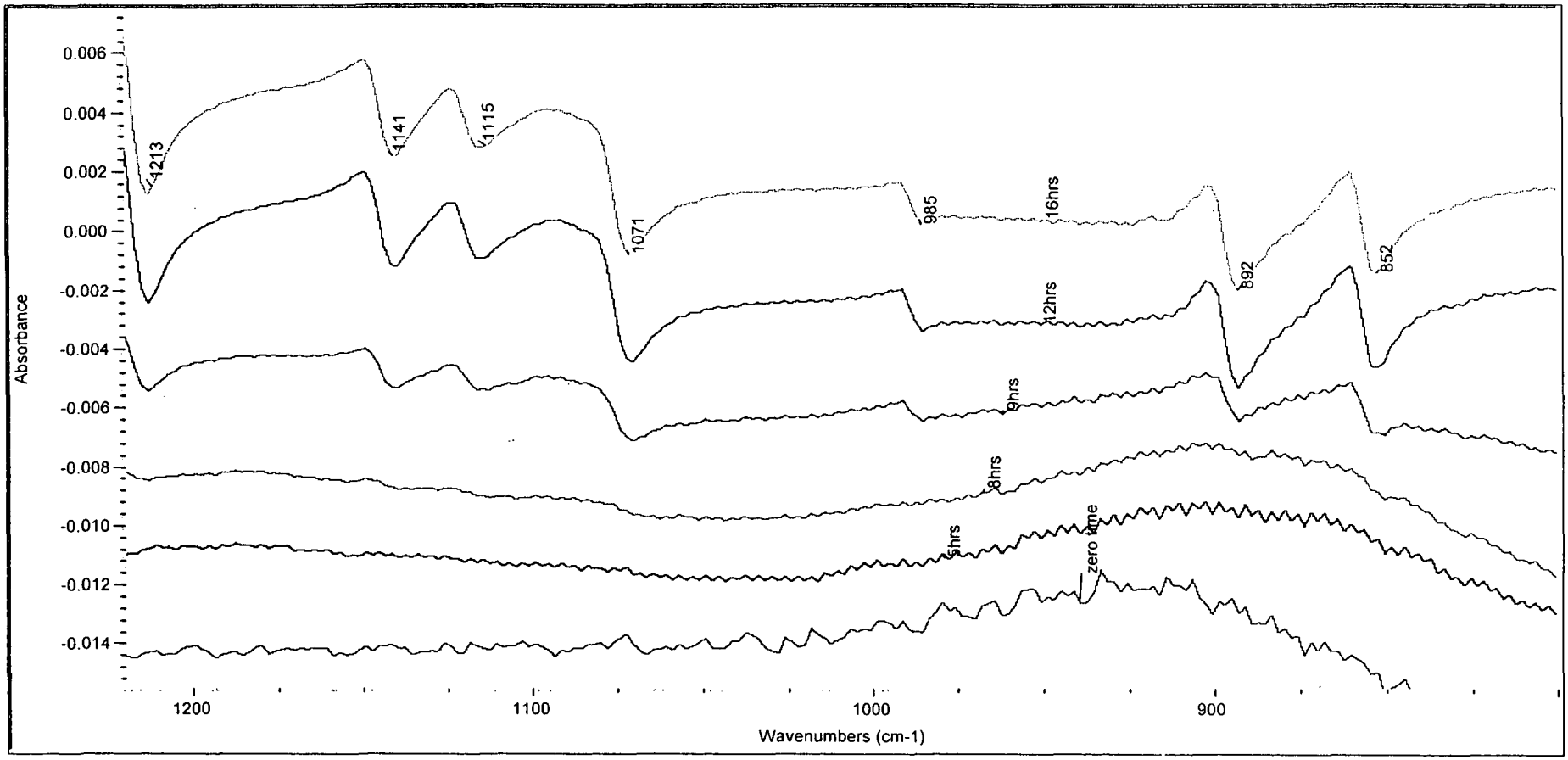

Fg. 4.24 External reflection FTIR spectra from 1220-800cm^{-1} for polycaprolactone spread on a 120% supersaturated solution of dl-aspartic acid at a compression surface pressure of 15.4 mN/m.

4.3.5. Poly-l-isoleucine:

Table 4.8 Important peaks of the FTIR spectrum (see figs. 4.25 and 4.26) from 4000-650cm^{-1} for poly-l-isoleucine film on a 120% supersaturated solution of dl-aspartic acid at a compression surface pressure of 11.6 mN/m.

The Time of Spectra Reading after Spreading the Film/(hour)						Assignment[37]
0	5	10	14	20	24	
			852	852	852	CH_2 rock for dl-aspartic acid
			895	895	895	CC stretch for dl-aspartic acid
			985	985	985	CC stretch for dl-aspartic acid (very weak)
			1071	1071	1071	CN stretch for dl-aspartic acid
			1115	1115	1115	NH_3^+ rocking for dl-aspartic acid
			1141	1141	1141	NH_3^+ rocking for dl-aspartic acid
			1213	1213	1213	CH_2 twist for dl-aspartic acid
2849	2848	2848	2848	2848	2848	CH_2 symmetric stretch for poly-l-isoleucine
2920	2917	2917	2917	2917	2917	CH_2 asymmetric stretch for poly-l-isoleucine
2962	2961	2960	2960	2960	2960	CH_3 asymmetric stretch for poly-l-isoleucine

Table 4.8

From the FTIR spectra (see figs. 4.25 and 4.26) and table 4.8 we can see that peaks due to dl-aspartic acid crystals first appeared ~14 hrs after spreading the film.

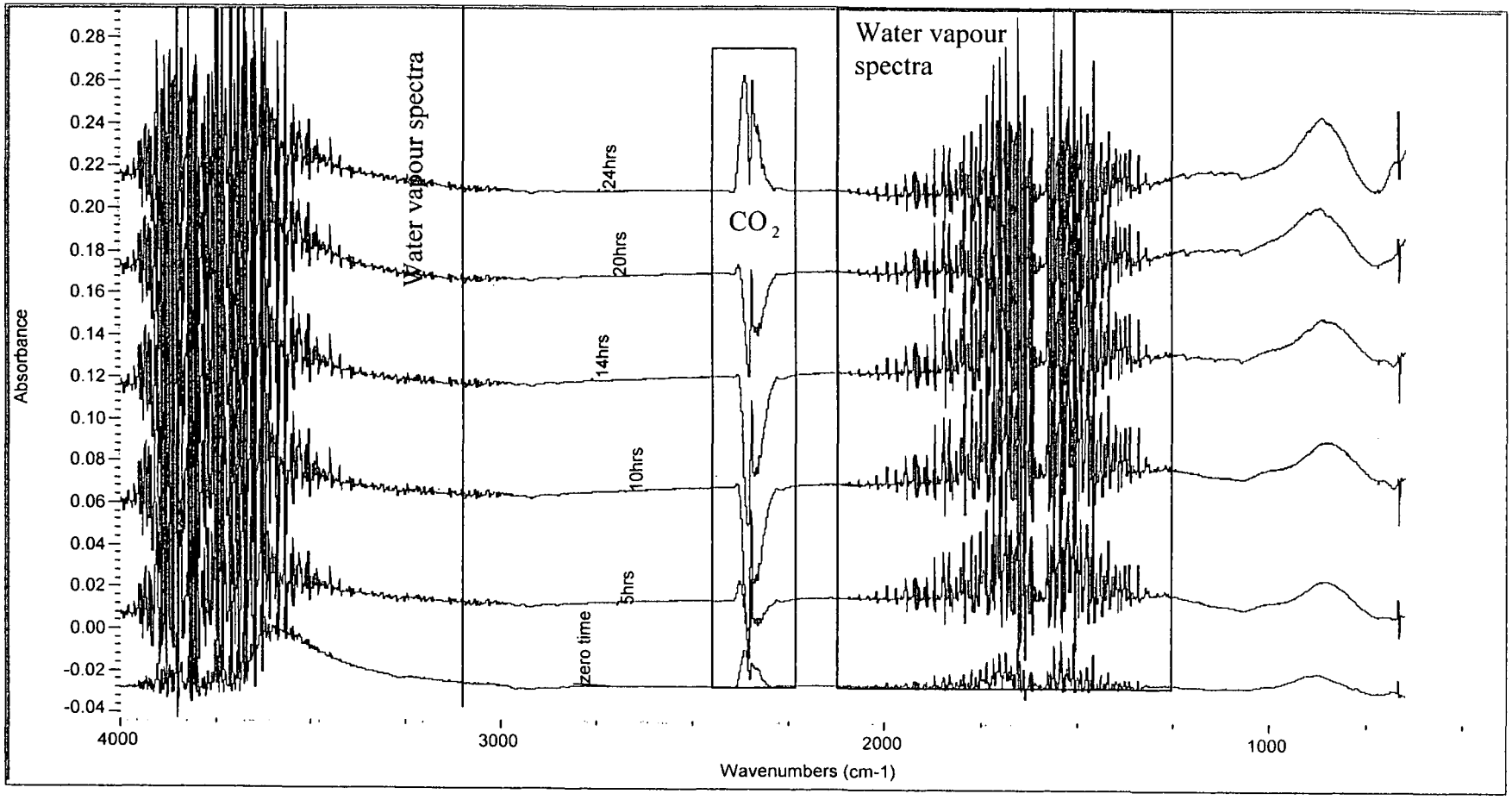

Fig. 4.25 External reflection FTIR spectra from 4000-650cm^{-1} for poly-l-isoleucine on a 120% supersaturated solution of dl-aspartic acid at a compression surface pressure of 11.6 mN/m.

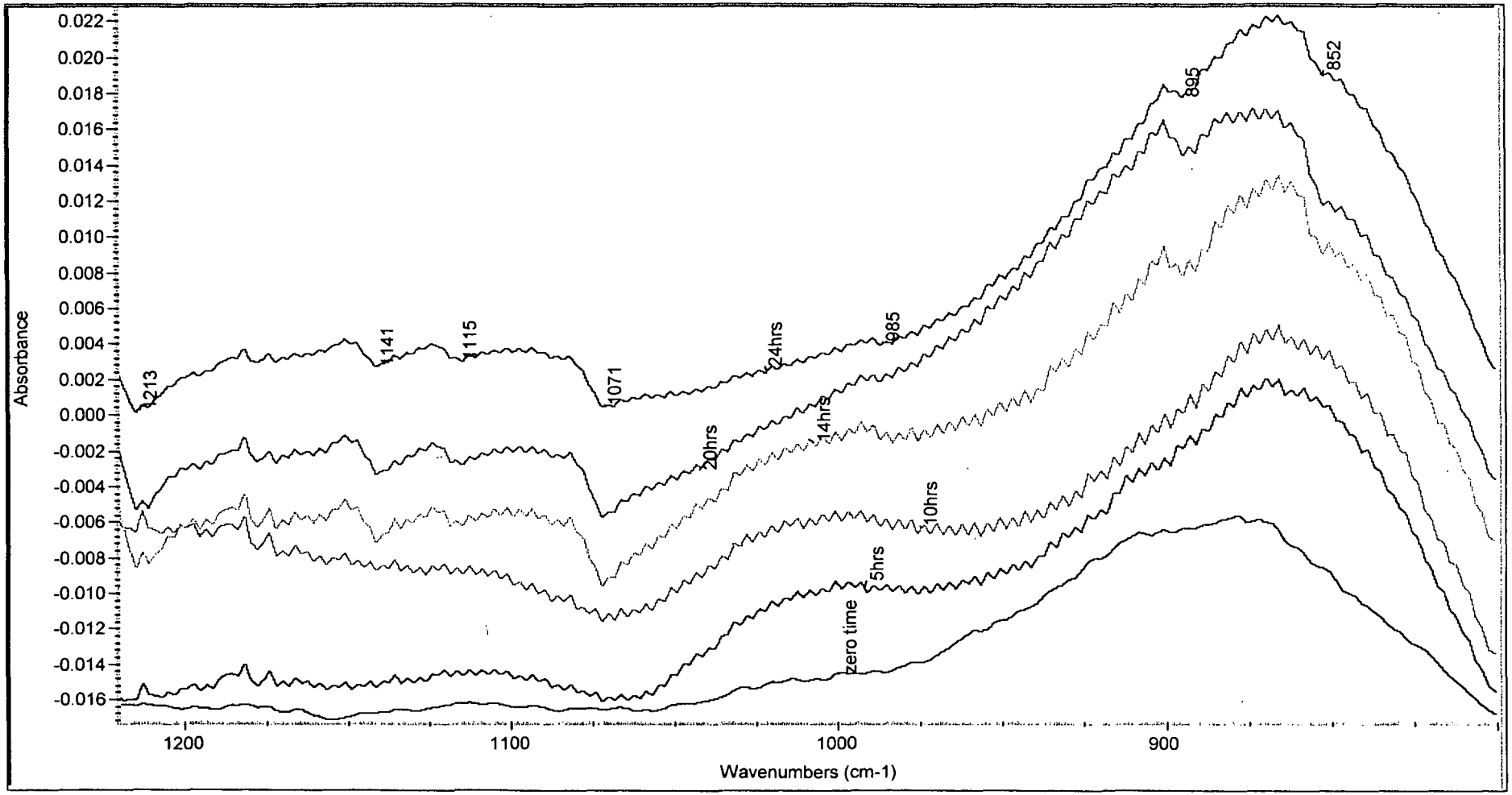

Fig. 4.26 External reflection FTIR spectra from 1220-800cm^{-1} for poly-l-isoleucine on a 120% supersaturated solution of dl-aspartic acid at a compression surface pressure of 11.6 mN/m.

4.3.6. Poly-γ-benzyl-l-glutamate:

Table 4.9. Important peaks of the FTIR spectra (see figs. 4.27 and 4.28) from 4000-650cm^{-1} for poly-γ-benzyl-l-glutamate on a 120% supersaturated solution of dl-aspartic acid at a compression surface pressure of 10.6 mN/m.

The Time of Spectra Reading after Spreading the Film/(hour)						Assignment [37]
0	4	9	12.5	16	19	
		852	852	852	852	CH_2 rock for dl-aspartic acid
		892	892	893	892	CC stretch for dl-aspartic acid
		985	985	985	985	CC stretch for dl-aspartic acid
		1071	1071	1071	1071	CN stretch for dl-aspartic acid
		1115	1115	1115	1115	NH_3^+ rocking for dl-aspartic acid
		1141	1141	1141	1141	NH_3^+ rocking for dl-aspartic acid
		1213	1213	1213	1213	CH_2 twist for dl-aspartic acid
2850	2850	2850	2850	2850	2850	CH_2 symmetric stretch for poly-γ-benzyl-l-glutamate
2916	2916	2917	2916	2917	2916	CH_2 asymmetric stretch for poly-γ-benzyl-l-glutamate
			3137	3137	3137	NH_3^+ asymmetric stretch for dl-aspartic acid

Table 4.9

From the FTIR spectra (see figs. 4.27 and 4.28) and table 4.9 we can see that peaks due to dl-aspartic acid crystals first appeared ~9 hrs after spreading the film.

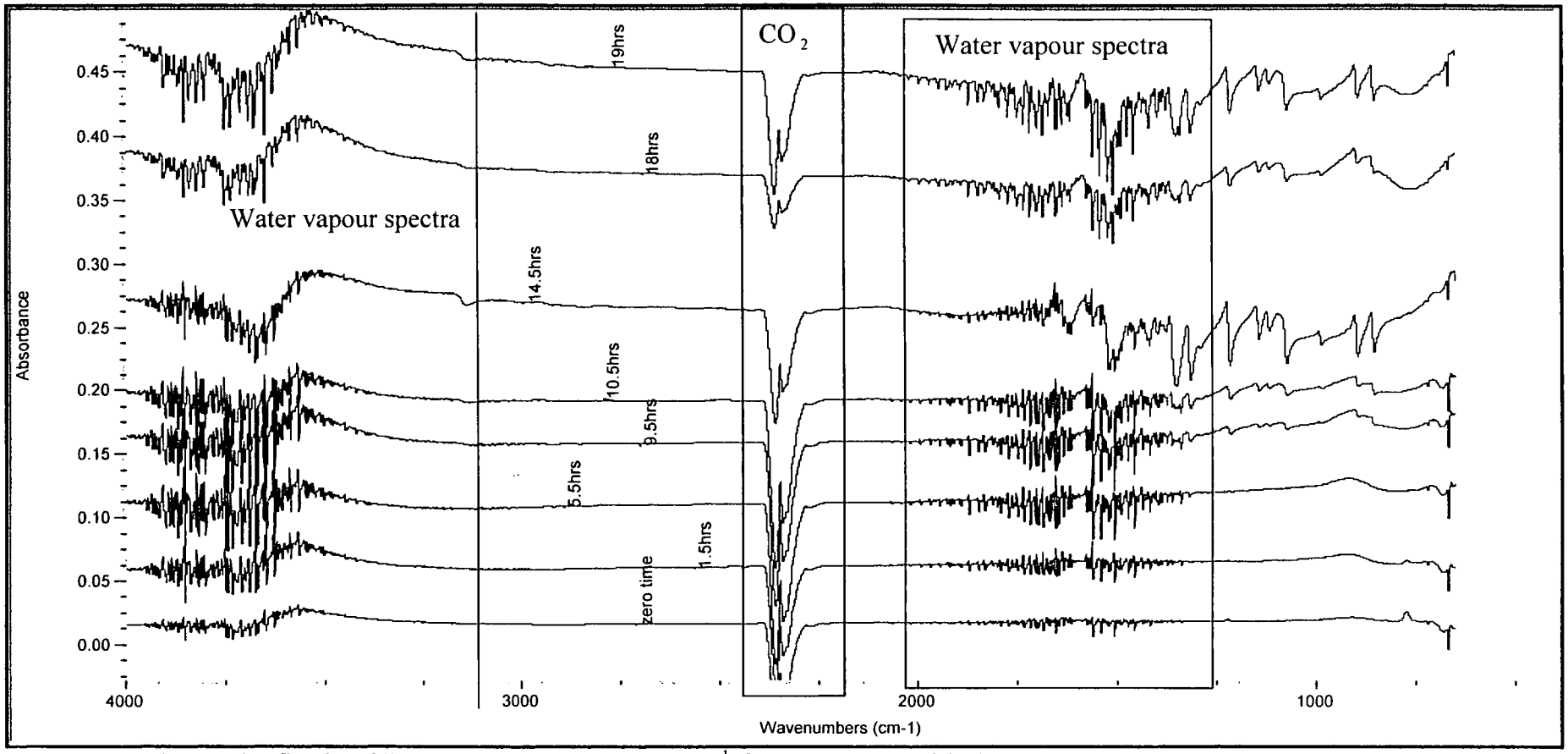

Fig. 4.27 External reflection FTIR spectra from 4000-650cm^{-1} for poly-γ-benzyl-l-glutamate on a 120% supersaturated solution of dl-aspartic acid at a compression surface pressure of 10.6mN/m.

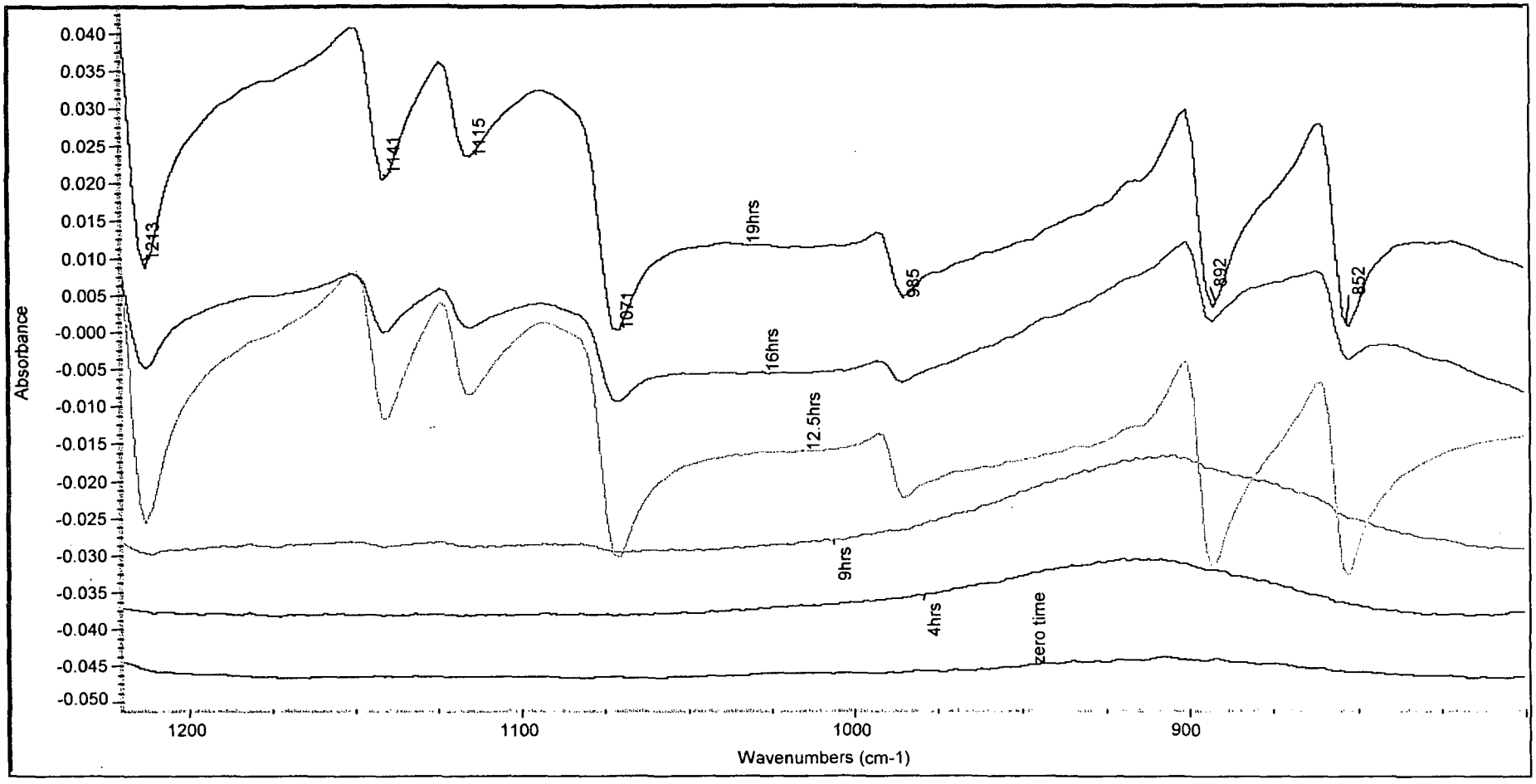

Fig. 4.28 External reflection FTIR spectra from 1220-800cm^{-1} for poly-γ-benzyl-l-glutamate on a 120% supersaturated solution of dl-aspartic acid at a compression surface pressure of 10.6mN/m.

4.3.7. Nylon 6 6:

Table 4.10 Important peaks of the FTIR spectrum (see figs. 4.29 and 4.30) from 4000-650cm^{-1} for nylon 6 6 spread on a 120% supersaturated dl-aspartic acid.

The Time of Spectra Reading after Spreading the Film/(hour)						Assignment [37]
0	7	9	12	19	23	
		854	854	854	854	CH_2 rock for dl-aspartic acid
		893	893	893	893	CC stretch for dl-aspartic acid
		985	985	985	985	CC stretch for dl-aspartic acid
		1071	1071	1071	1071	CN stretch for dl-aspartic acid
		1115	1115	1115	1115	NH_3^+ rocking for dl-aspartic acid
		1142	1142	1142	1142	NH_3^+ rocking for dl-aspartic acid
		1212	1212	1212	1212	CH_2 twist for dl-aspartic acid
2849	2849	2849	2849	2849	2849	CH_2 symmetric stretch for nylon 6 6 (very weak)
2916	2916	2916	2916	2916	2917	CH_2 asymmetric stretch for nylon 6 6 (very weak)
				3137	3137	NH_3^+ asymmetric stretch for dl-aspartic acid

Table 4.10

From the FTIR spectra (see figs 4.29 and 4.30) and table 4.10 we can see that peaks due to dl-aspartic acid crystals first appeared ~9 hrs after spreading the film. Unfortunately, the surface pressure was not measured for this experiment.

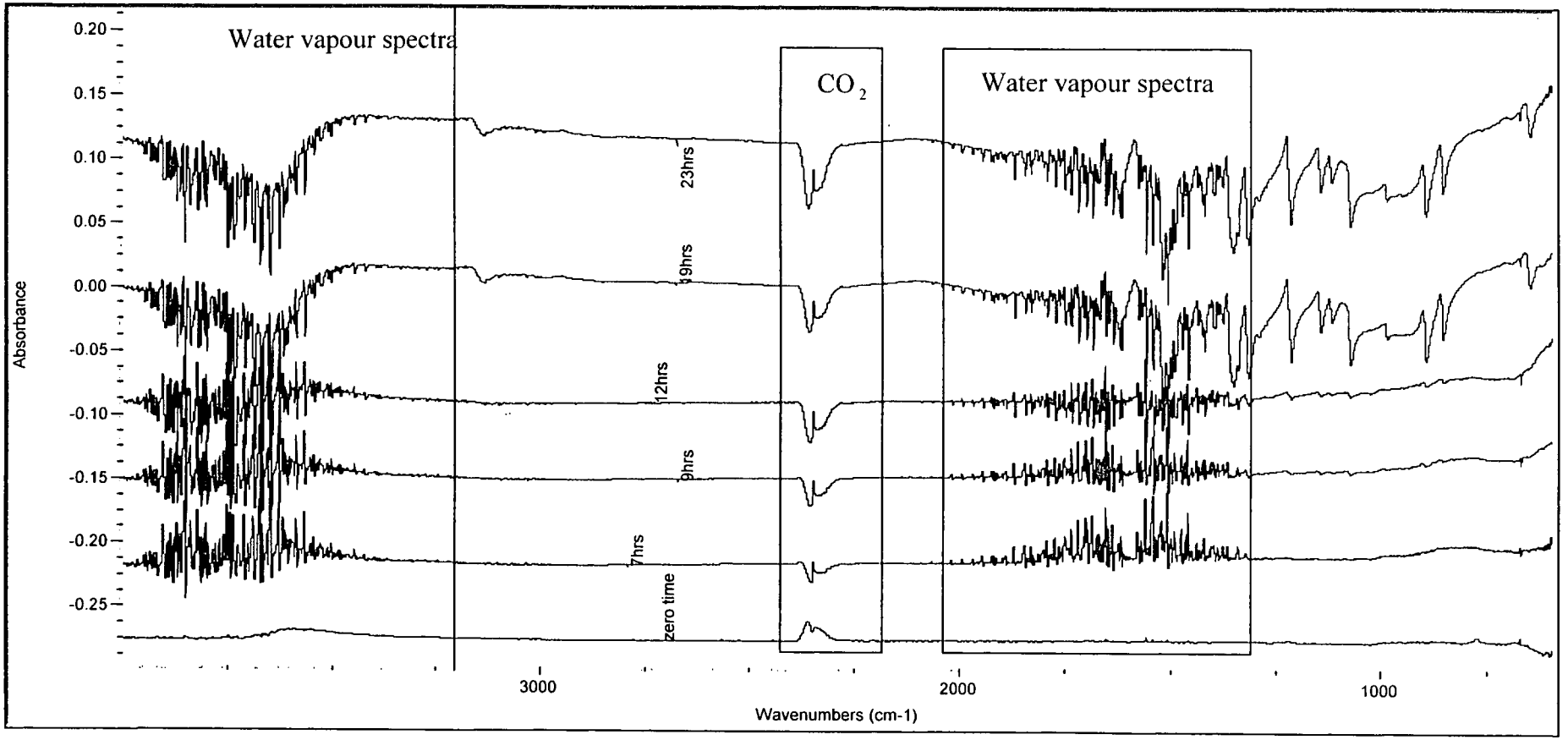

Fig. 4.29 External reflection FTIR spectra from 4000-650cm^{-1} for nylon 6 6 spread on a 120% supersaturated dl-aspartic acid solution.

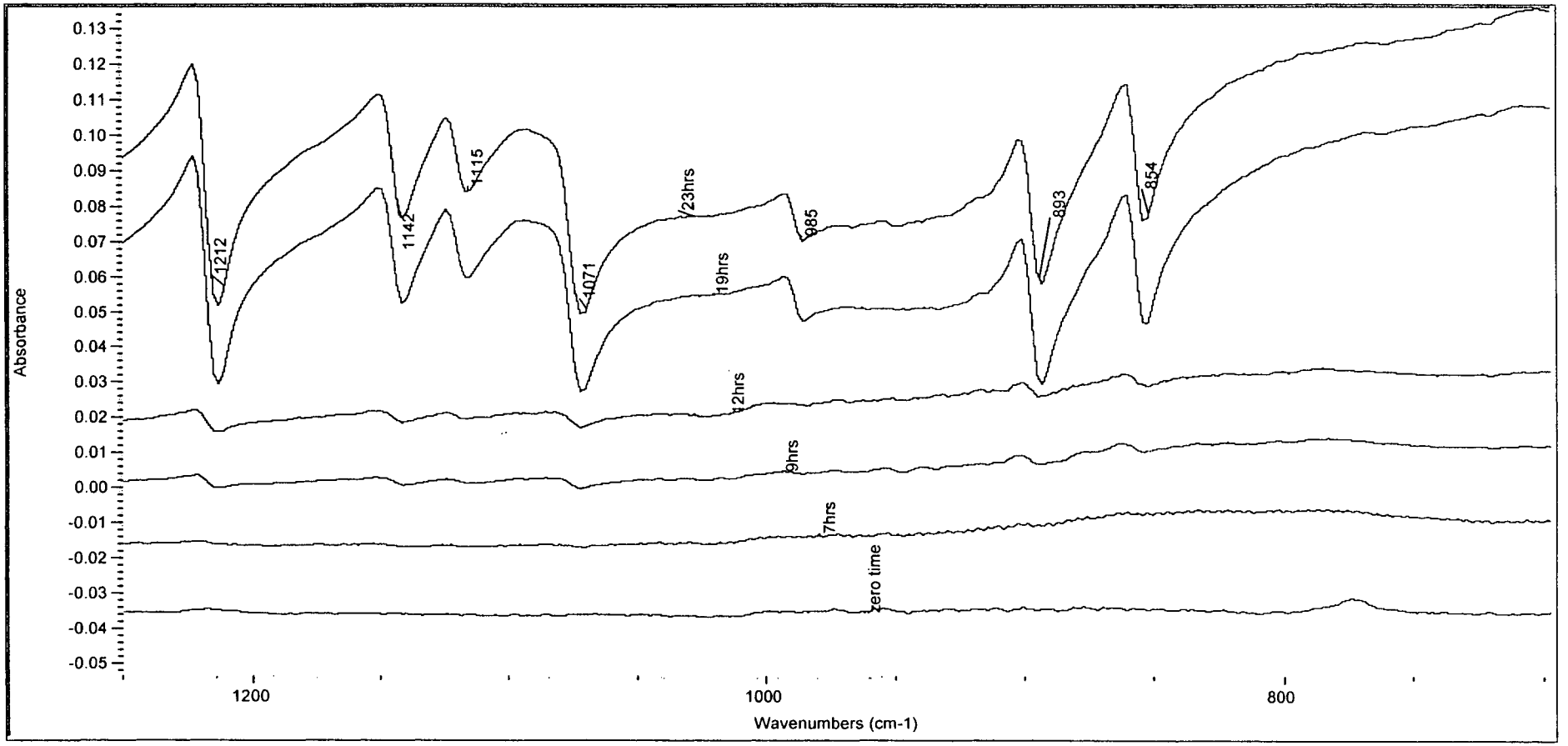

Fig. 4.30 External reflection FTIR spectra from 1220-700cm^{-1} for nylon 6 6 spread on a 120% supersaturated dl-aspartic acid solution.

4.3.8. Nylon 6 6 (spread from toluene-phenol solvent):

Table 4.11. Important peaks of the FTIR spectra (see figs. 4.31-4.33) from 4000-650 cm^{-1} for nylon 6 6 spread from toluene and phenol, on a 120% supersaturated dl-aspartic acid at a compression surface pressure of 12 mN/m.

The Time of Spectra Reading after Spreading the Film/(hour)						Assignment [37]
0	3	5	9	15	19	
		852	852	852	852	CH_2 rock for dl-aspartic acid
		983	983	983	983	CC stretch for dl-aspartic acid
		985	985	985	985	CC stretch for dl-aspartic acid
		1071	1071	1071	1071	CN stretch for dl-aspartic acid
		1115	1115	1115	1115	NH_3^+ rocking for dl-aspartic acid
		1141	1141	1141	1141	NH_3^+ rocking for dl-aspartic acid
		1212	1212	1212	1212	CH_2 twist for dl-aspartic acid
		2860	2860	2860	2860	CH_2 symmetric stretch for nylon 6 6
		2873	2873	2873	2873	CH_2 symmetric stretch for nylon 6 6
		2943	2940	2936	2937	CH_2 asymmetric stretch for nylon 6 6
		3137	3137	3137	3137	NH_3^+ asymmetric stretch for dl- aspartic acid
		3307	3307	3307	3307	NH stretch for nylon 6 6

Table 4.11

From the FTIR spectra (see figs. 4.31 and 4.33) and table 4.11 we can see that peaks due to dl-aspartic acid crystals first appeared ~5 hrs after spreading the film. Interestinly, for this film we saw the dramatic appearance of film peaks at 3307 cm^{-1} due to NH stretching and at 2890, 2873 and 2943 cm^{-1} due to CH_2 stretching when the dl-aspartic acid crystallised (see fig. 4.32). We also attribute this to film reorganisation. The NH and CH_2 groups of the nylon 6 6 film become more parallel to the surface and hence we suddenly see peaks due to these groups. Further experiments would be required to determine whether the difference between this and the previous nylon 6 6 spectra was due to the different film spreading solvent (which seems unlikely), or due to the different surface pressure in the two experiments.

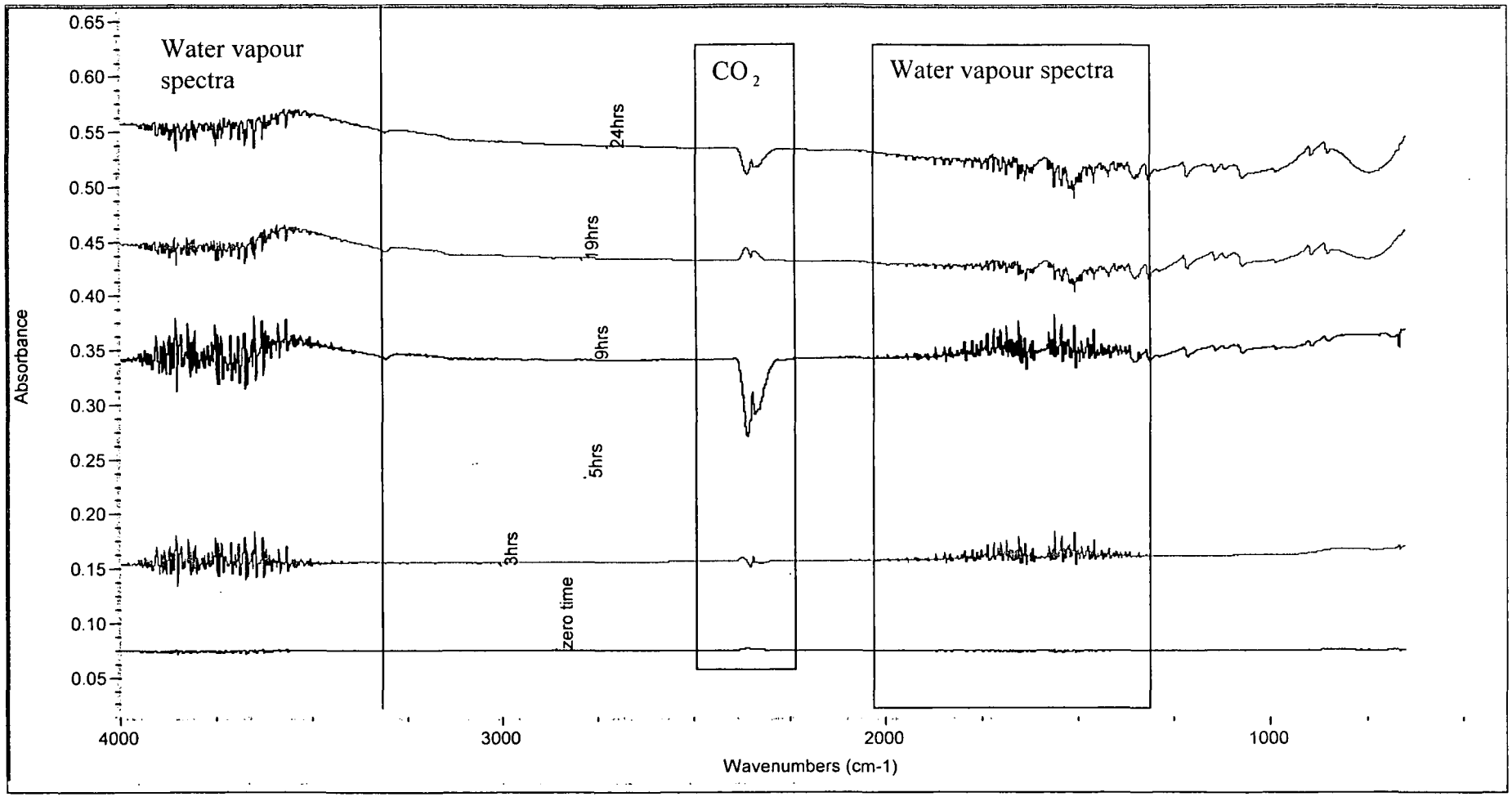

Fig. 4.31 External reflection FTIR spectra from 4000-650cm^{-1} of nylon 6 6 spread from toluene-phenol on a 120% supersaturated dl-aspartic acid solution at a compression surface pressure of 12mN/m.

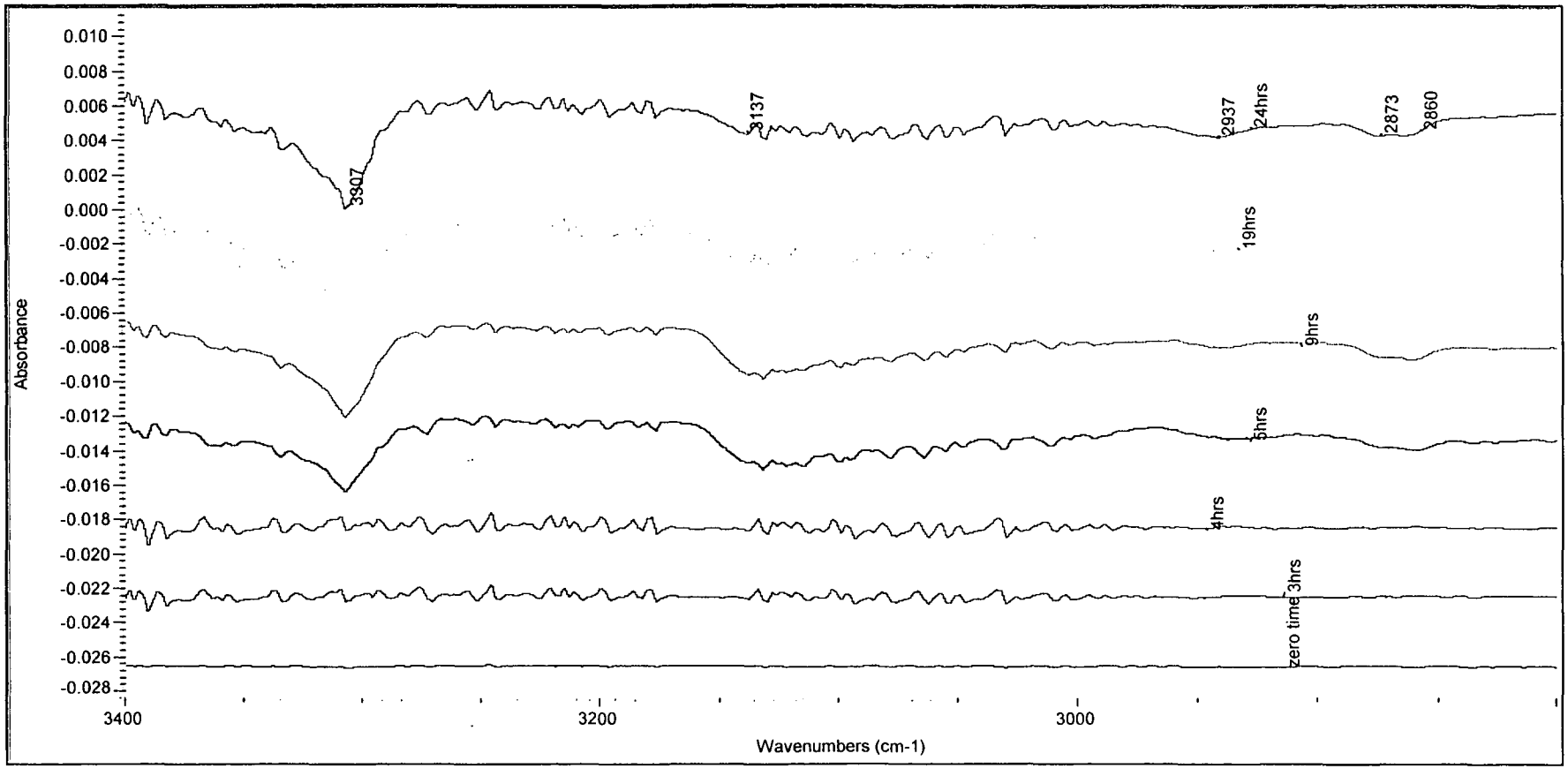

Fig. 4.32 External reflection FTIR spectra from 3400-2800cm^{-1} of nylon 6 6 spread from toluene-phenol on a 120% supersaturated dl-aspartic acid solution at a compression surface pressure of 12mN/m.

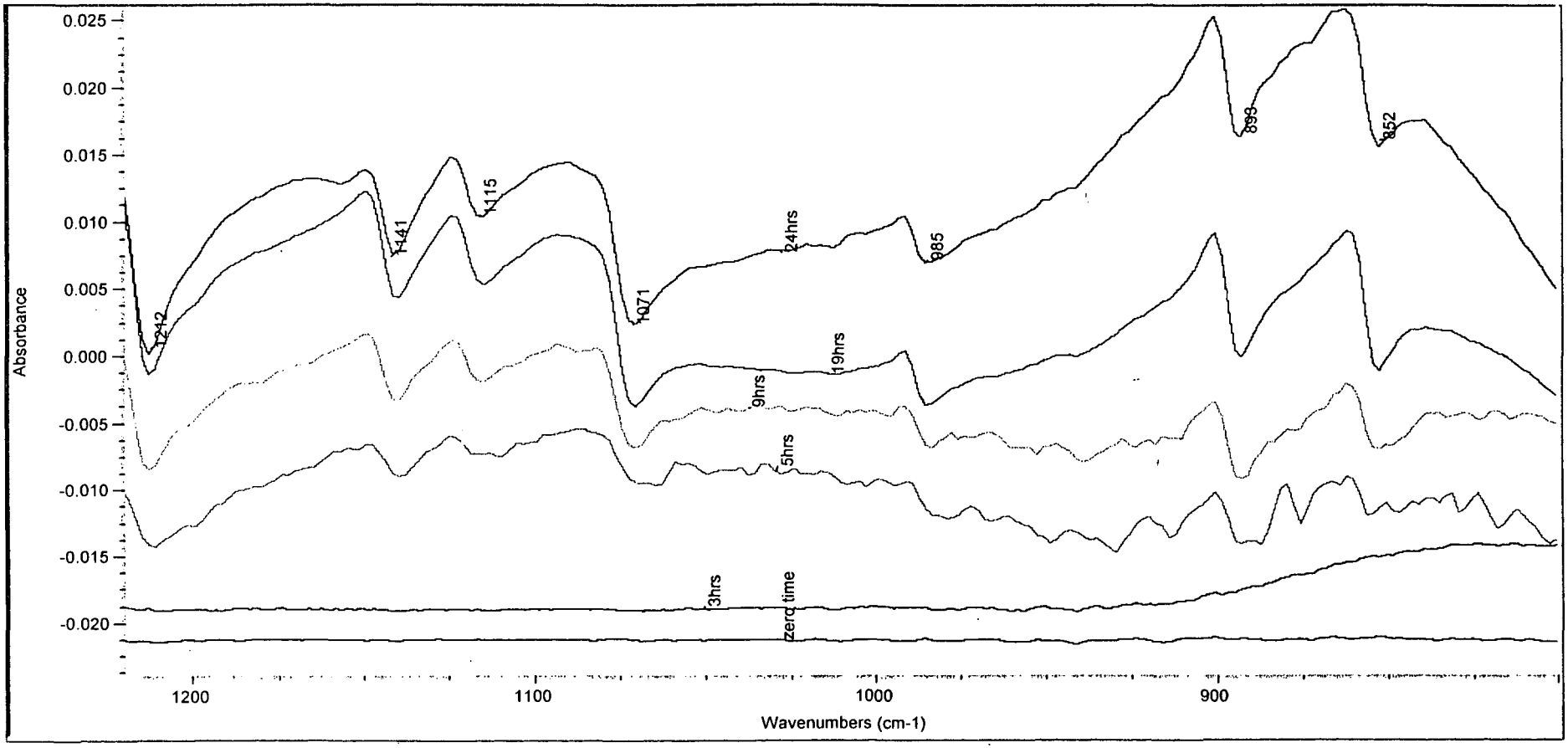

Fig.4.33 External reflection FTIR spectra from 1220-800cm^{-1} for nylon 6 6 spread from toluene-phenol on a 120% supersaturated dl-aspartic acid solution at a compression surface pressure of 12mN/m.

4.4. Conclusion:

We can conclude from this chapter the following results, summarised in the table below:

Film material	*Crystals faces*			*The approximate time of crystallisation from FTIR results*
	Main	Some	Few	
Stearic acid	$\{\bar{1}11\}$ & {110}	-	-	12hrs *
Methyl stearate	{110}	$\{\bar{1}11\}$	$\{\bar{2}02\}$	10hrs *
l-trysine	$\{\bar{1}11\}$	{110} & $\{\bar{2}02\}$	{200}	6hrs
Polycaprolactone	$\{\bar{1}11\}$ & {110}	$\{\bar{2}02\}$	{200}	9hrs
Poly-l-isoleucine	{110}	$\{\bar{1}11\}$	$\{\bar{2}02\}$	14hrs
Poly-γ-benzyl-l-glutamate	{110} & $\{\bar{1}11\}$	$\{\bar{2}02\}$	{200}	9hrs
Nylon 6 6	{110}	$\{\bar{1}11\}$ & $\{\bar{2}02\}$	{200}	9hrs
Nylon 6 6 (spread from toluene-phenol solution)	-			5 hrs *

Table 4.12

* Evidence of film reorganisation upon dl-aspartic crystallisation.

CHAPTER 5
CONCLUSION

From the results of this thesis, we can conclude that the polymeric spread films were better than small molecule films at nucleating dl-aspartic acid. The best polymeric films were polycaprolactone and nylon 6 6, and the best conditions were obtained at 120% supersaturation and under a medium compression surface pressure. In polycaprolactone the crystals typically grew in lines or groups, the average crystal length in the 120% supersaturated system was between 0.13 mm and 0.4 mm. I found that the main crystal faces of dl-aspartic acid growing beneath the polycaprolactone film were the $\{\bar{1}11\}$ and $\{110\}$ faces. The faces were identified using the Ceruis morphology module. The external reflection FTIR results showed that the polycaprolactone film nucleated dl-aspartic acid 9 hours after spreading. In nylon 6 6, the crystals also typically grew in lines or groups. The average crystal length in the 120% supersaturated system was between 0.1 mm and 0.26 mm. The main crystal face found was the $\{1\ 1\ 0\}$. From the external reflection FTIR I found that nylon spread from TFA-chloroform solvent could nucleate the dl-aspartic acid 9 hours after spreading, but nylon 6 6 spread from toluene-phenol solvent nucleated the dl-aspartic acid in a shorter time, i.e. 6 hours after spreading, as with the l-tyrosine film. The l-tyrosine film is good at nucleating dl-aspartic acid but not as good as nylon and polycaprolactone. The stearic acid film was very poor at nucleating the dl-aspartic acid compared with the other films. The crystal length in the 120% supersaturated system of between 0.1 mm and 0.2 mm. The main crystal faces found were the $\{\bar{1}11\}$ and $\{110\}$ faces. The external reflection FTIR results showed that the stearic acid film nucleated dl-aspartic acid 12 hours after spreading. The poly-l-isoleucine was the slowest film for nucleating dl-aspartic acid, as shown by the external reflection FTIR results, since it nucleated dl-aspartic acid 14 hours after spreading. We found that the concentration of the poly-l-isoleucine film affects its ability at nucleating dl-aspartic acid. However it was better at nucleating dl-aspartic acid than the stearic acid film. The average crystal length in the 120% supersaturated system was between 0.1 mm and 0.3 mm. The main crystal face found was the $\{110\}$ face. The methyl stearate film and the poly-γ-benzyl-l-glutamate were better at nucleating dl-aspartic acid than the stearic acid film and they nucleated

Film materials	*Ability of the film at nucleating dl-aspartic acid*	*Best compression surface pressure at nucleating the dl-aspartic acid*	*The main crystal faces*	*Average crystal length in 120% supersaturated system*	*The approximate nucleation time from FTIR data*
Stearic acid	Very poor at nucleating the dl-aspartic acid compared with other films in this table. The crystals were always few and tiny, see fig.3.4 .	16-30 mN/m	$\{\bar{1}11\}$ & {110}	0.1-0.2 mm	12 hrs *
Methyl stearate	Good at nucleating dl-aspartic acid. The results suggest that the methyl stearate is better than stearic acid, see fig 3.5	~20m N/m	{110}	0.1-0.2 mm	10 hrs *
l-tyrosine	Good at nucleating dl-aspartic acid, see fig. 3.6.	12-25 mN/m	$\{\bar{1}11\}$	0.2-0.3 mm	6 hrs
Polycaprolactone	Very good at nucleating dl-aspartic acid. The crystals typically grew in lines or groups, see fig.3.7 a & b.	14-16 mN/m	$\{\bar{1}11\}$ & {110}	0.13-0.4 mm	9 hrs
Poly-l-isoleucine	Good at nucleating dl-aspartic acid. The concentration of the film affects the ability of this film. See fig.3.10 a & b	The compression surface pressure was not a strong effect	{110}	0.1-0.3 mm	14 hrs
Poly-γ-benzyl-l-glutamate	Good at nucleating dl-aspartic acid, see fig 3.11.	10-20 mN/m	{110} & $\{\bar{1}11\}$	0.1-0.2 mm	9 hrs
Nylon 6 6	Very good at nucleating dl-aspartic acid. The crystals typically grew in lines or groups, see fig 3.12 a & b	Only low pressures studied ~4-7 mN/m	{110}	0.1-0.26 mm	5-9hrs *

Table 5.1 * evidence of film reorganisation during the crystallisation process.

dl-aspartic acid 9 to 10 hours after spreading. These results are summarised in the table 5.1. It was found that external reflection FTIR was a good method of studying films induced crystallisation since peaks due to both the film and dl-aspartic acid crystals can be observed. From the FTIR spectra, it appeared that film reorganisation occurred during dl-aspartic acid crystallisation for the stearic acid, methyl stearate and nylon 6 6 films. We believe this shows that the film is reorganising so as to maximise its interaction with the growing dl-aspartic acid crystals.

For further study, we suggest the following:

- Investigate the effects of the poly-l-isoleucine spreading solution concentration at nucleating dl-aspartic acid.
- Study the crystallisation of dl-aspartic acid beneath nylon 6 6 spread from phenol- toluene solvent.
- Determine the reason for the differences in the FTIR data between nylon 6 6 spread from TFA-chloroform solvent and that spread from toluene-phenol solvent.
- Perform more external reflection FTIR studies to determine whether film reorganisation occurred for any of the other films.

In addition, the experiments could be improved by having saturated water vapour atmospheres, so that water evaporation from the troughs was minimised.

References

1. E. M. Landau, M Levanon, L. Leiserowitz, M. Lahav, J. Sagiv, *Nature*, **318**, 353-356 (1985)
2. E. M. Landau, S. Grayer Wolf, M. Levanon, L. Leiserowitz, M. Lahav, J. Sagiv, *J. Am. Chem. Soc.*, **111**, 1436-1445 (1989)
3. M. Lahav, I. Weissbuch, F. Frolow, L. Leiserowitz, *J. Am. Chem. Soc.*, **112**, 7718 (1990)
4. M. Lahav, I. Weissbuch, G. Berkovice, L. Leiserowitz, *J. Am. Chem. Soc.*, **112**, 5874 (1990)
5. M. Lahav, R. Popovitz-Biro, L. Leiserowitz, *J. Am. Chem. Soc.*, **113**, 8943 (1991)
6. S. J. Cooper, *Nucleation Beneath Monolayer Film,* Doctoral Thesis, Univ. Bristol (1993)
7. S. J. Cooper, R. B. Sessions, S. D. Lubetkin, *J. Am. Chem. Soc.*, **120**, 2090-2098 (1998).
8. S. J. Cooper, R. B. Sessions, S. D. Lubetkin, *Langmuir*, **13**, 7165-7172 (1997)
9. D. J. Ahn, A. Berman, D. Charych,, *J. Phys. Chem. Soc,* **100**, 12455-12461 (1996).
10. P. Hartman, ed., by P. Bennema, *Crystal Growth: an introduction.* North Holland publ. Co. (1973) p343
11. I. V Markov, *Crystal Growth For Beginners.* World Scientific Publishing Co., Singapore. (1996) p3
12. P. Hartman, ed., by S. Toschev, *Crystal Growth: an introduction.* North-Holland publ. (1973). p10
13. I. V. Markov, *Crystal Growth For Beginners.* World Scientific Publishing Co. Singapore (1996) p43
14. R. Docherty, G. Clydesdale, K. J. Roberts, P. Bennema, *J. Phys. D: Appl. Phys.*, **24**, 89 (1991)
15. P. Hartman, P. Bennema, *J. Cryst. Growth,* **49**, 145 (1980).
16. G. L. Gainnes. JR. *Insoluble Monolayers at Liquid-Gas interfaces.* John Wiley & Sons, Inc., USA, (1966).
17. W. D. Harkins, L. E. Copeland, *J. Chem. Phys.*, **10**, 272 (1942)
18. E. K. Rideal, R. K. Schofield, *Proc. R. Soc.* (Lon.), **A109**, 57 (1925).

19. J. H. Brooks, A. E. Alexander, *Proceedings of the Third International Congress of Surface Activity,* **2**, 196 (1933).
20. R. D. Smith, J. C. Berg, *J. Coll. Inter. Sci.,* **74**, 273 (1980).
21. V. A. Asentiev, J. Leja, *Colloid and Interface Science,* vol. 5, ed. M. Kerker, Academic Press, N. Y., (1976), p251
22. R. Bienkowski, M. Skolrick, *J. Coll. Inter. Sci.*, **39**, 323 (1972)
23. R. A. Dluhy, *J. Phys. Chem.,* **89**, 3195-3197, (1985)
24. B. F. Sinnamon, R. A. Dluhy, G.T. Barnes., *Colloids and Surfaces A*, **146**, 49-61 (1999)
25. R. A. Dluhy, *J. Phys. Chem.,* **90**, 1373-1379, (1986)
26. M. L. Mitchell, R. A. Dluhy, *J. Am. Chem. Soc.*, **110**, 712-718 (1988)
27. J. A. Mielczarski, *J. Phys. Chem.*, **97**, 2649-2663 (1993)
28. G. L. Gainnes. JR. *Insoluble Monolayers at Liquid-Gas interfaces.* John Wiley & Sons, Inc., USA, (1966) p220
29. S. J. Cooper, *Nucleation Beneath Monolayer Film,* Doctoral Dissertation, Univ. Bristol, (1993) p115
30. D. Volhardt, *Colloids and Surfaces,* **143**, 185-195 (1998)
31. D. Marr-Leisy, R. Neumann, H. Ringsdorf, *Coll. Polym. Sci.,* **263**, 791-798 (1985)
32. S. J. Cooper, *Nucleation Beneath Monolayer Film,* Doctoral Dissertation, Univ. Bristol (1993) p130
33. W. Lee, J. A. Gardella, Jr., *Langmuir,* **16**, 3401-3406 (2000)
34. M. Fukuto, R. K. Heilmann, P. S. Pershan, *J. Chem. Phys.*, **111**, 9761-9777 (1999)
35. R. Popovitz-Biro, R. Edgar, I. Weissbuch, R. Lavie, S. Cohen, K. Kjaer, J. Als-Nielsen, E. Wassermann, L. Leiserowitz, M. Lahav, *Acta Polym*, **49**, 626-635 (1998)
36. G. D. Fasman *Handbook of Biochemistry and Molecular Biology* 3rd Edition (1976) vol 1, p115
37. J. T. L. Navarrete, V. Hernández, F. J. Ramírez, *Biopolymers*, **34**, 1065-1077 (1994)